A QUANTUM ELECTRODYNAMICAL APPROACH TO CHIRALITY AND PHOTONICS: NONLINEAR OPTICS, STRUCTURED LIGHT, AND OPTICAL FORCES

A thesis submitted by:

KAYN A. FORBES

as part of the requirements for the degree of PhD in the

School of Chemistry

University of East Anglia

NORWICH NR4 7TJ

January 2018

The research in this thesis has not been submitted previously for a degree at this or any other university. Except where explicitly mentioned, the work is of my own.

K. A. Forbes

January 2018

ABSTRACT

In this thesis, the theory of quantum electrodynamics (QED) is utilised to study the interaction between radiation and matter. In particular, the non-relativistic limit of the theory is employed, describing the optical processes and coupling between molecules and light.

The predictive power of this theory is highlighted from the outset, whereby it is shown that a new form of quantum uncertainty, with its origins in delocalised photon emission and absorption, exists in non-linear optics: a non-localised mechanism for the processes of both spontaneous parametric down-conversion and second harmonic generation is established by accounting for virtual photon propagation.

The subsequent chapter brings forth the often ignored diamagnetic couplings to optical processes. Their interesting and unique physical properties are shown to manifest themselves in scattering and two-photon absorption processes, and an argument for their inclusion in any multiphoton optical process is outlined.

Next, the question of whether the sign of the topological charge (handedness) of a beam possessing optical orbital angular momentum (structured light) engages in chiroptical processes with chiral molecules is resolved. It is shown that through the engagement of the electric quadrupole molecular moment, discriminatory effects with regards to the direction of the vortex twist are anticipated with anisotropic matter.

Finally, the laser-induced intermolecular forces that exist between molecules present within an intense laser beam are focused on. Specifically, it is shown that there exists a discriminatory force between chiral molecules when subjected to circularly polarised light.

For Mum and Georgia

"'Tis not in mortals to command success; but we'll do more, Sempronius, we'll deserve it."

-Joseph Addison, *Cato, a Tragedy*. (1712).

CONTENTS

CHAPTER 2: QUANTUM DELOCALISATION IN NONLINEAR OPTICS

CHAPTER 3: DIAMAGNETIC INTERACTIONS IN SCATTERING AND NONLINEAR OPTICS

CHAPTER 4: OPTICAL ORBITAL ANGULAR MOMENTUM: TWISTED LIGHT AND CHIRALITY

CHAPTER 5: CHIRAL DISCRIMINATION IN OPTICAL FORCES

PUBLICATIONS

The following list represents published papers that resulted from research that was undertaken for this thesis;

1.   **K. A. Forbes** and D. L. Andrews, Chiral discrimination in optical binding, *Physical review A*. **91** (5), 053824 (2015).

2.   D. S. Bradshaw, **K. A. Forbes**, J. M. Leeder, and D. L. Andrews, Chirality in optical trapping and optical binding, *Photonics*. **2** (2), 483-497 (2015).

3.   **K. A. Forbes**, D. S. Bradshaw, and D. L. Andrews, Discriminatory effects in the optical binding of chiral nanoparticles, in *Optical Trapping and Optical Micromanipulation XII,* ed. K. Dholakia and G. C. Spalding, *Proceedings of SPIE*, **9548**, 95480M (2015).

4.   **K. A. Forbes**, D. S. Bradshaw, and D. L. Andrews, Identifying diamagnetic interactions in scattering and nonlinear optics, *Physical Review A*. **94** (3), 033837 (2016).

5.   **K. A. Forbes**, M. D. Williams, and D. L. Andrews, Quantum theory for the nanoscale propagation of light through stacked thin film layers, in *Nanophotonics IV*, ed. D. L. Andrews, J-M. Nunzi, and A. Ostendorf, *Proceedings of SPIE,* **9884**, 988434 (2016).

6.   **K. A. Forbes**, J. S. Ford, and D. L. Andrews, Nonlocalized Generation of Correlated Photon Pairs in Degenerate Down-Conversion, *Physical Review Letters*. **118** (13), 133602. (2017).

7.   **K. A. Forbes**, J. S. Ford, G. A. Jones, and D. L. Andrews, Quantum delocalization in photon-pair generation, *Physical Review A*. **96** (2), 023850 (2017).

8.   **K. A. Forbes**, J. S. Ford, and D. L. Andrews, Quantum localization issues in nonlinear frequency conversion and harmonic generation, in *Quantum Nanophotonics*, ed. J. A. Dionne and M. Lawrence, *Proceedings of SPIE,* **10359**, 1035908 (2017).

9.   **K. A. Forbes** and D. L. Andrews, Optical orbital angular momentum: twisted light and chirality, *Optics Letters* **43** (3), 435-438 (2018)

10.   **K. A. Forbes** and D. L. Andrews, Chiroptical interactions between twisted light and chiral media, in *Complex Light and Optical Forces XII*, ed. E. J. Galvez, D. L. Andrews, and J. Glückstad, *Proceedings of SPIE*, **10549**, 1054915 (2018).

ACKNOWLEDGMENTS

1

QUANTUM ELECTRODYNAMICS

1.1 INTRODUCTION

The theory of quantum electrodynamics (QED) is often quoted as the most accurate physical theory that exists to date [1]. The key to its success is that it treats both the matter, radiation, and the interaction between the two, using a fully quantised formulation. This is in contrast to both the classical and semi-classical methods that pre-dated it. Whilst the shortcomings of the fully classical theory are well known, treating the matter quantum mechanically and the radiation classically (semi-classical theory) is still widely utilised to this day as it can be used to explain a multitude of physical phenomena, and in general gives adequate results [2]. However, its shortcomings were eventually highlighted through its inability to explain simple optical processes such as spontaneous emission, and it was clear that the only way to fully explain the way electrodynamics is observed in the universe is to treat the whole matter-radiation system as a quantised entity.

In the late 1920s, the quantum theory of the free electromagnetic field was formulated [3] and its first application was in the absorption and emission of light by atoms [4] : QED was born. In the decades that followed, many of the significant advances in the field were in the successful marrying of special relativity and QED, resulting in a fully-relativistic theory applicable to high energy particles coupling to the radiation field [5].

In this thesis, the interaction of radiation and matter will be concerned with molecules, where the energies of the bound electrons are much less than mc^2. As such, the issues of fermionic pair particle creation and destruction events does not concern us, and the number of charged

particles present in the system is conserved. However, these charged particles are free to exchange energy with the radiation field through the annihilation and creation of photons, and as such there is no conservation of photon number. When these limits are placed upon fully-covariant QED, the emerging result is a non-relativistic theory, more commonly known as molecular QED [6-12].

Molecular QED has found wide-ranging success in describing the interactions between photons and molecules. The most celebrated of these include the fully-retarded expression for the dispersion force between a pair of neutral molecules [13, 14], a plethora of nonlinear optical processes including the generation of optical harmonics [15, 16], intermolecular forces [12], resonance energy transfer [17, 18], light beams with orbital angular momentum interacting with molecules [19], and chirally discriminant processes including optical rotation [20], circular dichroism [21], differential Rayleigh and Raman scattering [22, 23].

This introductory chapter aims to present an outline of the underlying theory of molecular QED, suitable for the application to specific photon-molecule interactions in the ensuing chapters. It will follow the most well-known method of working through the canonical formalism: starting with the classical Lagrangian and applying canonical quantisation to yield the total quantum Hamiltonian for the system. This route is best undertaken working within the Schrödinger picture, where the time dependence occurs exclusively within the state of the system and the operators are time-independent. However, there does exist a less well-known viewpoint whereby the electromagnetic field interacts with a wavelike electron (rather than a charged particle) – this is sometimes referred to as the field theoretic approach [24-26]. This method is most easily understood through the Heisenberg picture, where all time dependence is contained within the dynamic variables.

Most standard texts on the issue of molecular QED begin with what is termed the minimal coupling Lagrangian, moving through the canonical quantisation procedure to secure the minimal coupling Hamiltonian. This Hamiltonian was widely utilised in the early studies of photon-molecule interactions and is therefore engrained within the literature. However, its implementation is rather cumbersome due to it being dependent on the vector potential and the conjugate momentum. Fortunately, there also exists another Hamiltonian, more suited to the interaction of radiation and molecules which is termed the multipolar Hamiltonian. This Hamiltonian is dependent on the multipole moments of the molecules and the fundamental electric and magnetic fields. It is therefore easier to implement in calculations and gives

much better physical insight to the optical processes to be studied. For this reason, it is the most-implemented Hamiltonian within modern molecular QED studies. Many texts still derive the minimal coupling Hamiltonian and carry out a suitable canonical transformation to yield the multipolar Hamiltonian. However, throughout this thesis we explicitly use the multipolar Hamiltonian, and therefore it will be derived starting with the multipolar Lagrangian.

1.2   QUANTISATION OF MATTER

The first step in developing the fully quantised theory light-matter interactions is to quantise the charges which make up the material part of the system. We proceed in the standard and most general way through the Lagrangian formulation in the absence of fields. The system is made up of particles ξ with generalised positions q_ξ and velocities $\dot{q}_\xi$. The Lagrangian itself is defined as the kinetic energy T minus the potential energy V: the motivation behind such a definition is that the difference between the average kinetic and average potential energy is stationary about a classical trajectory. As is standard, through Hamilton's principle of least action and the calculus of variations, the Euler-Lagrange equation of motion for a system of particles with N degrees of freedom is

$$\frac{d}{dt}\left(\frac{\partial L}{\partial \dot{q}_\xi}\right) - \frac{\partial L}{\partial q_\xi} = 0;\ \xi = 1, 2, ... N. \tag{1.2.1}$$

The description of motion in the Lagrangian formulation is by N second-order equations. However, it is possible to reduce this computational complexity, first by introducing the Hamiltonian function H, and then describing the system by generalised coordinates q_ξ, as in the Lagrangian method, but instead of generalised velocities, the Hamiltonian approach requires generalised momenta p_ξ. The Hamiltonian function takes the form

$$H = \sum_{\xi=1}^{N} p_\xi \dot{q}_\xi - L, \tag{1.2.2}$$

and the generalised momenta are defined by

$$p_\xi = \frac{\partial L}{\partial \dot{q}_\xi}; \ \xi = 1, 2, ... N. \tag{1.2.3}$$

By inserting (1.2.3) into (1.2.1) it is simple to show that

$$\dot{p}_\xi = \frac{\partial L}{\partial q_\xi}. \tag{1.2.4}$$

When the above is used in determining the total differential dH from (1.2.2), we yield Hamilton's canonical equations

$$\dot{q}_\xi = \frac{\partial H}{\partial p_\xi}; \quad \dot{p}_\xi = -\frac{\partial H}{\partial q_\xi}; \ \xi=1,2,...N, \tag{1.2.5}$$

and find that

$$\frac{\partial H}{\partial t} = -\frac{\partial L}{\partial t}. \tag{1.2.6}$$

Thus, it can be seen that Hamilton's canonical equations of motion consist of 2N first-order equations and are equivalent to N second-order Euler-Lagrange equations of motion, and that they depend on the canonically conjugate variables of generalised position coordinates

and generalised momenta. After having obtained the classical Hamiltonian function in terms of the canonically conjugate variables (1.2.2), the quantum mechanical Hamiltonian operator is found by simply promoting the classical variables to quantum operators. The quantum operators must obey the fundamental canonical commutation relations for particles ξ and ξ':

$$\left[\boldsymbol{q}_\xi, \boldsymbol{q}_{\xi'} \right] = 0; \quad \left[\boldsymbol{p}_\xi, \boldsymbol{p}_{\xi'} \right] = 0; \quad \left[\boldsymbol{q}_\xi, \boldsymbol{p}_{\xi'} \right] = i\hbar \delta_{\xi\xi'}. \tag{1.2.7}$$

1.3 MACROSCOPIC AND MICROSCOPIC FIELDS

In classical electromagnetism [27], Maxwell's equations relate electricity and magnetism to their macroscopic sources, namely the charge density ρ and current density $\boldsymbol{j}$, these being continuous functions of position. However, it is well known that at the microscopic scale, matter is made up of a collection of discrete charged particles. Therefore, in the following development of quantum electrodynamics, it is suitably advantageous to define the sources as charged particles α possessing electrical charge e_α, situated at a position $\boldsymbol{q}_\alpha$ and possessing a velocity $\dot{\boldsymbol{q}}_\alpha$, and as such $\rho(\boldsymbol{r})$ and $\boldsymbol{j}(\boldsymbol{r})$ are defined as

$$\rho(\boldsymbol{r}) = \sum_\alpha e_\alpha \delta(\boldsymbol{r} - \boldsymbol{q}_\alpha), \tag{1.3.1}$$

and

$$\boldsymbol{j}(\boldsymbol{r}) = \sum_\alpha e_\alpha \dot{\boldsymbol{q}}_\alpha \delta(\boldsymbol{r} - \boldsymbol{q}_\alpha), \tag{1.3.2}$$

respectively. In the above, $\delta(\boldsymbol{r})$ is the Dirac delta function, which is strongly localised when $\boldsymbol{r} = \boldsymbol{q}_\alpha$.

The microscopic counterpart to the macroscopic Maxwell equations are the Maxwell-Lorentz equations:

$$\nabla \cdot \boldsymbol{e} = \frac{\rho}{\varepsilon_0}, \qquad (1.3.3)$$

$$\nabla \cdot \boldsymbol{b} = 0, \qquad (1.3.4)$$

$$\nabla \times \boldsymbol{e} = -\frac{\partial \boldsymbol{b}}{\partial t}, \qquad (1.3.5)$$

$$\nabla \times \boldsymbol{b} = \frac{1}{c^2} \frac{\partial \boldsymbol{e}}{\partial t} + \frac{1}{\varepsilon_0 c^2} \boldsymbol{j}. \qquad (1.3.6)$$

In contrast to the macroscopic Maxwell equations, all charged particles in the system contribute to ρ and $\boldsymbol{j}$, and there are no auxiliary fields; they also only depend on the fundamental electric $\boldsymbol{e}$ and magnetic $\boldsymbol{b}$ fields. The constants ε_0 and μ_0 are the vacuum permittivity and magnetic permeability, respectively, and are related through $\varepsilon_0 \mu_0 = c^{-2}$.

1.4 ELECTROMAGNETIC POTENTIALS

The next issue is key in the management of the eventual quantisation of the radiation-matter system which is to come. The microscopic field equations as presented currently are expressed in terms of the force fields $\boldsymbol{e}$ and $\boldsymbol{b}$, however the ensuing canonical quantisation

process can be made easier via the use of potentials. It is therefore convenient to introduce the two electromagnetic potentials: the scalar ϕ and the vector $\boldsymbol{a}$, potentials. Using two results from vector analysis:

(i) If the divergence of a vector field vanishes $(\nabla \cdot \boldsymbol{F} = 0)$, the field can be expressed as the curl of a vector field $\boldsymbol{a}$:

$$\boldsymbol{F} = \nabla \times \boldsymbol{a}, \qquad (1.4.1)$$

since $\nabla \cdot (\nabla \times \boldsymbol{a}) = 0$ for any vector field.

(ii) If the curl of a vector field vanishes $(\nabla \times \boldsymbol{F} = 0)$, the field can be expressed as the gradient of a scalar field ϕ:

$$\boldsymbol{F} = \nabla \phi, \qquad (1.4.2)$$

since $\nabla \times (\nabla \boldsymbol{a}) = 0$ for any scalar field.

Taking into account the above, the *vector potential* $\boldsymbol{a}$, with the aid of the second Maxwell-Lorentz equation (1.3.4), can be defined as

$$\boldsymbol{b} = \nabla \times \boldsymbol{a}. \qquad (1.4.3)$$

Inserting (1.4.3) into the third Maxwell-Lorentz equation (1.3.5) gives

$$\nabla \times \left(\boldsymbol{e} + \frac{\partial \boldsymbol{a}}{\partial t} \right) = 0. \qquad (1.4.4)$$

Therefore, using the result (1.4.2), that the curl of the gradient of a scalar field is zero, the factor in parentheses of (1.4.4) can be written as

$$\boldsymbol{e} + \frac{\partial \boldsymbol{a}}{\partial t} = -\nabla \phi, \tag{1.4.5}$$

where ϕ is the scalar potential (the choice of negative sign aids later work). Inserting (1.4.5) into (1.3.3) yields

$$\nabla \cdot \left(-\nabla \phi - \frac{\partial \boldsymbol{a}}{\partial t} \right) = \nabla^2 \phi + \frac{\partial}{\partial t}(\nabla \cdot \boldsymbol{a}) = -\frac{\rho}{\varepsilon_0}, \tag{1.4.6}$$

whilst inserting both (1.4.3) and (1.4.5) into the final Maxwell-Lorentz equation (1.3.6) gives

$$\nabla^2 \boldsymbol{a} - \frac{1}{c^2}\frac{\partial^2 \boldsymbol{a}}{\partial t^2} - \nabla(\nabla \cdot \boldsymbol{a}) - \frac{1}{c^2}\nabla\frac{\partial \phi}{\partial t} = -\frac{1}{\varepsilon_0 c^2}\boldsymbol{j}, \tag{1.4.7}$$

which has been written with the aid of the vector identity

$$\nabla \times (\nabla \times \boldsymbol{a}) = -\nabla^2 \boldsymbol{a} + \nabla(\nabla \cdot \boldsymbol{a}). \tag{1.4.8}$$

The four Maxwell-Lorentz equations have now been reduced to two coupled equations, both written in terms of the electromagnetic potentials (not force fields) and are directly related to the sources.

1.5 LORENTZ AND COULOMB GAUGES

A potential is only determined up to a constant of integration. As such, the electromagnetic potentials a and ϕ are not uniquely defined, being determined up to an additive gauge function f. This gauge freedom of the potentials is easily exhibited through making the replacement of $a \rightarrow a + \nabla f$ in (1.4.3)

$$b = \nabla \times a = \nabla \times (a + \nabla f) = \nabla \times a + \nabla \times (\nabla f) = \nabla \times a, \tag{1.5.1}$$

where the vector identity $\nabla \times (\nabla f) = 0$ has been used. Evidently, the addition of the gradient of a scalar function leaves b invariant. The gauge transformation that must be simultaneously applied to ϕ which leaves e invariant can be found by inserting the transformation for the vector potential $a \rightarrow a + \nabla f$ into (1.4.5):

$$e = -\frac{\partial a}{\partial t} - \nabla \phi = -\frac{\partial}{\partial t}(a + \nabla f) - \nabla \phi', \tag{1.5.2}$$

and therefore

$$\nabla \phi' = \nabla \left(\phi - \frac{\partial f}{\partial t} \right). \tag{1.5.3}$$

The scalar potential is determined to within the time derivative of the same function f: $\phi \rightarrow \phi - \frac{\partial f}{\partial t}$. The two relations that constitute the gauge transformation are therefore

$$\boldsymbol{a} \rightarrow \boldsymbol{a} + \nabla f, \tag{1.5.4}$$

and

$$\phi \rightarrow \phi - \frac{\partial f}{\partial t}. \tag{1.5.5}$$

The fields and Maxwell-Lorentz equations are unaffected by making the substitution and gauge transformation when (1.5.4) and (1.5.5) are applied in conjunction: this invariance is described as gauge invariance and leaves the fundamental field vectors unaltered.

One choice of gauge function is the Lorentz gauge, which relates the scalar potential to the charges and the vector potential to the currents. The Lorentz gauge is a more suitable choice in the relativistic formulation of QED. A more useful gauge for the non-covariant theory developed and used throughout this thesis is known as the Coulomb gauge, and it is a gauge in which the vector potential is purely solenoidal

$$\nabla \cdot \boldsymbol{a} = 0. \tag{1.5.6}$$

Due to the ability to make a gauge transformation $\boldsymbol{a} \rightarrow \boldsymbol{a} + \nabla f$, a vector potential with zero divergence can always be found:

$$\begin{aligned} 0 &= \nabla \cdot \left(\boldsymbol{a} + \nabla f \right) \\ &= \nabla \cdot \boldsymbol{a} + \left(\nabla^2 f \right) \\ \nabla^2 f &= -\nabla \cdot \boldsymbol{a}, \end{aligned} \tag{1.5.7}$$

where the function f can always be chosen as to be a solution of the Poisson's equation.

Invoking the Coulomb gauge then, (1.4.6) and (1.4.7) become

$$\nabla^2 \phi = -\frac{\rho}{\varepsilon_0},$$

(1.5.8)

and

$$\left(\nabla^2 - \frac{1}{c^2} \frac{\partial^2}{\partial t^2} \right) \boldsymbol{a} = \frac{1}{c^2} \nabla \left(\frac{\partial \phi}{\partial t} \right) - \frac{1}{\varepsilon_0 c^2} \boldsymbol{j},$$

(1.5.9)

respectively. Therefore, the Poisson's equation (1.5.8) shows that in the Coulomb gauge the scalar potential represents the instantaneous Coulomb potential due to the charge density – hence the name Coulomb gauge. We have therefore separated the static and dynamic aspects of the sources of the electromagnetic field. In free space, devoid of any sources, the scalar potential clearly goes to zero – this is the basis behind the Maxwell-Lorentz equations in free space which we discuss in the next section.

Using Helmholtz's theorem of decomposition of vector fields into transverse and longitudinal components $\left(\boldsymbol{F} = \boldsymbol{F}^{\perp} + \boldsymbol{F}^{\parallel} \right)$, it can clearly been seen from (1.3.4) that the vector field $\boldsymbol{b}$ must be purely transverse and that (1.3.3) and (1.3.5) become

$$\nabla \cdot \boldsymbol{e}^{\parallel} = \frac{\rho}{\varepsilon_0},$$

(1.5.10)

and

$$\nabla \times \boldsymbol{e}^{\perp} = -\frac{\partial \boldsymbol{b}}{\partial t},$$

(1.5.11)

respectively. The final Maxwell-Lorentz equation (1.3.6) separates into

$$\nabla \times \boldsymbol{b} = \frac{1}{c^2}\frac{\partial \boldsymbol{e}^{\perp}}{\partial t} + \frac{1}{\varepsilon_0 c^2}\boldsymbol{j}^{\perp}, \tag{1.5.12}$$

and

$$0 = \frac{1}{c^2}\frac{\partial \boldsymbol{e}^{\parallel}}{\partial t} + \frac{1}{\varepsilon_0 c^2}\boldsymbol{j}^{\parallel}. \tag{1.5.13}$$

The equation of continuity,

$$\nabla \cdot \boldsymbol{j}^{\parallel} + \frac{\partial \rho}{\partial t} = 0, \tag{1.5.14}$$

is secured through taking the divergence of (1.5.13) and using (1.5.10), and it states that the total charge in a specified volume is constant unless there is a net flow of charge in or out of the volume: this is the principle of charge conservation.

The central characteristic of the Coulomb gauge is that the vector potential $\boldsymbol{a}$ has zero divergence (as shown in (1.5.6)), and therefore $\boldsymbol{a} = \boldsymbol{a}^{\perp}$. This, in conjunction with the fact that $\nabla \phi$ is irrotational (see (1.4.2)), equation (1.4.5) can be divided into longitudinal and transverse terms

$$\boldsymbol{e}^{\parallel} = -\nabla \phi, \tag{1.5.15}$$

and

$$e^{\perp} = -\frac{\partial \boldsymbol{a}}{\partial t}. \tag{1.5.16}$$

Therefore, equation (1.5.9) can now be written explicitly in terms of transverse components only

$$\left(\nabla^2 - \frac{1}{c^2}\frac{\partial^2}{\partial t^2} \right) \boldsymbol{a} = -\frac{1}{\varepsilon_0 c^2}\boldsymbol{j}^{\perp}, \tag{1.5.17}$$

and ϕ continues to satisfy Poisson's equation (1.5.8). Clearly then, in the Coulomb gauge, the irrotational (longitudinal) and solenoidal (transverse) fields are completely separated. The scalar potential (electrostatic potential) describes the static longitudinal fields fully, and the vector potential obeys a wave equation and fully describes the transverse dynamic fields. This is why the Coulomb gauge is useful and suitable for problems of the electromagnetic field coupling to atoms and molecules: the Coulomb potential separates out.

1.6 THE CLASSICAL ELECTROMAGNETIC FIELD IN SOURCE-FREE SPACE

Section 1.2 outlined the general method of constructing the quantum mechanics of a system of particles beginning with the classical Lagrangian function and progressing through the Hamiltonian formulation. In this section, the same general scheme and principles are applied to the classical radiation field in a region free of sources (*in vacuo*) leading to the quantisation of the free electromagnetic field. As has been noted previously, this is an essential step in the formulation of quantum electrodynamics, whose major difference to other dynamical theories is that the radiation is subject to the postulates of quantum mechanics, as well as the matter.

In regions free of charge, Maxwell's equations for the fundamental electromagnetic field vectors e and b for the microscopic field take the form

$$\nabla \cdot \boldsymbol{e} = 0, \tag{1.6.1}$$

$$\nabla \cdot \boldsymbol{b} = 0, \tag{1.6.2}$$

$$\nabla \times \boldsymbol{e} = -\frac{\partial \boldsymbol{b}}{\partial t}, \tag{1.6.3}$$

$$\nabla \times \boldsymbol{b} = \frac{1}{c^2} \frac{\partial \boldsymbol{e}}{\partial t}. \tag{1.6.4}$$

Evidently both e and b are divergence-free and therefore transverse in vacuum. A more convenient way to describe the fields is through the electromagnetic potentials defined in (1.4.3) and (1.4.5). Employing the Coulomb gauge ($\nabla \cdot \boldsymbol{a} = 0$) and $\boldsymbol{e} = -\dot{\boldsymbol{a}}$ - the latter due to the fact that the scalar potential ϕ is a constant which may be taken to be zero since the electric field is divergence-free in vacuum (see equation (1.5.8) - the elimination of e and b from (1.6.4) using (1.4.3) and (1.4.5) leads to d'Alembert's equation for the vector potential,

$$\left(\nabla^2 - \frac{1}{c^2} \frac{\partial^2}{\partial t^2} \right) \boldsymbol{a} = 0. \tag{1.6.5}$$

e and b satisfy identical equations of motion

$$\left(\nabla^2 - \frac{1}{c^2} \frac{\partial^2}{\partial t^2} \right) \boldsymbol{e} = 0, \tag{1.6.6}$$

$$\left(\nabla^2 - \frac{1}{c^2}\frac{\partial^2}{\partial t^2}\right)\boldsymbol{b} = 0. \tag{1.6.7}$$

One of the possible complex solutions to the wave equations for each of the fields $\boldsymbol{a}$, $\boldsymbol{e}$, and $\boldsymbol{b}$ are the monochromatic plane waves

$$\boldsymbol{a} = \boldsymbol{a}_0\, e^{i(\boldsymbol{k}\cdot\boldsymbol{r}-\omega t)}, \tag{1.6.8}$$

$$\boldsymbol{e} = e_0\boldsymbol{e}_0\, e^{i(\boldsymbol{k}\cdot\boldsymbol{r}-\omega t)}, \tag{1.6.9}$$

$$\boldsymbol{b} = b_0\boldsymbol{b}_0\, e^{i(\boldsymbol{k}\cdot\boldsymbol{r}-\omega t)}, \tag{1.6.10}$$

where the pre-exponential scalars and vectors denote the amplitude and polarisation vector, respectively. The magnitude of the wave vector $\boldsymbol{k}$, which describes the direction of propagation of the electromagnetic wave, can easily be found by substitution of the plane wave solution into the appropriate wave equation and it is seen to be $|\boldsymbol{k}| = k = \omega/c$, where ω is the angular frequency.

Inserting (1.6.8) and (1.6.9) into (1.6.6) and (1.6.7) produces

$$\hat{k}\times\boldsymbol{e}_0 = c\boldsymbol{b}_0, \tag{1.6.11}$$

and

$$\hat{k} \times \boldsymbol{b}_0 = -\frac{1}{c} \boldsymbol{e}_0, \tag{1.6.12}$$

respectively. In the above, $\hat{k} = \boldsymbol{k}/k$ is the unit vector of the wave vector. From (1.6.11) it can be seen that $\boldsymbol{b}_0$ is transverse to the propagation of the electromagnetic wave $\hat{k}$ and to the electric polarisation vector $\boldsymbol{e}_0$, its magnitude equal to $\left| e_0/c \right|$. Equally, (1.6.12) shows $\boldsymbol{e}_0$ is transverse to $\hat{k}$, highlighting the transverse nature of electromagnetic waves: it can be seen that $\boldsymbol{e}_0$, $\boldsymbol{b}_0$, and $\hat{k}$ form a right-handed triad. Another result that will become important in the quantisation procedure is noting that from (1.4.5)

$$\boldsymbol{e}_0 = ick\boldsymbol{a}_0. \tag{1.6.13}$$

1.7 ELECTROMAGNETIC WAVES IN A BOX

In the monochromatic plane wave solutions (1.6.8)-(1.6.10), the wave vector $\boldsymbol{k}$ that is associated with the propagating wave can assume an infinite range of values. Such an infinity of continuum states may be overcome in the transition to quantum theory using the technique of box normalisation [28]. The method of box normalisation allows the radiation field to be composed of field *modes*, with each mode being normalisable in a simple manner. Upon application of the method, it is assumed that the field is present within a finite arbitrary volume V (a cube in this case) and that the vector potential $\boldsymbol{a}$ (1.6.8) is required to take the same value on opposite faces of the volume (cube).

Solutions of the plane waves are now restricted to those where the wave vector values satisfy the boundary conditions of having the same values on opposite sides of a cube of volume $V=L_xL_yL_z$ (L being dimensions along the three sides of the box), namely

$$k_i = \frac{2\pi}{L_i} n_i, \tag{1.7.1}$$

where $i = x, y, z$ and n_i are integers and the result is secured through Euler's formula and the result $\cos(\pm n2\pi) = 1$. Each solution applies to two modes of the vector field and is characterised by three integers.

The vector potential $\boldsymbol{a}(\boldsymbol{r},t)$ can be written in the form of a Fourier series in the modes allowed by (1.7.1), giving the mode expansion of $\boldsymbol{a}$ as a sum over plane wave terms

$$\boldsymbol{a}(\boldsymbol{r},t) = \sum_{\boldsymbol{k}} \left[\boldsymbol{a}_{\boldsymbol{k}}(t) e^{i\boldsymbol{k}\cdot\boldsymbol{r}} + \bar{\boldsymbol{a}}_{\boldsymbol{k}}(t) e^{-i\boldsymbol{k}\cdot\boldsymbol{r}} \right], \tag{1.7.2}$$

the $\boldsymbol{a}_{\boldsymbol{k}}(t)$ being amplitude coefficients and the overbar denotes the complex conjugate. Substitution of (1.7.2) into (1.6.5) leads to $\boldsymbol{a}_{\boldsymbol{k}}(t)$ having to satisfy

$$\frac{\partial^2 \boldsymbol{a}_{\boldsymbol{k}}(t)}{\partial t^2} + c^2 k^2 \boldsymbol{a}_{\boldsymbol{k}}(t) = 0. \tag{1.7.3}$$

The solutions to the above equation are obvious: periodic functions of the form $e^{-i\omega t}$ and therefore

$$\boldsymbol{a}_{\boldsymbol{k}}(t) \propto e^{i(\boldsymbol{k}\cdot\boldsymbol{r} - \omega t)}, \tag{1.7.4}$$

which corresponds to a wave propagating in the $\hat{\boldsymbol{k}}$ direction with speed c, exactly as in the unconfined field (1.6.8). Since $\nabla \cdot \boldsymbol{a} = 0$, equation (1.7.2) shows that $\hat{\boldsymbol{k}} \cdot \boldsymbol{a}_{\boldsymbol{k}} = 0$ which means the mode amplitudes are orthogonal to the direction in which the wave is propagating. The $\boldsymbol{e}$ and $\boldsymbol{b}$ fields (which are also transverse) are parallel and perpendicular to the $\boldsymbol{a}$ field for each mode $\boldsymbol{k}$. The Fourier amplitudes being orthogonal to $\hat{\boldsymbol{k}}$ can therefore be specified in

terms of two components along two mutually orthogonal directions transverse to $\hat{\boldsymbol{k}}$, which are the polarisation vectors, chosen to form a right-handed triad with $\hat{\boldsymbol{k}}$. That is:

$$\boldsymbol{e}^{(1)}(\boldsymbol{k})\cdot\overline{\boldsymbol{e}}^{(2)}(\boldsymbol{k})=\boldsymbol{e}^{(1)}(\boldsymbol{k})\cdot\hat{\boldsymbol{k}}=\overline{\boldsymbol{e}}^{(2)}(\boldsymbol{k})\cdot\hat{\boldsymbol{k}}=0. \tag{1.7.5}$$

Therefore, $\boldsymbol{a}(\boldsymbol{r},t)$ can be written as

$$\boldsymbol{a}(\boldsymbol{r},t)=\sum_{\boldsymbol{k},\eta}\left[\boldsymbol{e}^{(\eta)}(\boldsymbol{k})a_{\boldsymbol{k}}^{(\eta)}(t)e^{i\boldsymbol{k}\cdot\boldsymbol{r}}+\overline{\boldsymbol{e}}^{(\eta)}(\boldsymbol{k})\overline{a}_{\boldsymbol{k}}^{(\eta)}(t)e^{-i\boldsymbol{k}\cdot\boldsymbol{r}}\right], \tag{1.7.6}$$

where $\boldsymbol{e}^{(\eta)}(\boldsymbol{k})$ is the unit electric polarisation vector of mode $(\boldsymbol{k},\eta)$, with η denoting the polarisation state. The mode expansion for the fundamental fields can easily be obtained from (1.7.6), however their fully normalised forms will be given once the field has been quantised.

1.8 POLARISATION

The unit electric field vector $\boldsymbol{e}^{(\eta)}(\boldsymbol{k})$ from (1.7.6) is a polarisation vector, containing the directional properties of the electric field component of propagating photon or electromagnetic wave in space and time. A wave or photon is said to be linearly polarised if the electric field vector remains, up to a sign, in a fixed direction for all space and time. However, a more general state of polarisation can be achieved by combining two mutually orthogonal and independent electric field unit vectors. A superposition of two different electric fields possessing a phase δ_1 and δ_2 gives

$$\boldsymbol{e}(\boldsymbol{r},t)=\left(e_1\boldsymbol{e}_1\,\mathrm{e}^{i\delta_1}+e_2\boldsymbol{e}_2\,\mathrm{e}^{i\delta_2}\right)\mathrm{e}^{i(\boldsymbol{k}\cdot\boldsymbol{r}-\omega t)}. \tag{1.8.1}$$

Assuming that the two waves are superposed out of phase, this general state produces elliptical polarisation. If both components have the same phase, the result is linear polarisation. If the phase difference is $\delta_1 - \delta_2 = \pm \pi/2$ and both waves have equal amplitudes, the resultant state is circularly polarised. For orthogonal unit vectors, the left- and right-handed circular polarisations are defined as

$$e^{(\text{L/R})} = \frac{1}{\sqrt{2}}\left(e_1 \pm ie_2\right). \tag{1.8.2}$$

1.9 LAGRANGIAN AND HAMILTONIAN FOR THE FREE FIELD

The essential characteristics of the classical field in regions free of sources has been outlined. In order to progress from the classical theory to the fully quantised form, the canonical formalism can be applied to the electromagnetic field in an analogous manner to that in Section 1.2. In contrast to the particle formulation, the field varies continuously throughout space and is described by a density functional $\mathcal{L}$. The total Lagrangian is

$$L = \int \mathcal{L}\left(a, \nabla a, \dot{a}\right)\mathrm{d}^3 r. \tag{1.9.1}$$

As is usual, the principle of least action and calculus of variations are utilised to secure the Euler-Lagrange equations of motions for the field as

$$\frac{\partial}{\partial t}\left(\frac{\partial \mathcal{L}}{\partial \dot{a}_i}\right) + \frac{\partial}{\partial x_j}\frac{\partial \mathcal{L}}{\partial\left(\partial a_i/\partial x_j\right)} - \frac{\partial \mathcal{L}}{\partial a_i} = 0. \tag{1.9.2}$$

To proceed, it is necessary to find a Lagrangian density functional satisfying the requirement that it leads to the correct equations of motion for electromagnetic fields – namely the Maxwell-Lorentz equations free of sources. We choose for the Lagrangian density

$$\mathcal{L} = T - V = \frac{\varepsilon_0}{2}\left(e^2 - c^2 b^2\right) = \frac{\varepsilon_0}{2}\left[\dot{a}^2 - c^2\left(\nabla \times a\right)^2\right], \tag{1.9.3}$$

where we have used $e = -\dot{a}$ and $b = \nabla \times a$, along with taking the square of the electric field to be proportional to the kinetic energy and the electromagnetic potential energy as the square of the magnetic field. We can now evaluate each of the three terms explicitly in (1.9.2)

$$\frac{\partial}{\partial t}\left(\frac{\partial \mathcal{L}}{\partial \dot{a}_i}\right) = \varepsilon_0 \ddot{a}_i, \tag{1.9.4}$$

and

$$\frac{\partial}{\partial x_j}\frac{\partial \mathcal{L}}{\partial\left(\partial a_i / \partial x_j\right)} = -\varepsilon_0 c^2 \nabla^2 a_i, \tag{1.9.5}$$

and finally

$$\frac{\partial \mathcal{L}}{\partial a_i} = 0. \tag{1.9.6}$$

Therefore, substituting (1.9.4)-(1.9.6) into (1.9.2) produces (1.6.5), the correct equation of motion, validating (1.9.3) as the correct choice of Lagrangian density functional for the free electromagnetic field. The next step is to construct the Hamiltonian: the first step is finding

the momentum canonically conjugate to $\boldsymbol{a}$. We define the canonical momentum density for the field as

$$\Pi(\boldsymbol{r}) = \frac{\partial \mathcal{L}}{\partial \dot{\boldsymbol{a}}}, \tag{1.9.7}$$

and therefore the Hamiltonian density is found from the Hamiltonian function

$$\mathcal{H} = \Pi \cdot \dot{\boldsymbol{a}} - \mathcal{L}. \tag{1.9.8}$$

Carrying out the partial differentiation of the Lagrangian density as in (1.9.7) using (1.9.3), leads to the canonical momentum density being

$$\Pi = \varepsilon_0 \dot{\boldsymbol{a}} = -\varepsilon_0 \boldsymbol{e}, \tag{1.9.9}$$

whose relationship with the electric field is qualified by (1.6.3). We can now go back to the Hamiltonian density, which from (1.9.8) and (1.9.3) is seen to be

$$\mathcal{H} = \Pi \cdot \dot{\boldsymbol{a}} - \frac{\varepsilon_0}{2} \left[\dot{\boldsymbol{a}}^2 - c^2 (\nabla \times \boldsymbol{a})^2 \right]. \tag{1.9.10}$$

By using the result (1.9.9), we can eliminate $\dot{\boldsymbol{a}}$ in favour of Π, as this gives the Hamiltonian density in terms of the canonical variables (which will aid us when quantising the Hamiltonian):

$$\mathcal{H} = \frac{1}{2}\left[\frac{\boldsymbol{\Pi}^2}{\varepsilon_0} + c^2\left(\nabla\times\boldsymbol{a}\right)^2\right] = \frac{\varepsilon_0}{2}\left(\boldsymbol{e}^2 + c^2\boldsymbol{b}^2\right) = \int\left(T+V\right)\mathrm{d}^3\boldsymbol{r}, \tag{1.9.11}$$

this is therefore seen to be equal to the electromagnetic energy density, and we can see that we produce the formal definition of the Hamiltonian function – the sum of kinetic and potential energy.

1.10 THE ELECTROMAGNETIC FIELD AS A SUM OF MODE OSCILLATORS

Obtaining the mode expansion for $\boldsymbol{\Pi}$ through (1.9.9) and inserting both it and the expansion for $\boldsymbol{a}$ (1.7.6) into the Hamiltonian density (1.9.11) it is easily verified that the Hamiltonian can be expressed as

$$H = \int \mathcal{H}\left(\boldsymbol{a},\boldsymbol{\Pi},\nabla\boldsymbol{a}\right)\mathrm{d}^3\boldsymbol{r} = 2V\varepsilon_0 c^2\sum_{\boldsymbol{k},\lambda}k^2 a_{\boldsymbol{k}}^{(\eta)}\overline{a}_{\boldsymbol{k}}^{(\eta)}. \tag{1.10.1}$$

We can now introduce two canonically conjugate variables $q_{\boldsymbol{k},\eta}$ and $p_{\boldsymbol{k},\eta}$ which are defined as

$$q_{\boldsymbol{k},\eta} = \left(V\varepsilon_0\right)^{1/2}\left(a_{\boldsymbol{k}}^{(\eta)} + \overline{a}_{\boldsymbol{k}}^{(\eta)}\right); \quad p_{\boldsymbol{k},\eta} = -ick\left(V\varepsilon_0\right)^{1/2}\left(a_{\boldsymbol{k}}^{(\eta)} - \overline{a}_{\boldsymbol{k}}^{(\eta)}\right), \tag{1.10.2}$$

and re-write the Hamiltonian as

$$H = \sum_{k,\eta} H_{k,\eta} = \sum_{k,\eta} \frac{1}{2}\left(p_{k,\eta}^2 + \omega^2 q_{k,\eta}^2\right). \tag{1.10.3}$$

Thus, H is now written as a set of harmonic oscillator Hamiltonians, one for each mode (k, η), in the new canonically conjugate variables $p_{k,\eta}$ and $q_{k,\eta}$. It is readily shown that H leads to the correct Hamilton's equations (i.e. (1.2.5)): firstly by using (1.6.8) in (1.10.2)

$$\frac{dq_{k,\eta}}{dt} = p_{k,\eta}; \qquad \frac{dp_{k,\eta}}{dt} = -\omega^2 q_{k,\eta}, \tag{1.10.4}$$

and therefore using (1.10.3)

$$\frac{\partial H}{\partial p_{k,\lambda}} = p_{k,\lambda} = \dot{q}_{k,\lambda}; \qquad \frac{\partial H}{\partial q_{k,\lambda}} = \omega^2 q_{k,\lambda} = -\dot{p}_{k,\lambda}, \tag{1.10.5}$$

thus satisfying Hamilton's canonical equations.

1.11   QUANTISATION OF THE FREE FIELD

From (1.10.3) it is seen that the radiation field can be composed of a collection of non-interacting harmonic oscillators, and therefore, quantisation of such a set will also lead to quantisation of the free field [29, 30]. However, the solution is began by consideration of a one-dimensional harmonic oscillator whose classical Hamiltonian function is,

$$H = \frac{1}{2m}\left(p^2 + m^2\omega^2 q^2\right). \tag{1.11.1}$$

The corresponding quantum mechanical Hamilton is achieved by promoting the canonical variables with their quantum operator counterparts subject to the fundamental commutator

$$[q, p] = i\hbar. \tag{1.11.2}$$

We now define a pair of mutually adjoint operators a and $a^\dagger$ to replace q and p – this makes finding the eigenvalue spectrum of H much more straightforward and physically meaningful as we will come to discover:

$$a = (2\hbar\omega)^{-\frac{1}{2}}(\omega q + ip), \tag{1.11.3}$$

and

$$a^\dagger = (2\hbar\omega)^{-\frac{1}{2}}(\omega q - ip). \tag{1.11.4}$$

It is to be stressed that although a and $a^\dagger$ are both real, they are not Hermitian and do not represent observables of the harmonic oscillator unlike q and p. Properties of the operators can be found through

$$
\begin{aligned}
a^\dagger a &= (2\hbar\omega)^{-1}\left(p^2 + \omega^2 q^2 + i\omega qp - i\omega pq\right) \\
&= (2\hbar\omega)^{-1}\left(p^2 + \omega^2 q^2 + i\omega[qp - pq]\right) \\
&= (\hbar\omega)^{-1}\left(H - \frac{1}{2}\hbar\omega\right),
\end{aligned}
\tag{1.11.5}
$$

and similarly

$$aa^\dagger = \left(\hbar\omega \right)^{-1} \left(H + \frac{1}{2}\hbar\omega \right).$$

(1.11.6)

Therefore, the commutator of the new operators is easily found to be

$$\left[a, a^\dagger \right] = aa^\dagger - a^\dagger a = 1.$$

(1.11.7)

Using the above results allows the quantum mechanical Hamiltonian to now be expressed in three different, but equivalent forms

$$\begin{aligned}
H &= \left(a^\dagger a + \frac{1}{2} \right) \hbar\omega \\
&\equiv \left(aa^\dagger - \frac{1}{2} \right) \hbar\omega \\
&\equiv \frac{1}{2}\left(a^\dagger a + aa^\dagger \right) \hbar\omega.
\end{aligned}$$

(1.11.8)

The solutions to the Hamiltonian are therefore given by the eigenvalues and eigenfunctions of the operator $a^\dagger a$, such a combination is termed the number operator n . Its eigenvalues are the positive integers and zero, which represent the number of quantised particles in the eigenstate $|n\rangle$. In the case of the electromagnetic field, the quanta are the massless bosons termed *photons*. The concept of the photon underpins all quantum electrodynamics, and its physicality and fundamental nature is the driving force behind the research presented in this thesis. Being bosons, photons obey Bose-Einstein statistics and therefore there exists no restriction on the occupation number of any given quantum state:

$$a^\dagger a\left|n\right\rangle = n\left|n\right\rangle; \quad n=0,1,2,....$$ (1.11.9)

From (1.11.8), it is readily verified that the eigenvalues for the harmonic oscillator are $\left(n+1/2\right)\hbar\omega, \; n=0,1,2,....$. The lowest energy ($n$=0) corresponds to a non-zero value for the energy of the field, termed the zero-point energy or vacuum energy, and this has extremely important consequences as will be seen throughout QED and the work in this thesis.

It is can be easily identified that the harmonic oscillator is built up in a ladder of states, with each step separated by a quantum of energy $\hbar\omega$. The individual operators a and $a^\dagger$ acting on a state, respectively decreasing or increasing its occupation number by unity – they are annihilation and creation operators. This ability to account for the changes in particle number together with the correct statistical laws that the particles adhere to is called second quantisation. It is especially helpful in QED, as the number of photons in any specific mode is sometimes not constant in any given optical processes, for example emission, absorption, or non-forward scattering. The operator equations for the annihilation and creation operators are as follows

$$a\left|n\right\rangle = \begin{cases} 0, & n=0 \\ \sqrt{n}\left|n-1\right\rangle, & n=1,2,3,... \end{cases},$$ (1.11.10)

and

$$a^\dagger\left|n\right\rangle = \sqrt{n+1}\left|n+1\right\rangle \quad n=0,1,2,....$$ (1.11.11)

Which translate as that for the annihilation operator acting on a state $\left|n\right\rangle$, the square root is taken, and then it is lowered by unity; for the creation operator the state is raised by unity and then square rooted.

Section 1.10 outlined how the Hamiltonian for the vacuum electromagnetic field can be composed of one-dimensional harmonic oscillator Hamiltonians (Equation (1.10.3). The eigenvalues and eigenfunctions that were found for a one-dimensional harmonic oscillator can be adapted to form a solution for a sum of uncoupled harmonic oscillator Hamiltonians. For a such a case, the annihilation and creation operators of a photon in the mode (k, η), with wave vector k and polarisation η, subject to the following commutation rules [31]

$$
\begin{aligned}
&\left[a^{(\eta)}(k), a^{(\eta')}(k') \right] = 0 \\
&\left[a^{\dagger(\eta)}(k), a^{\dagger(\eta')}(k') \right] = 0 \\
&\left[a^{(\eta)}(k), a^{\dagger(\eta')}(k') \right] = \left(8\pi^3 V^{-1} \right) \delta^3 (k - k') \delta_{\eta\eta'},
\end{aligned}
\tag{1.11.12}
$$

are employed to construct analogous Hamiltonians of the form (1.11.8), which now take on the forms of

$$
\begin{aligned}
H &= \sum_{k,\eta} \frac{1}{2} \left[a^{(\eta)}(k) a^{\dagger(\eta)}(k) + a^{\dagger(\eta)}(k) a^{(\eta)}(k) \right] \hbar c k \\
&\equiv \sum_{k,\eta} \left[a^{\dagger(\eta)}(k) a^{(\eta)}(k) + \frac{1}{2} \right] \hbar c k \\
&\equiv \sum_{k,\eta} \left[a^{(\eta)}(k) a^{\dagger(\eta)}(k) - \frac{1}{2} \right] \hbar c k,
\end{aligned}
\tag{1.11.13}
$$

where $k = |k|$. The eigenenergy of (1.11.13) is simply a sum over all individual oscillators α

$$
H \left| n_1(k_1, \eta_1), n_2(k_2, \eta_2), ... \right\rangle = \sum_{\alpha} \left(n_\alpha(k_\alpha, \eta_\alpha) + \frac{1}{2} \right) \hbar \omega_\alpha \left| n_1(k_1, \eta_1), n_2(k_2, \eta_2), ... \right\rangle, \tag{1.11.14}
$$

where n_α is the occupation number of the oscillator and $\omega_\alpha = ck_\alpha$.

Evidently from (1.11.10), a particle cannot be absorbed from the ground state ($n = 0$). In the case of the electromagnetic field, when $n_\alpha = 0$ for all α the ground state is the electromagnetic vacuum. Successive application of the appropriate creation operator upon the vacuum state leads to occupation of other basis states, as in

$$\left| n_1(\boldsymbol{k}_1, \eta_1), n_2(\boldsymbol{k}_2, \eta_2), \ldots \right\rangle = \prod_\alpha \frac{\left[a^{\dagger(\eta_\alpha)}(\boldsymbol{k}_\alpha) \right]^{n_\alpha}}{\left(n_\alpha!\right)^{1/2}} \left| 0(\boldsymbol{k}_1, \eta_1), 0(\boldsymbol{k}_2, \eta_2), \ldots \right\rangle. \qquad (1.11.15)$$

The states are known as number states and they correspond to the number of photons in a specific mode. Therefore

$$a^{\dagger(\eta)}(\boldsymbol{k}) a^{(\eta)}(\boldsymbol{k}) \left| n(\boldsymbol{k}, \eta) \right\rangle = n \left| n(\boldsymbol{k}, \eta) \right\rangle, \qquad (1.11.16)$$

$$a^{(\eta)}(\boldsymbol{k}) \left| n(\boldsymbol{k}, \eta) \right\rangle = \sqrt{n} \left| (n-1)(\boldsymbol{k}, \eta) \right\rangle, \qquad (1.11.17)$$

$$a^{\dagger(\eta)}(\boldsymbol{k}) \left| n(\boldsymbol{k}, \eta) \right\rangle = \sqrt{n+1} \left| (n+1)(\boldsymbol{k}, \eta) \right\rangle. \qquad (1.11.18)$$

The creation and annihilation operators are time-independent, and all time dependence is manifest in the states of the system. This is the Schrödinger picture.

At $t = 0$, the quantum mechanical analogues to the classical mode expansions are of the form

$$a(r) = \sum_{k,\eta} \left(\frac{\hbar}{2\varepsilon_0 ckV} \right)^{1/2} \left[e^{(\eta)}(k) a^{(\eta)}(k) e^{ik\cdot r} + \bar{e}^{(\eta)}(k) a^{\dagger(\eta)}(k) e^{-ik\cdot r} \right], \qquad (1.11.19)$$

$$e(r) = i\sum_{k,\eta} \left(\frac{\hbar ck}{2\varepsilon_0 V} \right)^{1/2} \left[e^{(\eta)}(k) a^{(\eta)}(k) e^{ik\cdot r} - \bar{e}^{(\eta)}(k) a^{\dagger(\eta)}(k) e^{-ik\cdot r} \right], \qquad (1.11.20)$$

$$b(r) = i\sum_{k,\eta} \left(\frac{\hbar k}{2\varepsilon_0 cV} \right)^{1/2} \left[b^{(\eta)}(k) a^{(\eta)}(k) e^{ik\cdot r} - \bar{b}^{(\eta)}(k) a^{\dagger(\eta)}(k) e^{-ik\cdot r} \right], \qquad (1.11.21)$$

$$\Pi(r) = -i\sum_{k,\eta} \left(\frac{\hbar ck\varepsilon_0}{2V} \right)^{1/2} \left[e^{(\eta)}(k) a^{(\eta)}(k) e^{ik\cdot r} - \bar{e}^{(\eta)}(k) a^{\dagger(\eta)}(k) e^{-ik\cdot r} \right]. \qquad (1.11.22)$$

The normalisation factor appearing at the front of the mode expansions is obtained by evaluating the expectation value of the energy of the field for a number state, which is known to be $(n+1/2)\hbar\omega$.

1.12 PUTTING IT ALL TOGETHER: MATTER AND RADIATION IN MUTUAL INTERACTION

So far we have treated matter and radiation in isolation from one another, moving through the canonical quantisation process beginning with the classical Lagrangian for charged particles and the electromagnetic field, and progressing to the eventual quantum Hamiltonian. The standard treatment of formulating the quantum Hamiltonian for an *interacting* particle-radiation field system begins with what is known as the minimal coupling Lagrangian. Then, by utilising the fact that there is no unique choice of the total Lagrangian - only that it must lead to the correct equations of motion − the equations of

motion derived from the minimal coupling Lagrangian are unaltered by the addition to the Lagrangian of a total time derivative of a function of the coordinates q and time t.

Using the addition of a function first suggestive by Göppert-Mayer [32], a new Lagrangian is formed known as the multipolar Lagrangian. Both the minimal coupling and multipolar Lagrangian are said to be equivalent. The resultant Hamiltonians will, however, differ in form, but are related to one another by a canonical transformation [7, 11, 33-37]. It is to be recognised that one can begin with the minimal coupling Lagrangian, and progress through to the multipolar Lagrangian followed then by the multipolar Hamiltonian. Equally, one may begin with the minimal coupling Lagrangian, then progress to the minimal coupling Hamiltonian and then carry out a canonical transformation to produce the multipolar Hamiltonian. Thus, it can be seen there are two routes to achieving the desired multipolar Hamiltonian.

In most contemporary QED and quantum optics studies, the multipolar Hamiltonian (most often referred to as the Power-Zienau-Wooley Hamiltonian (PZW Hamiltonian) when quantised) is predominantly utilised over other Hamiltonians – such as the minimal coupling form. As we will come to discover in the ensuing sections, this is because the PZW Hamiltonian offers many distinct physical and calculational advantages, especially for when the particles are molecules. For these reasons, in the following sections we do away with the minimal coupling regime in full, and begin with the multipolar Lagrangian, follow through the canonical formalism, and produce the resulting multipolar Hamiltonian. It will be this PZW Hamiltonian that is used to calculate energy shifts and optical rates throughout this thesis.

1.13   ELECTRIC AND MAGNETIC POLARISATION FIELDS

Before the formulation of the correct Lagrangian and the subsequent Hamiltonian for the quantised light-matter system takes place, it is necessary to define some properties that characterise a medium (due to the fact that neither the matter or the radiation are now free from each other's influence). One such property is the charge distribution, which may be written in the following way when expressed using the conventional Taylor series expansion in terms of point multipole moments about the position R

$$\rho(\boldsymbol{r}) = \sum_\alpha e_\alpha \delta(\boldsymbol{r} - \boldsymbol{q}_\alpha)$$

$$= \sum_\alpha e_\alpha \delta(\boldsymbol{r} - \boldsymbol{R}) - \nabla \cdot \boldsymbol{p}(\boldsymbol{r})$$

$$= \rho^{\text{true}}(\boldsymbol{r}) - \nabla \cdot \boldsymbol{p}(\boldsymbol{r}). \tag{1.13.1}$$

In the above, the true charge density is the overall net charge density of the total distribution, and the following terms can be expressed as the divergence of a vector field $\boldsymbol{p}(\boldsymbol{r})$, which is known as the electric polarisation field and can be written in closed form as the parametric integral [7]

$$\sum_\xi \boldsymbol{p}(\xi, \boldsymbol{r}) = \boldsymbol{p}(\boldsymbol{r}) = e_\alpha \sum_\alpha \left(\boldsymbol{q}_\alpha(\xi) - \boldsymbol{R}_\xi\right) \int_0^1 \delta\left(\boldsymbol{r} - \boldsymbol{R}_\xi - \lambda\left(\boldsymbol{q}_\alpha(\xi) - \boldsymbol{R}_\xi\right)\right) d\lambda. \tag{1.13.2}$$

For example, the first two terms in the expansion relate to the dipole and quadrupole multipole moments about $\boldsymbol{R}$, respectively. In the above, the charged particles α have been grouped together to form atoms and molecules ξ, and the approximation that the nuclei are fixed in space relative to the freely moving electrons has been legitimately assumed in the knowledge of the optical processes studied in the ensuing chapters. Therefore, the dynamical variables of the particle-system are the electron coordinates and momenta. This simplification is known as the Born-Oppenheimer approximation, and is frequently employed in molecular physics. However, it is to be stressed that for many situations nuclear motions cannot be ignored, such as vibrational and rotational motion, or the dynamics of chemical reactions.

The magnetisation field $\mathbf{m}(\boldsymbol{r})$ is related to the current density $\boldsymbol{j}(\boldsymbol{r})$, which is given by

$$\boldsymbol{j}(\boldsymbol{r}) = \sum_\alpha e_\alpha \dot{\boldsymbol{q}}_{(\alpha)} \delta(\boldsymbol{r} - \boldsymbol{q}_\alpha). \tag{1.13.3}$$

The current density in a system of neutral atoms or molecules at rest can be partitioned into electric and magnetic polarisation terms, as

$$j(r) = \frac{\mathrm{d}p(r)}{\mathrm{d}t} + \nabla \times \mathbf{m}(r). \tag{1.13.4}$$

Therefore, subtracting the time derivative of (1.13.2) from the current density (1.13.4) leads to the expression for the magnetisation field $\mathbf{m}(r)$ as

$$\sum_{\xi} \mathbf{m}(\xi, r) = \mathbf{m}(r) = \sum_{\alpha} e_{\alpha} \left[\left(q_{\alpha}(\xi) - R_{\xi} \right) \times \dot{q}_{\alpha} \right] \int_{0}^{1} \lambda \delta \left(r - R_{\xi} - \lambda \left(q_{\alpha}(\xi) - R_{\xi} \right) \right) d\lambda. \tag{1.13.5}$$

1.14 MULTIPOLAR LAGRANGIAN

The total Lagrangian for a matter-radiation system in the multipolar form can be written as

$$L^{\mathrm{mult}} = L^{\mathrm{mol}} + L^{\mathrm{rad}} + L^{\mathrm{int}}, \tag{1.14.1}$$

where

$$L^{\mathrm{mol}} = \sum_{\xi} \left\{ \frac{m}{2} \sum_{\alpha} \dot{q}_{\alpha}^{2}(\xi) - V(\xi) \right\}, \tag{1.14.2}$$

$$L^{\mathrm{rad}} = \frac{\varepsilon_{0}}{2} \int \left\{ \dot{a}^{2}(r) - c^{2} \left(\nabla \times a(r) \right)^{2} \right\} \mathrm{d}^{3}r, \tag{1.14.3}$$

and

$$L^{\text{int}} = \int \left(\nabla \times \mathbf{m}(\boldsymbol{r}) \right) \cdot \boldsymbol{a}(\boldsymbol{r}) \mathrm{d}^3 \boldsymbol{r} - \int \boldsymbol{p}^{\perp}(\boldsymbol{r}) \cdot \dot{\boldsymbol{a}}(\boldsymbol{r}) \mathrm{d}^3 \boldsymbol{r} - \sum_{\xi < \xi'} V_{\text{inter}}(\xi, \xi') \qquad (1.14.4)$$

The total electrostatic potential energy has been divided into a sum of one-particle and two-particle terms:

$$V = \sum_{\xi} V(\xi) + \sum_{\xi < \xi'} V(\xi, \xi'). \qquad (1.14.5)$$

Evidently, in the interaction Lagrangian the coupling of molecules to the radiation occurs through the electric and magnetisation polarisation fields - this is characteristic of the multipolar Lagrangian. It is also to be noted that the Lagrangian for the uncoupled radiation field and particles in a radiation-matter system take on the same form as their free-field and particle counterparts.

A key facet to the Lagrangian formalism is securing the result that the Euler-Lagrange equations of motion are invariant. The Euler-Lagrange equation of motion for particles is given in (1.2.1). Inserting the multipolar Lagrangian (1.14.1) into the Euler-Lagrange equation, it can be shown [11] that the expected equations of motion are secured: namely, Newton's force law with the Lorentz force terms

$$m_{\alpha} \ddot{q}_{i(\alpha)} = -\frac{\partial V}{\partial q_{i(\alpha)}} + e_{\alpha} e_i^{\perp}(\boldsymbol{q}_{\alpha}) + e_{\alpha} \left[\dot{\boldsymbol{q}}_{\alpha} \times \boldsymbol{b}(\boldsymbol{q}_{\alpha}) \right]_i. \qquad (1.14.6)$$

1.15 ATOMIC FIELD EQUATIONS

In the above, it has been highlighted that the multipolar Lagrangian gives the correct equations of motion for free particles. It is now shown that it also gives the correct Maxwell-Lorentz equations in the presence of sources [34, 38].

Due to the fact that in the multipolar formalism the bound charges form part of the medium, the fields are therefore modified by the surrounding charges. These fields are the electric displacement field d and the magnetic displacement field h, which take account of the medium locally.

There are two source-dependent Maxwell-Lorentz equations, the first of which can be written in terms of (1.13.1) as

$$\nabla \cdot e(r) = \varepsilon_0^{-1} \rho(r) = \varepsilon_0^{-1} \left[\rho^{\text{true}}(r) - \nabla \cdot p(r) \right]. \tag{1.15.1}$$

The electric displacement field $d(r)$ can be defined as

$$d(r) = \varepsilon_0 e(r) + p(r), \tag{1.15.2}$$

and therefore taking the divergence of $d(r)$ and using (1.15.1) it can be seen that the sole sources of the d field are the true charges, thus in a system with no net charge

$$\nabla \cdot d(r) = 0. \tag{1.15.3}$$

The other source-dependent Maxwell-Lorentz equation is obtained from the Euler-Lagrange equation (1.9.2) by inserting the Lagrangian density from (1.14.1)

$$\frac{\partial}{\partial t}\left(\frac{\partial \mathcal{L}}{\partial \dot{a}_i}\right) = \frac{\partial}{\partial t}\left[\varepsilon_0 \dot{a}_i(\boldsymbol{r}) - p_i^{\perp}(\boldsymbol{r})\right] = \frac{\partial}{\partial t}\left[-\varepsilon_0 e_i^{\perp}(\boldsymbol{r}) - p_i^{\perp}(\boldsymbol{r})\right] = -\frac{\partial d_i^{\perp}(\boldsymbol{r})}{\partial t}, \qquad (1.15.4)$$

$$\frac{\partial}{\partial x_j}\frac{\partial \mathcal{L}}{\partial(\partial a_i/\partial x_j)} = c^2\varepsilon_0 \nabla_j \varepsilon_{ijk}(\nabla \times \boldsymbol{a})_k$$
$$= c^2\varepsilon_0(\nabla \times \boldsymbol{b})_i, \qquad (1.15.5)$$

$$\frac{\partial \mathcal{L}}{\partial a_i} = (\nabla \times \mathbf{m}(\boldsymbol{r}))_i. \qquad (1.15.6)$$

Therefore, after substitution into of each term (1.15.4)-(1.15.6) into the Euler-Lagrange equation of motion for the radiation field

$$\nabla \times \boldsymbol{b} = \frac{1}{c^2\varepsilon_0}\left(\frac{\partial \boldsymbol{d}^{\perp}(\boldsymbol{r})}{\partial t} + \nabla \times \mathbf{m}(\boldsymbol{r})\right)$$
$$= \frac{1}{c^2}\frac{\partial \boldsymbol{e}^{\perp}(\boldsymbol{r})}{\partial t} + \frac{1}{c^2\varepsilon_0}\left(\frac{\partial \boldsymbol{p}^{\perp}(\boldsymbol{r})}{\partial t} + \nabla \times \mathbf{m}(\boldsymbol{r})\right)$$
$$= \frac{1}{c^2}\frac{\partial \boldsymbol{e}^{\perp}(\boldsymbol{r})}{\partial t} + \frac{1}{c^2\varepsilon_0}\boldsymbol{j}^{\perp}(\boldsymbol{r}), \qquad (1.15.7)$$

recovering (1.3.6), the correct equation of motion for the field. The remaining Maxwell-Lorentz equations are source-free and are automatically satisfied by the choice of gauge (Coulomb).

1.16 MULTIPOLAR HAMILTONIAN

The canonical formalism can now be applied to the multipolar Lagrangian to yield the multipolar Hamiltonian. The multipolar Hamiltonian function is therefore

$$H_{\text{mult}} = \sum_{\xi,\alpha} \boldsymbol{p}_\alpha(\xi) \cdot \dot{\boldsymbol{q}}_\alpha(\xi) + \int \boldsymbol{\varPi}(\boldsymbol{r}) \cdot \dot{\boldsymbol{a}}(\boldsymbol{r}) \, \mathrm{d}^3 \boldsymbol{r} - L_{\text{mult}}.$$
(1.16.1)

The momentum $\boldsymbol{p}_\alpha(\xi)$ is canonically conjugate to the position vector $\boldsymbol{q}_\alpha(\xi)$ and is found by

$$
\begin{aligned}
\boldsymbol{p}_\alpha(\xi) = \frac{\partial L_{\text{mult}}}{\partial \dot{\boldsymbol{q}}_\alpha(\xi)} &= m\dot{\boldsymbol{q}}_\alpha(\xi) + e\big(\boldsymbol{q}_\alpha(\xi) - \boldsymbol{R}_\xi\big) \\
&\times \iint_0^1 \lambda \delta\big(\boldsymbol{r} - \boldsymbol{R}_\xi - \lambda\big(\boldsymbol{q}_\alpha(\xi) - \boldsymbol{R}_\xi\big)\big)\mathrm{d}\lambda \times \boldsymbol{b}(\boldsymbol{r})\mathrm{d}^3\boldsymbol{r}.
\end{aligned}
$$
(1.16.2)

It is convenient to define a new vector field $\boldsymbol{n}_\alpha(\xi,\boldsymbol{r})$:

$$\boldsymbol{n}_\alpha(\xi,\boldsymbol{r}) = -e\big(\boldsymbol{q}_\alpha(\xi) - \boldsymbol{R}_\xi\big)\int_0^1 \lambda \delta\big(\boldsymbol{r} - \boldsymbol{R}_\xi - \lambda\big(\boldsymbol{q}_\alpha(\xi) - \boldsymbol{R}_\xi\big)\big)\mathrm{d}\lambda,$$
(1.16.3)

this is the same expression as that for the electric polarisation field, except for a factor λ in the integrand. As such, $\boldsymbol{n}_\alpha(\xi,\boldsymbol{r})$ is a polarisation distribution that differs from the electric polarisation field in its multipolar weightings, with the nth multipolar component weighting being reduced by $1/(n+1)$. Then, inserting $\boldsymbol{n}_\alpha(\xi,\boldsymbol{r})$ into (1.16.2) gives

$$p_\alpha(\xi) = m\dot{q}_\alpha(\xi) - \int n_\alpha(\xi, r) \times b(r) \mathrm{d}^3 r. \tag{1.16.4}$$

The momentum conjugate to the vector potential $a(r)$ is

$$\Pi(r) = \frac{\partial \mathcal{L}_{\text{mult}}}{\partial \dot{a}} = \varepsilon_0 \dot{a}(r) - p^\perp(r) = -d^\perp(r). \tag{1.16.5}$$

Rearranging (1.16.4) and (1.16.5), then substituting for $\dot{q}$ and $\dot{a}$ in (1.16.1) gives

$$H_{\text{mult}} = \frac{1}{2m} \sum_{\xi,\alpha} p_\alpha^2(\xi) + \sum_\xi V(\xi) + \frac{\varepsilon_0}{2} \int \left[\left(\frac{\Pi(r)}{\varepsilon_0} \right)^2 + c^2 b^2(r) \right] \mathrm{d}^3 r$$

$$+ \varepsilon_0^{-1} \int p^\perp(r) \cdot \Pi(r) \mathrm{d}^3 r - \int m(r) \cdot b(r) \mathrm{d}^3 r + \frac{1}{2m} \sum_{\xi,\alpha} \left[\int n_\alpha(\xi, r) \times b(r) \mathrm{d}^3 r \right]^2$$

$$+ \frac{1}{2\varepsilon_0} \int \left| p^\perp(r) \right|^2 \mathrm{d}^3 r + \sum_{\xi < \xi'} V_{\text{inter}}(\xi, \xi'), \tag{1.16.6}$$

where the magnetisation field $m(r)$ is different from $\mathbf{m}(r)$ in (1.13.5), because the kinetic and canonical momenta are now no longer equal to each other,

$$m(r) = \frac{1}{2m} \sum_{\xi,\alpha} \left(n_\alpha(\xi, r) \times p_\alpha(\xi) - p_\alpha(\xi) \times n_\alpha(\xi, r) \right). \tag{1.16.7}$$

The penultimate term of (1.16.6) is proportional to the square modulus of the transverse electric polarisation, and is composed of intra- and intermolecular terms

$$\frac{1}{2\varepsilon_0} \int \left| p^\perp(r) \right|^2 \mathrm{d}^3 r = \frac{1}{2\varepsilon_0} \int \sum_\xi \left| p^\perp(\xi, r) \right|^2 \mathrm{d}^3 r + \frac{1}{2\varepsilon_0} \int \sum_{\xi < \xi'} p^\perp(\xi, r) \cdot p^\perp(\xi', r) \mathrm{d}^3 r. \tag{1.16.8}$$

Noting that the total polarised vector field is composed of both transverse and longitudinal components $\boldsymbol{p}(\boldsymbol{r}) = \boldsymbol{p}^{\perp}(\boldsymbol{r}) + \boldsymbol{p}^{\parallel}(\boldsymbol{r})$ and is strongly localised in the region of molecules, meaning that the total *intermolecular* polarisation product vanishes for non-overlapping charge distributions (i.e. $\xi < \xi'$)

$$\frac{1}{2\varepsilon_0}\int\sum_{\xi<\xi'}\boldsymbol{p}^{\perp}(\xi,\boldsymbol{r})\cdot\boldsymbol{p}^{\perp}(\xi',\boldsymbol{r})\,\mathrm{d}^3\boldsymbol{r} = -\frac{1}{2\varepsilon_0}\int\sum_{\xi<\xi'}\boldsymbol{p}^{\parallel}(\xi,\boldsymbol{r})\cdot\boldsymbol{p}^{\parallel}(\xi',\boldsymbol{r})\,\mathrm{d}^3\boldsymbol{r}. \tag{1.16.9}$$

Though arduous, the right hand side of (1.16.9) can be shown to be equal to the final term of (1.16.6) $\sum_{\xi<\xi'}V_{\text{inter}}(\xi,\xi')$ and as such, in the multipolar Hamiltonian, the intermolecular Coulomb interaction potential is cancelled by the intermolecular transverse electric polarisation [11], leaving an intramolecular self-energy term, which leaves the Hamiltonian in the form of

$$H^{\text{mult}} = H_{\text{mol}}^{\text{mult}} + H_{\text{rad}}^{\text{mult}} + H_{\text{int}}^{\text{mult}} + \frac{1}{2\varepsilon_0}\int\sum_{\xi}\left|\boldsymbol{p}^{\perp}(\xi,\boldsymbol{r})\right|^2\mathrm{d}^3\boldsymbol{r}, \tag{1.16.10}$$

where

$$H_{\text{mol}}^{\text{mult}} = \frac{1}{2m}\sum_{\xi,\alpha}\boldsymbol{p}_{\alpha}^2(\xi) + \sum_{\xi}V(\xi), \tag{1.16.11}$$

$$H_{\text{rad}}^{\text{mult}} = \frac{\varepsilon_0}{2}\int\left[\left(\frac{\boldsymbol{\Pi}(\boldsymbol{r})}{\varepsilon_0}\right)^2 + c^2\boldsymbol{b}^2(\boldsymbol{r})\right]\mathrm{d}^3\boldsymbol{r} = \frac{1}{2\varepsilon_0}\int\left[\boldsymbol{d}^{\perp 2}(\boldsymbol{r}) + \varepsilon_0^2 c^2\boldsymbol{b}^2(\boldsymbol{r})\right]\mathrm{d}^3\boldsymbol{r}, \tag{1.16.12}$$

and

$$H_{\text{int}}^{\text{mult}} = \varepsilon_0^{-1} \int \boldsymbol{p}^{\perp}(\boldsymbol{r}) \cdot \boldsymbol{\Pi}(\boldsymbol{r}) \mathrm{d}^3\boldsymbol{r} - \int \boldsymbol{m}(\boldsymbol{r}) \cdot \boldsymbol{b}(\boldsymbol{r}) \mathrm{d}^3\boldsymbol{r} + \frac{1}{2m} \sum_{\xi,\alpha} \left[\int \boldsymbol{n}_\alpha(\xi,\boldsymbol{r}) \times \boldsymbol{b}(\boldsymbol{r}) \mathrm{d}^3\boldsymbol{r} \right]^2$$

$$= -\varepsilon_0^{-1} \int \boldsymbol{p}(\boldsymbol{r}) \cdot \boldsymbol{d}^{\perp}(\boldsymbol{r}) \mathrm{d}^3\boldsymbol{r} - \int \boldsymbol{m}(\boldsymbol{r}) \cdot \boldsymbol{b}(\boldsymbol{r}) \mathrm{d}^3\boldsymbol{r}$$

$$+ \frac{1}{2} \int O_{ij}(\boldsymbol{r},\boldsymbol{r}') b_i(\boldsymbol{r}) b_j(\boldsymbol{r}') \mathrm{d}^3\boldsymbol{r} \, \mathrm{d}^3\boldsymbol{r}'. \tag{1.16.13}$$

The final term of (1.16.10) is, as mentioned above, the intramolecular self-energy term and it is independent of the radiation field and therefore does not contribute to processes that involve changes in the state of the radiation field. The final term of (1.16.13) represents the diamagnetic interaction, and the diamagnetisation field $O_{ij}(\boldsymbol{r},\boldsymbol{r}')$ is given by

$$O_{ij}(\boldsymbol{r},\boldsymbol{r}') = \sum_{\xi,\xi'} \frac{1}{m} \varepsilon_{ikl} \varepsilon_{jml} n_k(\xi,\boldsymbol{r}) n_m(\xi',\boldsymbol{r}')$$

$$= \frac{e^2}{m} \varepsilon_{ikl} \varepsilon_{jml} \sum_{\xi,\xi'} \sum_{\alpha,\beta} \left(\boldsymbol{q}_\alpha(\xi) - \boldsymbol{R}_\xi \right)_k \left(\boldsymbol{q}_\alpha(\xi') - \boldsymbol{R}_{\xi'} \right)_m$$

$$\times \int_0^1 \int_0^1 \lambda\lambda' \delta\left(\boldsymbol{r} - \boldsymbol{R}_\xi - \lambda\left(\boldsymbol{q}_\alpha(\xi) - \boldsymbol{R}_\xi \right) \right)$$

$$\times \delta\left(\boldsymbol{r}' - \boldsymbol{R}_{\xi'}' - \lambda'\left(\boldsymbol{q}_\beta(\xi') - \boldsymbol{R}_{\xi'}' \right) \right) \mathrm{d}\lambda\mathrm{d}\lambda'. \tag{1.16.14}$$

Some interesting features of the multipolar Hamiltonian (1.16.13) include its dependence on the transverse electromagnetic fields $\boldsymbol{d}^{\perp}$ and $\boldsymbol{b}$, rather than the electromagnetic potentials. This has the distinct advantage of making the multipolar Hamiltonian independent of the gauge chosen. There is no electrostatic intermolecular interaction term, and molecules couple directly to the radiation fields through the electric polarisation, magnetisation, and diamagnetisation fields. Therefore, interactions between molecules are mediated by the field via the exchange of transverse photons which propagate with speed c in a vacuum. This leads to the multipolar Hamiltonian giving fully-retarded results, as required by causality.

Expanding the interaction Hamiltonian into specific multipole moments puts it in a more convenient form for subsequent application throughout the thesis, using (1.13.2), (1.13.5), and (1.16.14) the first few terms are

$$
H_{\text{int}}^{\text{mult}} = \sum_{\xi} \left[-\varepsilon_0^{-1} \boldsymbol{\mu}(\xi) \cdot \boldsymbol{d}^{\perp}\left(\boldsymbol{R}_{\xi}\right) - \varepsilon_0^{-1} Q_{ij}(\xi) \nabla_j d_i^{\perp}\left(\boldsymbol{R}_{\xi}\right) - \boldsymbol{m}(\xi) \cdot \boldsymbol{b}\left(\boldsymbol{R}_{\xi}\right) \right]
$$
$$
+ \frac{e^2}{8m} \sum_{\xi,\alpha} \left[\left(\boldsymbol{q}_{\alpha}(\xi) - \boldsymbol{R}_{\xi}\right) \times \boldsymbol{b}\left(R_{\xi}\right) \right]^2 + ..., \tag{1.16.15}
$$

where $\boldsymbol{\mu}(\xi)$, $Q_{ij}(\xi)$, $\boldsymbol{m}(\xi)$ are the electric dipole, electric quadrupole and magnetic dipole moments of molecule ξ, respectively; the final term in (1.16.15) is lowest order diamagnetic coupling interaction. Retention of just the first term that involves the electric dipole moment constitutes the electric dipole approximation, well-known throughout optical and molecular physics. As will be seen, however, inclusion of the higher-order terms is necessary for certain optical processes.

1.17 PERTURBATION THEORY

Exact analytic solutions to the Schrödinger equation exist for only an extremely limited set of simple physical situations. However, a plethora of techniques of approximation is available. One such method, perturbation theory [2, 39], naturally lends itself to QED calculations as the radiation-molecule couplings are weak in comparison to the Coulomb forces present within atoms and molecules. Although time-independent perturbation theory provides adequate results in specific cases, nearly all perturbations are time-dependent and in the specific case of molecules interacting with electromagnetic fields that oscillate indefinitely, time-dependent perturbation theory is essential. The dynamics are therefore governed by the time-dependent Schrödinger equation

$$i\hbar \frac{\partial}{\partial t}\left|\Psi\left(t\right)\right\rangle = H\left|\Psi\left(t\right)\right\rangle, \qquad (1.17.1)$$

where $\left|\Psi\left(t\right)\right\rangle$ represents the state of the total system. Inspection of the Hamiltonian (1.16.10), where we can neglect the final term which represents self-energy corrections, highlights the fact we can use the first two terms as a basis for solving the full Hamiltonian: secular perturbation theory.

$$H = H_0 + H_{\text{int}}, \qquad (1.17.2)$$

where $H_0 = H_{\text{mol}} + H_{\text{rad}}$ is the unperturbed Hamiltonian. This is a satisfactory partition because the intramolecular binding energies in molecules are much larger than the interaction between the field and a molecule – which H_{int} represents. Only for extremely intense radiation fields does the perturbation theory breakdown, and other methods are sought. Importantly, H_{int} contains all the time-dependence of the overall Hamiltonian, and it can cause transitions that are real or virtual between the states of H_0. The eigenstates of H_0 are written as the product of both the molecule and radiation field - $\left|E_m\left(\xi\right)\right\rangle\left|n\left(\boldsymbol{k},\eta\right)\right\rangle$ - corresponding to a molecule ξ in the electronic state E_m, and the electromagnetic field in a mode $\left(\boldsymbol{k},\eta\right)$ that is occupied by n photons.

Expressing the time variation of the state function from (1.17.1) in terms of the unitary time evolution operator gives

$$\left|\Psi\left(t\right)\right\rangle = U\left(t,t_0\right)\left|\Psi\left(t_0\right)\right\rangle. \qquad (1.17.3)$$

$U\left(t,t_0\right)$ acts on the state at t_0 to give the state at time t, enabling (1.17.3) to be determined at any time. When the system is in the initial state $\left|\Psi\left(t_0\right)\right\rangle$ and there is no coupling between

the radiation field and the molecule through H_{int}, the perturbation is zero and the evolution operator can be written as $e^{-iH_0(t-t_0)/\hbar}$. Removing this term from (1.17.3) gives

$$\left|\Psi(t)\right\rangle = e^{-iH_0(t-t_0)/\hbar}\, U_I\left(t,t_0\right)\left|\Psi(t_0)\right\rangle \tag{1.17.4}$$

which allows the evolution operator, now in the interaction picture, to be interpreted as giving a modification to the time evolution of the system state due to the interaction. Operating on both sides of (1.17.4) with $i\hbar\dfrac{\partial}{\partial t}$ and using the product rule gives

$$i\hbar\frac{\partial}{\partial t}\left|\Psi(t)\right\rangle = H_0\, e^{-iH_0(t-t_0)/\hbar}\, U_I\left(t,t_0\right)\left|\Psi(t_0)\right\rangle + i\hbar e^{-iH_0(t-t_0)/\hbar}\frac{\partial}{\partial t}U_I\left(t,t_0\right)\left|\Psi(t_0)\right\rangle. \tag{1.17.5}$$

Evidently

$$H\left|\Psi(t)\right\rangle = \left(H_0 + H_{\text{int}}\right)e^{-iH_0(t-t_0)/\hbar}\, U_I\left(t,t_0\right)\left|\Psi(t_0)\right\rangle, \tag{1.17.6}$$

and therefore equating (1.17.5) and (1.17.6) (i.e. producing the time-dependent Schrödinger equation (1.17.1)) then operating on both sides by $e^{-iH_0(t-t_0)/\hbar}$ eventually leads to the operator equation

$$i\hbar\frac{\partial}{\partial t}U_I\left(t,t_0\right) = H_{\text{int}}^{I}\left(t\right)U_I\left(t,t_0\right), \tag{1.17.7}$$

where

$$H_{\text{int}}^{I}(t) = e^{iH_0(t-t_0)/\hbar} \, H_{\text{int}} \, e^{-iH_0(t-t_0)/\hbar}.$$ (1.17.8)

Evaluating the time evolution of the system reduces to solving (1.17.7) for $U_I(t,t_0)$. Integration of (1.17.7), subject to the initial condition $U_I(t_0,t_0)=1$, gives

$$U_I(t,t_0) = 1 + \left(\frac{1}{i\hbar}\right)\int_{t_0}^{t} H_{\text{int}}^{I}(t_1)U_I(t_1,t_0)\,dt_1.$$ (1.17.9)

The right-hand side of (1.17.9) can be continuously reinserted as an expression for $U_I(t,t_0)$ and successively performing this iteration leads to an infinite power series solution

$$U_I(t,t_0) = 1 + \sum_{n=1}^{\infty}\left(\frac{1}{i\hbar}\right)^{n}\int_{t_0}^{t}dt_1\int_{t_0}^{t_1}dt_2...\int_{t_0}^{t_n-1}dt_n H_{\text{int}}^{I}(t_1)...H_{\text{int}}^{I}(t_n).$$ (1.17.10)

The power series (1.17.10) can now be used to calculate the quantum amplitude for the transition from the initial state at time t_0 to the final state at time t, due to the perturbation from H_{int}^{I}. Ignoring the constant of integration in (1.17.10) as it only leads to trivial process whereby there is no perturbation and no interaction between the radiation and matter, gives the matrix elements for the time evolution operator as

$$\langle f|U_I(t,t_0)|i\rangle = -\sum_{\xi}M_{fi}(\xi)\frac{e^{i(E_f-E_i)(t-t_0)/\hbar}-1}{E_f-E_i}.$$ (1.17.11)

By using the completeness relation, the matrix element M_{fi} can be expanded in powers of the perturbation operator

$$M_{fi}(\xi) = \langle f|H_{int}(\xi)|i\rangle + \sum_I \frac{\langle f|H_{int}(\xi)|I\rangle\langle I|H_{int}(\xi)|i\rangle}{E_i - E_I}$$

$$+ \sum_{I,II} \frac{\langle f|H_{int}(\xi)|II\rangle\langle II|H_{int}(\xi)|I\rangle\langle I|H_{int}(\xi)|i\rangle}{(E_i - E_I)(E_i - E_{II})}$$

$$+ \sum_{I,II,III} \frac{\langle f|H_{int}(\xi)|III\rangle\langle III|H_{int}(\xi)|II\rangle\langle II|H_{int}(\xi)|I\rangle\langle I|H_{int}(\xi)|i\rangle}{(E_i - E_I)(E_i - E_{II})(E_i - E_{III})} + ... \qquad (1.17.12)$$

The Born interpretation allows the time-dependent probability of the $f \leftarrow i$ transition to be given as

$$P_{f\leftarrow i}(t) = \left|\langle f|U_I(t,t_0)|i\rangle\right|^2$$

$$= \sum_\xi 4|M_{fi}(\xi)|^2 \frac{\sin^2 \omega_{fi}(t-t_0)/2}{\hbar^2 \omega_{fi}^2}, \qquad (1.17.13)$$

where $\hbar\omega_{fi} = E_f - E_i$. Many optical processes involve transitions taking place between states which may lay within a continuous spectrum. In all such optical processes, the transition probabilities must be summed over the continuous range of states

$$P_{tot}(t) = \sum_f P_{f\leftarrow i}(t)$$

$$\sum_\xi \frac{2\pi}{\hbar}|M_{fi}(\xi)|^2 (t-t_0)\rho_f, \qquad (1.17.14)$$

where $\rho_f = dn_f/dE_f$ is the number of levels per unit energy, or more commonly known as the density of final states. Finally, we can study how (1.17.14) changes with time, producing the famous Fermi golden rate rule

$$\frac{d}{dt}\sum_\xi \frac{2\pi}{\hbar}|M_{fi}(\xi)|^2 (t-t_0)\rho_f = \sum_\xi \frac{2\pi}{\hbar}|M_{fi}(\xi)|^2 \rho_f = \Gamma. \qquad (1.17.15)$$

Within this thesis we will be looking at optical processes and phenomena. In optical processes, the initial and final states of the radiation and/or matter components are not identical. A description of these processes requires the time-dependent approach outlined above, and therefore a rate calculation ensues. This is because the perturbation gives rise to transitions between the unperturbed eigenstates of H_0. For certain optical phenomena, however, both the initial and final state of the total system is identical, and the perturbation is time-independent, causing shifts of the eigenvalues of H_0. In this case, a calculation of the matrix element alone is needed, and it corresponds to the energy shift for the phenomena:

$$\Delta E = E_i^{(0)} + \left\langle f \left| H_{\text{int}} \right| i \right\rangle + \sum_I \frac{\left\langle f \left| H_{\text{int}} \right| I \right\rangle \left\langle I \left| H_{\text{int}} \right| i \right\rangle}{E_i - E_I} + ..., \qquad \left| i \right\rangle = \left| f \right\rangle. \qquad (1.17.16)$$

The evaluation of optical rates and energy shifts using the expansions (1.17.12) and (1.17.16) is most easily carried out with the aid of diagrammatic techniques. The most routinely employed are the time-ordered diagrams introduced by Feynman [40]. These simple graphs reduce the complexity of mathematical calculations, but more importantly offer a valuable insight into the underlying physical process through presenting all the possible time-ordered sequences of photon creation and annihilation events. Through this summation over all possible sequences of photon events, a summation over all intermediate states that link the initial and final states of the system is achieved. A main facet in the success of QED theory is its extremely precise theoretical calculations to match experiment; however it is the opinion of the author that the true power of QED is through its ability to predict new electrodynamical phenomena, the origin of this being the use of time-ordered Feynman diagrams. Other diagrammatic techniques are available, such as the state sequence method [41]. In this body of work, however, we will be primarily utilising Feynman's method.

REFERENCES

[1]   R. P. Feynman, *QED : The Strange Theory of Light and Matter* (Princeton University Press, Princeton, N.J., 1985).

[2]   G. Grynberg, A. Aspect, and C. Fabre, *Introduction to Quantum Optics: From the Semi-Classical Approach to Quantized Light* (Cambridge University Press, Cambridge, 2010).

[3]   M. Born, W. Heisenberg, and P. Jordan, *Zur Quantenmechanik. II*, Zeitschrift für Physik **35**, 557 (1926).

[4]   P. A. M. Dirac, *The quantum theory of the emission and absorption of radiation*, Proc. R. Soc. A **114**, 243 (1927).

[5]   J. Schwinger, *Selected Papers on Quantum Electrodynamics* (Dover, New York, 1958).

[6]   E. A. Power, *Introductory Quantum Electrodynamics* (American Elsevier Pub. Co., New York, 1965).

[7]   R. Woolley, *Molecular quantum electrodynamics*, Proc. R. Soc. A **321**, 557 (1971).

[8]   R. Woolley, *The electrodynamics of atoms and molecules*, Adv. Chem. Phys **33**, 153 (1975).

[9]   W. Healy, *Non-relativistic Quantum Electrodynamics* (Academic Press Inc. London, 1982).

[10]   C. Cohen-Tannoudji, J. Dupont-Roc, and G. Grynberg, *Photons and Atoms: Introduction to Quantum Electrodynamics* (Wiley, New York, 1989).

[11]   D. P. Craig and T. Thirunamachandran, *Molecular Quantum Electrodynamics: An Introduction to Radiation-Molecule Interactions* (Dover Publications, Mineola, NY, 1998).

[12]   A. Salam, *Molecular Quantum Electrodynamics. Long-Range Intermolecular Interactions* (Wiley, Hoboken, NJ, 2010).

[13]   H. B. G. Casimir and D. Polder, *The influence of retardation on the London-van der Waals forces*, Phys. Rev. **73**, 360 (1948).

[14]   P. W. Milonni, *The Quantum Vacuum: An Introduction to Quantum Electrodynamics* (Academic Press, San Diego, 1993).

[15] S. Mukamel, *Principles of Nonlinear Optical Spectroscopy* (Oxford University Press, New York, 1995).

[16] D. L. Andrews and P. Allcock, *Optical Harmonics in Molecular Systems* (Wiley-VCH, Weinheim, 2002).

[17] D. L. Andrews and A. A. Demidov, *Resonance Energy Transfer* (Wiley, Chichester, 1999).

[18] G. J. Daniels, R. D. Jenkins, D. S. Bradshaw, and D. L. Andrews, *Resonance energy transfer: The unified theory revisited*, J. Chem. Phys. **119**, 2264 (2003).

[19] L. C. Dávila Romero, D. L. Andrews, and M. Babiker, *A quantum electrodynamics framework for the nonlinear optics of twisted beams*, J. Opt. B: Quantum Semiclass. Opt. **4**, S66 (2002).

[20] P. W. Atkins and L. D. Barron, *Quantum field theory of optical birefringence phenomena. I. Linear and nonlinear optical rotation*, Proc. R. Soc. A **304**, 303 (1968).

[21] E. A. Power and T. Thirunamachandran, *Circular dichroism: A general theory based on quantum electrodynamics*, J. Chem. Phys. **60**, 3695 (1974).

[22] D. L. Andrews and T. Thirunamachandran, *A quantum electrodynamical theory of differential scattering based on a model with two chromophores. I. Differential Rayleigh-scattering of circularly polarized-light*, Proc. R. Soc. A **358**, 297 (1978).

[23] D. L. Andrews and T. Thirunamachandran, *A quantum electrodynamical theory of differential scattering based on a model with two chromophores. II. Differential Raman-scattering of circularly polarized-light*, Proc. R. Soc. A **358**, 311 (1978).

[24] E. A. Power and T. Thirunamachandran, *Quantum electrodynamics with nonrelativistic sources. I. Transformation to the multipolar formalism for second-quantized electron and Maxwell interacting fields*, Phys. Rev. A **28**, 2649 (1983).

[25] E. A. Power and T. Thirunamachandran, *Quantum electrodynamics with nonrelativistic sources. II. Maxwell fields in the vicinity of a molecule*, Phys. Rev. A **28**, 2663 (1983).

[26] A. Salam, *Molecular quantum electrodynamics in the Heisenberg picture: A field theoretic viewpoint*, Int. Rev. Phys. Chem. **27**, 405 (2008).

[27] A. Zangwill, *Modern Electrodynamics* (Cambridge University Press, Cambridge, U.K., 2013).

[28] L. Rayleigh, *Remarks upon the law of complete radiation*, The London, Edinburgh, and Dublin Philosophical Magazine and Journal of Science **49**, 539 (1900).

[29] W. Heitler, *The Quantum Theory of Radiation* (Dover, Mineola, New York, 1954).

[30] R. Loudon, *The Quantum Theory of Light* (Oxford University Press, Oxford, 2000).

[31] M. Williams, D. Bradshaw, and D. Andrews, *Quantum issues with structured light*, Complex Light and Optical Forces X, 976407 (2016).

[32] M. Göppert-Mayer, *Über elementarakte mit zwei quantensprüngen*, Ann. Phys. (Berlin) **401**, 273 (1931).

[33] E. A. Power and S. Zienau, *Coulomb gauge in non-relativistic quantum electrodynamics and the shape of spectral lines*, Philos. Trans. R. Soc. A **251**, 427 (1959).

[34] M. Babiker, E. Power, and T. Thirunamachandran, *On a generalization of the Power-Zienau-Woolley transformation in quantum electrodynamics and atomic field equations*, Proc. R. Soc. Lond A: Math. Phys. Eng. Sci. **338**, 235 (1974).

[35] E. A. Power and T. Thirunamachandran, *On the nature of Hamiltonian for interaction of radiation with atoms and molecules: (e/mc)p.A, -µ.E, and all that*, Am. J. Phys. **46**, 370 (1978).

[36] E. A. Power and T. Thirunamachandran, *The multipolar Hamiltonian in radiation theory*, Proc. R. Soc. A **372**, 265 (1980).

[37] E. A. Power and T. Thirunamachandran, *A note on the derivation of the multipolar Hamiltonian*, Phys. Lett. A **87**, 449 (1982).

[38] M. Babiker, E. Power, and T. Thirunamachandran, in Proceedings of the Royal Society of London A: Mathematical, Physical and Engineering Sciences (The Royal Society, 1973), pp. 187.

[39] J. J. Sakurai and J. J. Napolitano, *Modern quantum mechanics* (Pearson Higher Ed, 2014).

[40] R. P. Feynman, *Space-time approach to quantum electrodynamics*, Phys. Rev. **76**, 769 (1949).

[41] R. D. Jenkins, D. L. Andrews, and L. C. Dávila Romero, *A new diagrammatic methodology for non-relativistic quantum electrodynamics*, J. Phys. B: At. Mol. Opt. Phys. **35**, 445 (2002).

2

QUANTUM DELOCALISATION IN NONLINEAR OPTICS

## 2.1   INTRODUCTION

Within the well-established restraints of quantum uncertainty, it is generally assumed that the spatial extent of multiphoton annihilation or creation events in nonlinear optics is small. That is to say, photons are created and destroyed at distinct optical centres - molecules, for example. Of course, the exact location of these photon events can never be inferred by a direct experimental observation, but in nonlinear optical processes the annihilation and creation of photons are assumed to be collocated. For example, in any given generation of an nth-harmonic, n photons are annihilated at a single optical centre, and the corresponding output harmonic is emitted from the same centre [1, 2] – the process can be termed 'localised' with regards to the annihilated input and the corresponding emitted output photons.

In QED theory, it is well established that intermolecular coupling occurs through the process of virtual photon propagation [3, 4]. Well-known examples include the Casimir-Polder potential, laser-induced intermolecular interactions [5], and resonance energy transfer [6]. Virtual photons are manifestations of the quantum vacuum, where the vacuum fluctuations associated with the non-commuting electric and magnetic fields account for a non-vanishing electromagnetic field energy.

In this chapter, by duly accounting for the possibility of virtual photon propagation in the nonlinear optical processes of spontaneous parametric down-conversion (SPDC) [7, 8] and second harmonic generation (SHG), it emerges that photon annihilation and creation events need not necessarily occur in a localised fashion as described above. Through a fifth-order

nonlocal electric-dipole response, a rate for a delocalised mechanism of producing down-converted photons pairs and the generation of optical harmonics is secured. The derivation will concentrate on the process of SPDC, whereby each down-converted photon that constitutes the correlated photon pair are emitted from spatially distinct and separated points in space, schematically shown in Figure 2.1. The results secured are general in the sense that they are readily applicable to the time-inverse process of SPDC, namely SHG. In the delocalised mechanism for SHG, the two input photons that form the harmonic are annihilated at two completely distinct points in space.
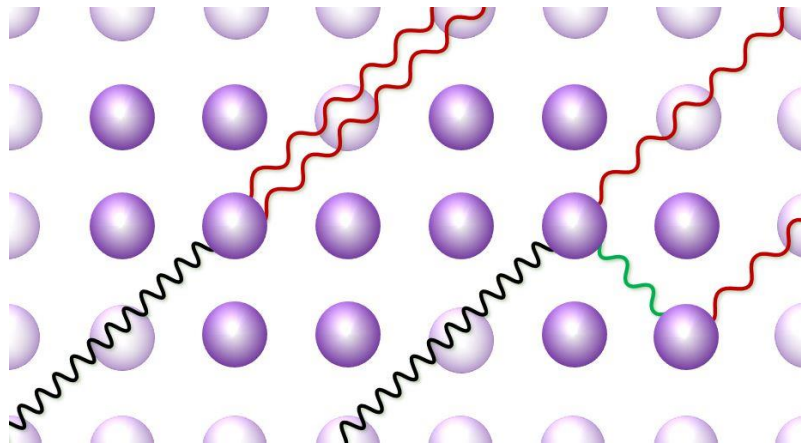
Figure 2.1 Array of optical centres (purple spheres): single-centred mechanism for SPDC on the left; delocalised mechanism for SPDC on the right. Green wavy line represents virtual photon propagation.

First, the localised mechanism of SPDC is studied, followed by the development of the theory for nonlocalised generation of down-converted photon pairs. Then, by combining both the localised and delocalised contributions to the overall rate of SPDC, the result is quantitatively analysed using a numerical lattice simulation to give an indicative figure for how much the delocalised mechanism contributes to the overall rate, and to gauge whether the possibility of observing the nonlocal effect is a legitimate endeavour.

2.2   MEDIA CORRECTIONS

In the development of QED theory outlined in Chapter 1, no mention was made of the dynamical influence that the surrounding media may have on any given interaction between the radiation field and a single, distinct optical centre or molecule. In the condensed phase, the electronic influence of surrounding molecules and atoms on the fields experienced and produced by the active optical centre need to be taken account of for a fully-correct description of the optical process. In QED, such media corrections are accounted for within the electric displacement field operator $d^{\perp}(r)$. Through a rather involved analysis [9-12], where the propagation and interaction of quantised radiation is described in terms of *polaritons*, the modified auxiliary field operator, $d^{\perp}(r)$, takes the form of

$$d^{\perp}(r) = i\sum_{k,\eta,m}\left(\frac{\hbar\varepsilon_0 v_g^{(m)}\omega_k^{(m)}}{2cVn\left(\omega_k^{(m)}\right)}\right)^{\frac{1}{2}}\left(\frac{n\left(\omega_k^m\right)+2}{3}\right)\left[e_k^{(\eta)}P_{k,m}^{(\eta)}e^{ik\cdot r}-\bar{e}_k^{(\eta)}P_{k,m}^{\dagger(\eta)}e^{-ik\cdot r}\right], \qquad (2.2.1)$$

where $n\left(\omega_k^{(m)}\right)$ is the complex, frequency-dependent refractive index for the polariton frequency $\omega_k^{(m)}$; $v_g^{(m)}$ is the group velocity; $P_{k,m}^{(\eta)}$ and $P_{k,m}^{\dagger(\eta)}$ are polariton annihilation and creation operators, respectively.

In all the applications of QED in this thesis, and in general throughout quantum and nonlinear optics, it is only the photon-like polaritons that are of interest. As such, the *m* index in Equation (2.2.1), which labels the branches of polariton dispersion, is implicit. This also means that is it the standard vacuum annihilation and creation operators that are to be used (Equations (1.11.17) and (1.11.18)), rather than $P_{k,m}^{(\eta)}$ and $P_{k,m}^{\dagger(\eta)}$, respectively.

In this chapter, the correct Lorentz local-field factors and complex refractive index will be explicitly accounted for where appropriate. This is to give the analysis of the result a firmer grounding if one is to make physical predictions of a quantitative nature. However, the remaining chapters in the thesis will assume these media corrections implicit in order to

simplify the ensuing calculations and results. This does not alter any of the physics presented as all the work is based on the photon interactions, and the addition of media effects are easily accounted for.

2.3   LOCALISED SPDC

In the photonic formulation of QED, the nonlinear optical process of SPDC occurs through the annihilation of a single pump photon possessing a wave vector $\boldsymbol{k}$ and the creation of two output photons with a wave vector $\boldsymbol{k'}$, where $\boldsymbol{k} = 2\boldsymbol{k'}$. Therefore, this elastic process fulfils wave vector matching and the output is coherent. The output photons in this process are termed 'correlated photon pairs' due to the fact their polarisations are entangled quantum states [13, 14].

As is standard, the input photon annihilation and the creation of the two output photons are assumed to occur at a single optical centre or molecule. That is to say, the positional range of the location for the emission of the two down-converted photons (and input photon annihilation) is small. Therefore, the SPDC photonic mechanism occurs in a localised fashion, with the output emitted in a collocated fashion, and only the usual constraints of quantum uncertainty put a limit on the precision with which the location of the SPDC process can be said to occur.

The three topologically distinct Feynman time-ordered diagrams that represent localised SPDC are shown in Figure 2.3.1-2.3.3. The initial state of the total matter-radiation system is $|i\rangle = \left|E_i^{\mathrm{A}}\right\rangle \left|q(\eta, \boldsymbol{k})\right\rangle \left|0(\eta', \boldsymbol{k'})\right\rangle$, where we have labelled the single interacting optical centre of interest within the nonlinear optical medium, 'A'; the final state of the system is $|f\rangle = \left|E_f^{\mathrm{A}}\right\rangle \left|q-1(\eta, \boldsymbol{k})\right\rangle \left|2(\eta', \boldsymbol{k'})\right\rangle$. Both the initial and final states of the material system are ground states $|0\rangle$. The interaction is third-order in H_{int} and therefore within the electric dipole approximation the matrix element is seen to be

$$
\begin{aligned}
M_{fi}^{\mathrm{A}} = \sum_{s,r} \frac{1}{\left(E_0 - E_s\right)\left(E_0 - E_r\right)} &\Big[\big\langle 0\big| -\varepsilon_0^{-1}\mu_i(\mathrm{A})d_i^{\perp}(\boldsymbol{r}_{\mathrm{A}})\big| s\big\rangle \\
&\times \big\langle s\big| -\varepsilon_0^{-1}\mu_i(\mathrm{A})d_i^{\perp}(\boldsymbol{r}_{\mathrm{A}})\big| r\big\rangle \big\langle r\big| -\varepsilon_0^{-1}\mu_i(\mathrm{A})d_i^{\perp}(\boldsymbol{r}_{\mathrm{A}})\big| 0\big\rangle\Big],
\end{aligned}
\tag{2.3.1}
$$

where we use the modified transverse electric displacement operator defined by (2.2.1), and r and s represent virtual intermediate states that link the final and initial states of the system.

The photon annihilation and creation operations in (2.3.1) when carried out on radiation modes occupied by q photons gives the following

$$
\begin{aligned}
&\big\langle 2(\eta',\boldsymbol{k}');q-1(\eta,\boldsymbol{k})\big| a^{\dagger}(\eta',\boldsymbol{k}')a^{\dagger}(\eta',\boldsymbol{k}')a(\eta,\boldsymbol{k})\big| q(\eta,\boldsymbol{k});0(\eta',\boldsymbol{k}')\big\rangle \\
&= \sqrt{q}\,\big\langle 2(\eta',\boldsymbol{k}');q-1(\eta,\boldsymbol{k})\big| a^{\dagger}(\eta',\boldsymbol{k}')a^{\dagger}(\eta',\boldsymbol{k}')\big| q-1(\eta,\boldsymbol{k});0(\eta',\boldsymbol{k}')\big\rangle \\
&= \sqrt{q}\sqrt{1}\,\big\langle 2(\eta',\boldsymbol{k}');q-1(\eta,\boldsymbol{k})\big| a^{\dagger}(\eta',\boldsymbol{k}')\big| q-1(\eta,\boldsymbol{k});1(\eta',\boldsymbol{k}')\big\rangle \\
&= \sqrt{q}\sqrt{1}\sqrt{2}\,\big\langle 2(\eta',\boldsymbol{k}');q-1(\eta,\boldsymbol{k})\big| q-1(\eta,\boldsymbol{k});2(\eta',\boldsymbol{k}')\big\rangle \\
&= \sqrt{q}\sqrt{2}.
\end{aligned}
\tag{2.3.2}
$$

The remainder of the quantum amplitude can then be calculated with the aid of the three Feynman graphs in Figure 2.3.1-2.3.3 to give

$$
\begin{aligned}
M_{\mathrm{A}} = -\frac{i^3}{\varepsilon_0^3}\sum_{\boldsymbol{k}',\eta'} \sqrt{q}\sqrt{2} &\left(\frac{\hbar\varepsilon_0 v_g ck}{2cVn(\omega_k)}\right)^{1/2}\left(\frac{\hbar\varepsilon_0 v_g' ck'}{2cVn(\omega_{k'})}\right) \\
&\times \left(\frac{n^2(\omega_k)+2}{3}\right)\left(\frac{n^2(\omega_{k'})+2}{3}\right)^2 e_i^{(\eta)}(\boldsymbol{k})\bar{e}_j^{(\eta')}(\boldsymbol{k}')\bar{e}_k^{(\eta')}(\boldsymbol{k}') \\
&\times \sum_{r,s}\left[\frac{\mu_i^{0r}\mu_j^{rs}\mu_k^{s0}}{\left(E_{s0}-\hbar ck'\right)\left(E_{r0}-2\hbar ck'\right)} + \frac{\mu_j^{0r}\mu_i^{rs}\mu_k^{s0}}{\left(E_{s0}-\hbar ck'\right)\left(E_{r0}+\hbar ck'\right)}\right. \\
&\left.+ \frac{\mu_j^{0r}\mu_k^{rs}\mu_i^{s0}}{\left(E_{s0}+2\hbar ck'\right)\left(E_{r0}+\hbar ck'\right)}\right]e^{i(\boldsymbol{k}-2\boldsymbol{k}')\cdot\boldsymbol{r}_{\mathrm{A}}},
\end{aligned}
\tag{2.3.3}
$$

where the three terms in square brackets correspond to the three time-orderings in Figure 2.3.1-2.3.3. In (2.3.3), there is an implied summation over subscript component indices. This Einstein summation convention is a notation that is implicit throughout the rest of this thesis. In the denominators in (2.3.3), terms of the form E_{r0} signify $E_{r0} = E_r - E_0$.
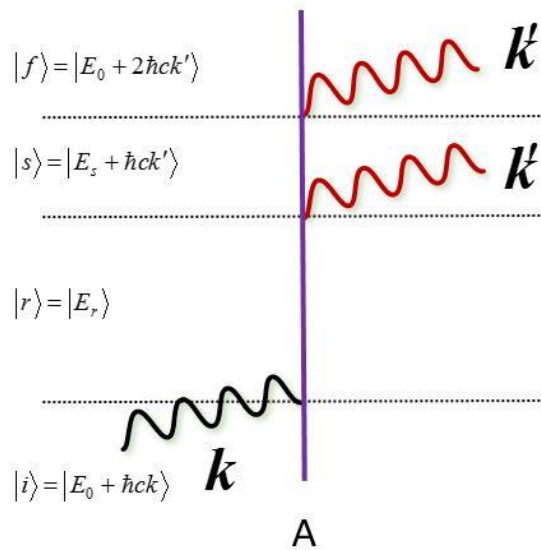
Figure 2.3.1 Feynman time-ordered diagram for localised SPDC at optical centre A. In these two-dimensional Feynman diagrams, time progresses in an upwards manner, whilst the horizontal axis represents space. The wavy lines represent single photons. The initial, final, and intermediate states are read off between the time shown by the horizontal lines. This particular graph corresponds to the first term in square brackets in (2.3.3).
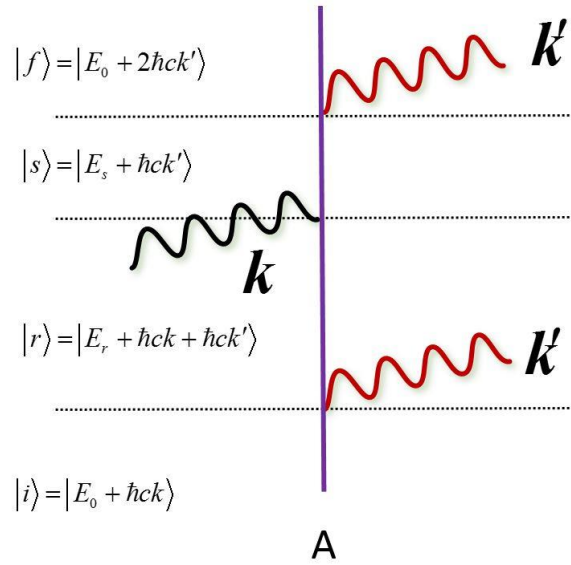
Figure 2.3.2 Time-ordered diagram for localised SPDC at centre A, corresponding to the second term in square brackets in (2.3.3)
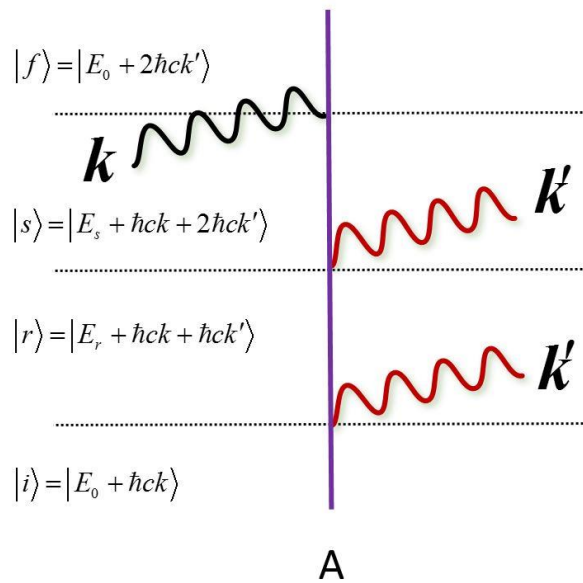
Figure 2.3.3 Time-ordered diagram for localised SPDC at centre A, corresponding to the third term in square brackets in (2.3.3)

It has been assumed that no down-converted photons are initially present, and therefore $q' = 0$. In doing so demands the retention of the sum over the output mode. However, SPDC is a coherent process $(\boldsymbol{k} = 2\boldsymbol{k}')$, and therefore conservation of photon momentum is intrinsic. This also means that for SPDC to occur at any sizeable rate in the condensed phase, the process must occur with refractive index-matching – and for simplicity we can neglect any minor difference in refractive index at frequencies ω and ω': the index therefore appears as simply n below. In the absence of significant optical dispersion, group velocity reduces to phase velocity such that $v_g = c/n$. Equation (2.3.3) can be further modified to highlight the role that the frequency-dependent nonlinear-susceptibility $\chi^{(2)}(\omega)$ takes in SPDC, the form of which is conventionally cast in tensor form as follows;

$$
\begin{aligned}
\chi^{(2)}_{i(jk)}\left(-\omega,-\omega;2\omega\right) &= \frac{N'}{2\varepsilon_0}\left(\frac{n^2+2}{3}\right)^3 \sum_{r,s}\left[\left\{\frac{\mu_i^{0r}\mu_j^{rs}\mu_k^{s0}}{\left(E_{s0}-\hbar\omega\right)\left(E_{r0}-2\hbar\omega\right)}\right.\right.\\
&\quad + \frac{\mu_j^{0r}\mu_i^{rs}\mu_k^{s0}}{\left(E_{s0}-\hbar\omega\right)\left(E_{r0}+\hbar\omega\right)}\\
&\quad \left.\left. + \frac{\mu_j^{0r}\mu_k^{rs}\mu_i^{s0}}{\left(E_{s0}+2\hbar\omega\right)\left(E_{r0}+\hbar\omega\right)}\right\}+\left\{j\leftrightarrow k\right\}\right]\\
&= \frac{N'}{2\varepsilon_0}\left(\frac{n^2+2}{3}\right)^3 \beta_{i(jk)}\left(-\omega,-\omega;2\omega\right),
\end{aligned}
$$

(2.3.4)

where N' is the number density of the active optical centres, equivalent to V^{-1}; $\left\{j\leftrightarrow k\right\}$ signifies the other terms by exchanging these indices; $\beta_{i(jk)}\left(-\omega,-\omega;2\omega\right)$ is the *molecular hyperpolarisability* tensor. Taking into account all of the above, assuming the correct photon-mode dependencies implicit, allows the complicated result (2.3.3) to be written as

$$
\begin{aligned}
M_A &= \frac{i}{4}\left(\frac{\hbar\omega}{\varepsilon_0 V n^2}\right)^{3/2} q^{1/2}\frac{N'}{\varepsilon_0}\left(\frac{n^2+2}{3}\right)^3 e_i\vec{e}_j'\vec{e}_k'\beta_{i(jk)}\left(-\omega,-\omega;2\omega\right)\\
&\equiv \frac{i}{4}\left(\frac{\hbar\omega}{n^2}\right)^{3/2}\left(\frac{q}{\varepsilon_0 V}\right)^{1/2}e_i\vec{e}_j'\vec{e}_k'\chi^{(2)}_{i(jk)}\left(-\omega,-\omega,2\omega\right),
\end{aligned}
$$

(2.3.5)

where the product polarisation tensor $e_i \bar{e}'_j \bar{e}'_k$ is j, k-symmetric, and therefore in its contraction with the nonlinear susceptibility tensor (2.3.4), only the j, k-symmetric part of the latter contributes. Equation (2.3.5) represents the quantum amplitude for *single-centre*, localised SPDC within a dielectric medium.

2.4 HIGHER ORDER OPTICAL MECHANISMS

The localised mechanism of SPDC outlined in the previous Section is the lowest-order and most dominant contribution to the rate of producing down-converted photon pairs. It was shown to be third-order in H_{int}, and we can label it an [AAA] interaction as all photon creation and annihilation events occur at the same optical centre 'A' – see Figure 2.4.1. The quantum amplitude can therefore be labelled as $M_A^{(3)}$.
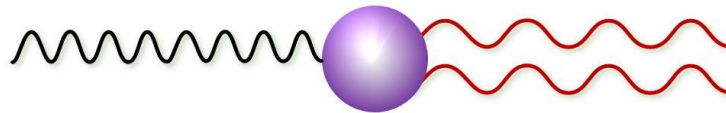
Figure 2.4.1 Schematic representation of the dominant [AAA] localised contribution to the rate of SPDC.

Beyond this leading term, there exists a multitude of higher-order mechanisms which contribute to the rate of SPDC, and some are shown schematically in Figures 2.4.2-2.4.5. Clearly, such additional terms can only be of order $3p + 2$ (where p is a positive integer). Therefore, all of the leading *corrections* come from fifth-order interactions. Some of these high-order corrections occur at the same distinct optical centre [AAAAA], and their matrix elements can be written as $M_A^{(5)}$, whilst others occur in pairwise fashion with coupling between two distinct localities within the optical crystal: $M_{AB}^{(5)}$. However, the majority of

these high-order mechanisms deliver no new physics, and act as small corrections to the overall rate of SPDC.
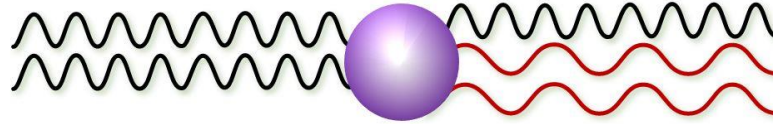
Figure 2.4.2 [AAAAA]-type minor correction to the overall rate of localised SPDC. A mechanism of this type is not separately identifiable and represents the effect of an optical Kerr shift in energy levels on the process of SPDC.
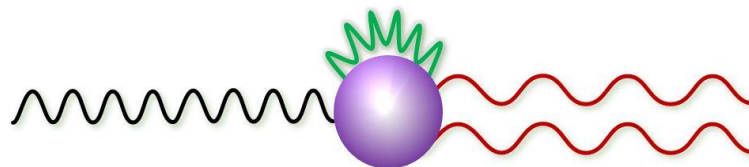
Figure 2.4.3 [AAAAA]-type minor correction to the overall rate of localised SPDC. This is a self-energy correction to the fundamental process at A and although it includes a virtual photon it has no bearings on issues of nonlocality.
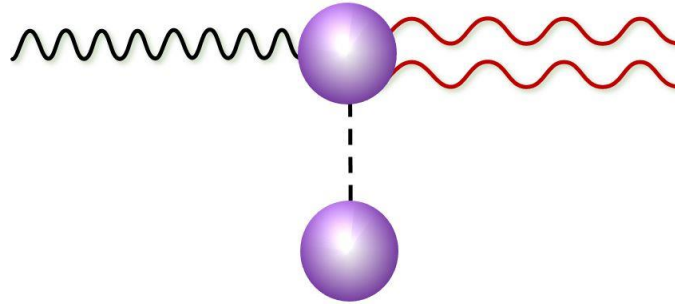
Figure 2.4.4 [AAAAB] mechanism highlighting a static contribution to the rate of localised SPDC – the dotted line signifying a static electric field associated with polar components. Once again, this mechanism has no bearing on the issues of where the output photon pair are emitted from, both clearly originating from the same centre as one another and the input photon annihilation site.
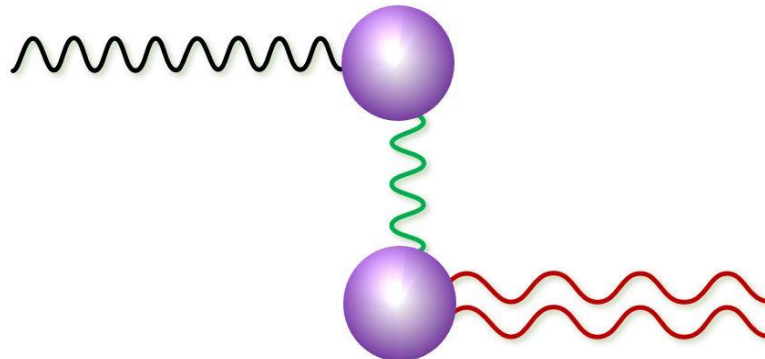
Figure 2.4.5 [AAABB]-type mechanism that appears to be a nonlocal contribution, but again the photon pair is emitted from the same distinct location as one another. This contribution is also not specifically identifiable as it is simply a forward scattering mechanism which is accounted for by the inclusion of material-induced field corrections, manifest in using media-corrected field expansions implicit in this analysis.

We now focus our attention on the contribution that does delivers new physics, namely the [AAABB] mechanism shown in Figure 2.4.6. This non-localised mechanism of generating down-converted photon pairs requires virtual photon propagation to produce single photons from completely separate points in space, but they still constitute a down-converted photon pair.
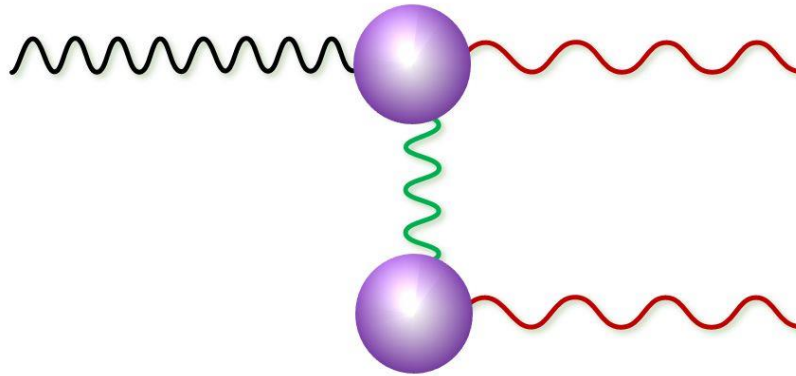
Figure 2.4.6 [AAABB] mechanism for nonlocalised generation of down-converted photon pairs at separate and distinct optical centres. The green wavy line represents virtual photon propagation which acts to couple the optical centres and transfer energy across the medium, allowing for the photons that constitute the down-converted pair to be born from different locations.

2.5   NONLOCALISED SPDC

The nonlocalised mechanism briefly outlined above will now be rigorously identified, and characterised, in this section. As intimated, the nonlocalised [AAABB] mechanism involves the coupling of the optical centre A with a new point in the medium, which we label B. There are no constraints on the positions of A or B, and we assume they are both electronically equivalent, such that any labelling of A or B is arbitrary (only that the former is associated

with the position of the input photon annihilation). As such, there is no need to entertain the role reversal A-B.

The mechanism of [AAABB] is as follows: An input photon of frequency ω is annihilated at an optical centre A (just as in the localised mechanism); however, A only emits a single real photon of frequency ω', whilst also coupling to another optical centre B, via virtual photon propagation, B itself then emitting another single real photon of frequency ω'. Thus, the down-converted photon pair emerges from two, fully distinct delocalised points within the optical medium.

The initial and final states of the system are analogous to those in Section 2.3, this time containing the optical centre B as a constituent of the total system: $|i\rangle = \left| E_0^A; E_0^B \right\rangle \left| q(\eta, \boldsymbol{k}) \right\rangle \left| 0(\eta', \boldsymbol{k}') \right\rangle$ and $|f\rangle = \left| E_0^A; E_0^B \right\rangle \left| q - 1(\eta, \boldsymbol{k}) \right\rangle \left| 2(\eta', \boldsymbol{k}') \right\rangle$ - where both the initial and final matter states are once again ground states. The delocalised mechanism entails five photon-matter interaction events, and so we have recourse to fifth-order perturbation theory to compute the corresponding quantum amplitude. The sum over all intermediate states $r^{(1)}\ldots r^{(4)}$ decomposes into $5! = 120$ topologically distinct time-ordered permutations of the five interaction events.

To highlight the procedure, we take as an example calculation, the uppermost pathway in the state sequence diagram [15] Figure 2.5.2 which corresponds to the Feynman diagram in Figure 2.5.1. The quantum amplitude for this single pathway is given as

$$
\begin{aligned}
M_{AB(1)} = {} & \frac{i}{4} \sum_{r,s} \sum_{\boldsymbol{p},\phi} \sqrt{q} \left(\frac{\hbar c k}{\varepsilon_0 V n^2} \right)^{\frac{3}{2}} \left(\frac{\hbar c p}{2\varepsilon_0 V n^2} \right) \left(\frac{n^2 + 2}{3} \right)^5 \\
& \times e_i \overline{e}_k' \overline{e}_m' \overline{e}_l^{(\phi)} e_j^{(\phi)} \mu_m^{r0(B)} \mu_k^{r0(A)} \mu_l^{sr(A)} \mu_i^{0s(A)} \mu_j^{0r(B)} \\
& \left[\left(E_{0r}^B - \hbar c k' \right) \left(E_{0r}^A + E_{0r}^B - 2\hbar c k' \right) \right. \\
& \left. \times \left(E_{0s}^A + E_{0r}^B - \hbar c \left(2k' + p \right) \right) \left(E_{0r}^B - \hbar c p \right) \right]^{-1} \mathrm{e}^{i(\boldsymbol{k} - \boldsymbol{p} - \boldsymbol{k}') \cdot \boldsymbol{r}_A} \, \mathrm{e}^{i(\boldsymbol{p} - \boldsymbol{k}') \cdot \boldsymbol{r}_B},
\end{aligned}
\tag{2.5.1}
$$

which includes a sum over all virtual photon modes that possess a wave vector $\boldsymbol{p}$ and polarisation ϕ.
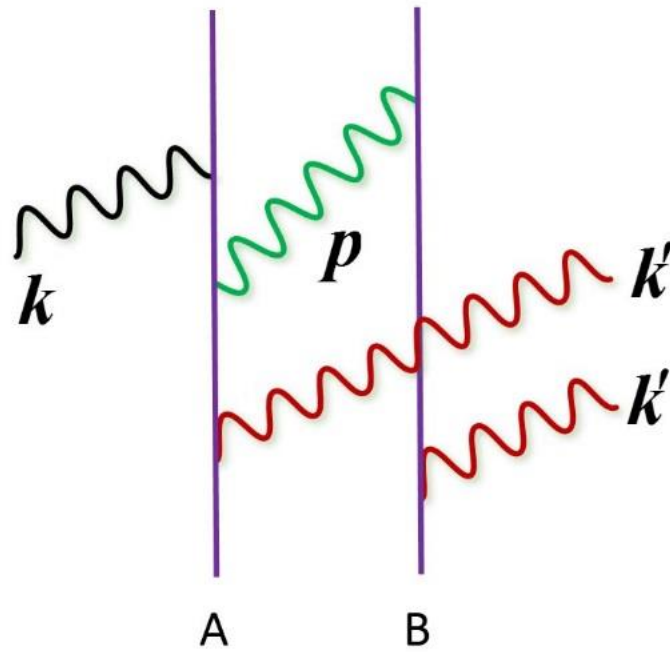
Figure 2.5.1 1 of 120 topologically distinct Feynman diagrams for the nonlocalised mechanism of SPDC. This particular time-ordered graph corresponds to the uppermost pathway in the state sequence diagram Figure 2.5.2.
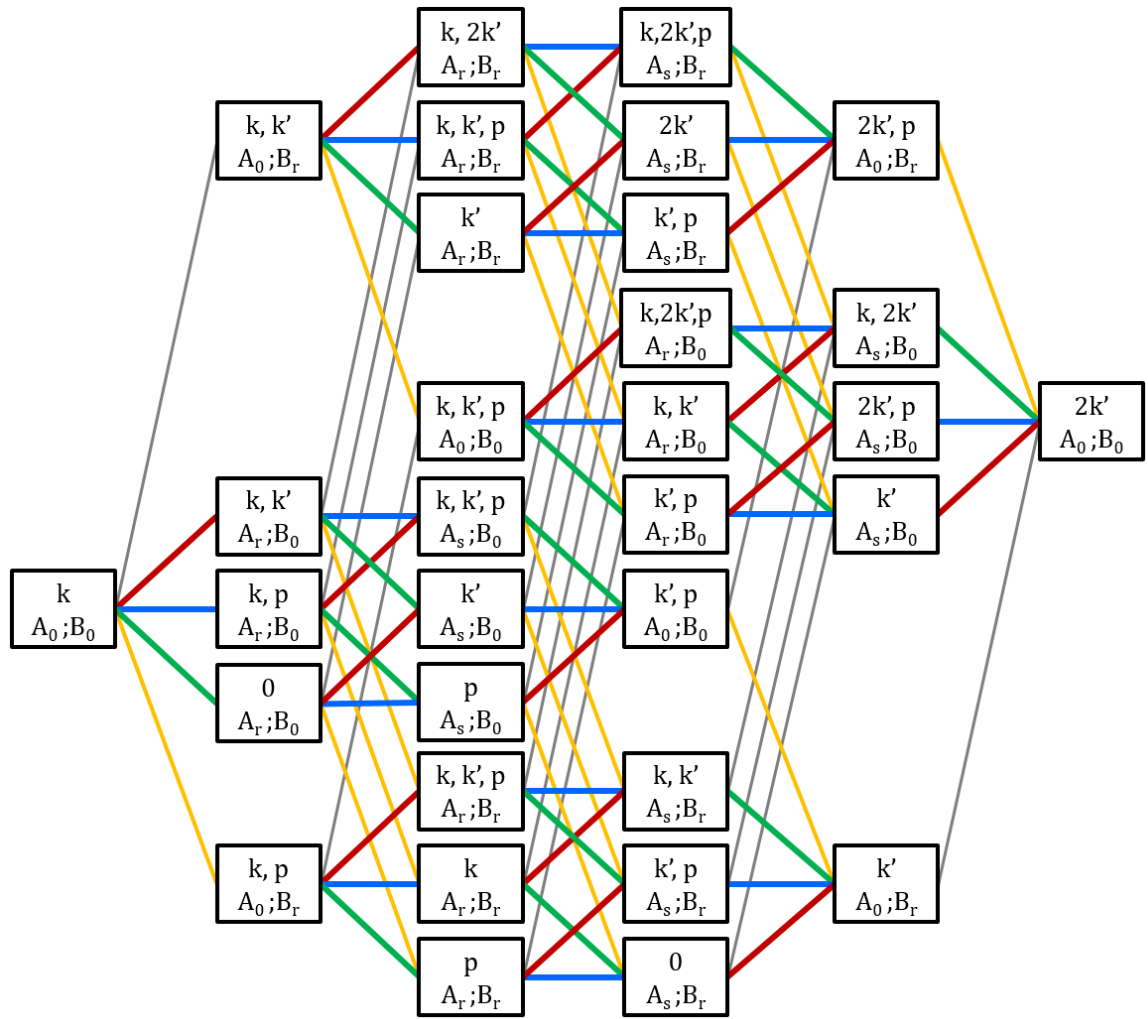
Figure 2.5.2 State-sequence diagram for the nonlocalised mechanism of SPDC, incorporating 120 Feynman graphs in a single diagrammatic representation. The state for the system (comprising three parts: A, B, and radiation) evolves from left to right, from state *i* shown at the far left, to state *f* at the far right. The process entails five distinct interaction events, each illustrated with parallel lines of a given colour: absorption of the input photon by A (green); creation of an output photon k' by A (red); creation of an output photon k' by B (grey); interaction of the virtual photon p by A (blue); and interaction of the virtual photon p by B (gold). (courtesy of Jack S. Ford)

Combining the result (2.5.1) with the other 119 contributions $M_{AB(2)} - M_{AB(120)}$ to the rate secures the full nonlocalised SDPC quantum amplitude [16, 17]

$$
M_{AB} = \frac{i}{4N'} \left(\frac{\hbar c k}{n^2} \right)^{\frac{3}{2}} \left(\frac{q\varepsilon_0}{V} \right)^{\frac{1}{2}} \frac{1}{n^2} e^{i(k-k')\cdot r_A} e^{-ik'\cdot r_B}
$$
$$
\times e_i \bar{e}'_k \bar{e}'_m \chi^{(2)}_{i(jk)} \left(-\omega, -\omega; 2\omega \right) \chi^{(1)}_{lm} \left(-\omega; \omega \right) V_{jl} \left(n, k', r \right), \tag{2.5.2}
$$

where $r = r_B - r_A$. As in the single-centre localised SPDC (2.3.5), the nonlocalised mechanism (2.5.2) also depends on the nonlinear-susceptibility. However, the delocalised contribution also depends on the *linear* susceptibility, which takes the form

$$
\chi^{(1)}_{lm} \left(-\omega, \omega \right) = \frac{N'}{\varepsilon_0} \left(\frac{n^2+2}{3} \right)^2 \sum_r \left[\frac{\mu_l^{0r} \mu_m^{r0}}{E_{r0} + \hbar\omega} + \frac{\mu_m^{0r} \mu_l^{r0}}{E_{r0} - \hbar\omega} \right]
$$
$$
= \frac{N'}{\varepsilon_0} \left(\frac{n^2+2}{3} \right)^2 \alpha_{lm} \left(-\omega, \omega \right), \tag{2.5.3}
$$

where $\alpha_{lm} \left(-\omega, \omega \right)$ is the molecular polarisability tensor. The other difference, besides pre-multiplicative factors, is the dependence on the retarded resonance electric-dipole coupling tensor [9]

$$
V_{jl} \left(n, k', r \right) = \frac{e^{ink'r}}{4\pi\varepsilon_0 r^3} \left[\left(\delta_{jl} - 3\hat{r}_j \hat{r}_l \right) \left(1 - ink'r \right) - \left(\delta_{jl} - \hat{r}_j \hat{r}_l \right) n^2 k'^2 r^2 \right], \tag{2.5.4}
$$

where n is the complex refractive index. By engaging the complex value, dissipative effects can be incorporated in the theory without the need of contriving an additional term to account for optical losses as light traverses the bulk medium.

It is worth highlighting the origin of the coupling tensor (2.5.4). Through a computationally demanding manipulation of all the 120 quantum amplitudes that contribute to (2.5.2), the following entity θ can be identified:

$$\theta = \sum_{p,\phi} \left(\frac{hcp}{2\varepsilon_0 V}\right) \frac{1}{n^2} \left(\frac{n^2+2}{3}\right)^2 e_j^{(\phi)}(\mathbf{p}) \bar{e}_l^{(\phi)}(\mathbf{p}) \left\{ \frac{e^{i\mathbf{p}\cdot\mathbf{r}}}{n\hbar ck - hcp} + \frac{e^{-i\mathbf{p}\cdot\mathbf{r}}}{-n\hbar ck - hcp} \right\}. \tag{2.5.5}$$

This can be further manipulated using the following relations [18]:

$$\frac{1}{V}\sum_p \to \frac{1}{(2\pi)^3}\int d^3\mathbf{p}, \tag{2.5.6}$$

$$d^3\mathbf{p} = p^2 dp d\Omega, \tag{2.5.7}$$

$$\sum_\phi e_j^{(\phi)}(\mathbf{p}) \bar{e}_l^{(\phi)}(\mathbf{p}) = \left(\delta_{jl} - \hat{p}_j \hat{p}_l\right), \tag{2.5.8}$$

to give

$$\theta = \left(\frac{hcp}{2\varepsilon_0}\right) \frac{1}{n^2} \left(\frac{n^2+2}{3}\right)^2 \frac{1}{(2\pi)^3} \int \left(\delta_{jl} - \hat{p}_j \hat{p}_l\right) \left\{ \frac{e^{i\mathbf{p}\cdot\mathbf{r}}}{n\hbar ck - hcp} + \frac{e^{-i\mathbf{p}\cdot\mathbf{r}}}{-n\hbar ck - hcp} \right\} p^2 dp d\Omega. \tag{2.5.9}$$

Using the following result on angular integration

$$\frac{1}{4\pi} \int \left(\delta_{jl} - \hat{p}_j \hat{p}_l\right) e^{\pm i\mathbf{p}\cdot\mathbf{r}} d\Omega = \frac{1}{p^3} \left(-\nabla^2 \delta_{jl} + \nabla_j \nabla_l\right) \frac{\sin pr}{r}, \tag{2.5.10}$$

then gives

$$\theta = \frac{1}{n^2}\left(\frac{n^2+2}{3}\right)^2 \frac{1}{4\pi^2\varepsilon_0}\left(-\nabla^2\delta_{jl} + \nabla_j\nabla_l\right)\int \frac{\sin pr}{r}\left\{\frac{1}{nk-p} + \frac{1}{-nk-p}\right\}\mathrm{d}p. \tag{2.5.11}$$

Extending the limits of integration from 0 to ∞ to $-\infty$ to ∞, and using special functions [6] provides the solution of the Green's function as

$$\frac{1}{2r}\int_{-\infty}^{\infty} \sin pr\left\{\frac{1}{nk-p} + \frac{1}{-nk-p}\right\}\mathrm{d}p = -\frac{\pi}{r}\mathrm{e}^{\mp inkr}. \tag{2.5.12}$$

And finally, by inserting (2.5.12) into (2.5.11) yields the result

$$\begin{aligned}
\theta &= -\frac{1}{n^2}\left(\frac{n^2+2}{3}\right)^2 \frac{1}{4\pi\varepsilon_0}\left(-\nabla^2\delta_{jl} + \nabla_j\nabla_l\right)\frac{1}{r}\mathrm{e}^{\mp inkr} \\
&= \frac{1}{n^2}\left(\frac{n^2+2}{3}\right)^2 \frac{1}{4\pi\varepsilon_0 r^3}\left[\left(\delta_{jl} - 3\hat{r}_j\hat{r}_l\right)(1\pm inkr) - \left(\delta_{jl} - \hat{r}_j\hat{r}_l\right)n^2k^2r^2\right]\mathrm{e}^{\mp inkr} \\
&= V_{jl}^{\pm}\left(n,k,\boldsymbol{r}\right),
\end{aligned} \tag{2.5.13}$$

where $V_{jl}^{\pm}\left(n,k,\boldsymbol{r}\right)$ is the retarded dipole-dipole coupling tensor, either choice of sign being perfectly legitimate, however it is the lower sign that is most often employed. The retarded dipole-dipole coupling tensor arises in QED every time there is a E1-E1 or M1-M1 intermolecular coupling through virtual photon propagation [19]. In the short range limit, this retarded coupling tensor becomes the static, or instantaneous, coupling tensor. There exists a generalised formula for all orders of electric multipole coupling (i.e. electric dipole-electric quadrupole) [20, 21], as well as a coupling tensor for interactions between electric and magnetic dipoles, and the general scheme of the derivation for these multipole-multipole

tensors is analogous to that of the dipole-dipole [6]. The coupling tensor presented here is suitable for working in dispersive media, as it possesses the correct media corrections through the Lorentz factors and refractive indices. However, as stated earlier, most theories work in vacuo, on the assumption that media corrections are easily incorporated if necessary. The coupling tensor in vacuo is related to the one derived here through [22]

$$V_{jl}\left(n,k,\boldsymbol{r}\right)=\frac{1}{n^2}\left(\frac{n^2+2}{3}\right)^2 V_{jl}^{\text{vac}}\left(nk,\boldsymbol{r}\right).$$

(2.5.14)

2.6 PAIR-GENERATION RATE

The localised [AAA] matrix element (2.3.5) as it stands applies to a single centre A, and so do the high-order single centre correction terms [AAAAA]. However, for a collection of N optical centres as in an optical medium, the corresponding matrix element is easily secured by introducing a sum over all N

$$M_{\text{A}}^{(3)}=\sum_{\text{A}}^{N}M_{\text{A}}^{(3)};\qquad M_{\text{A}}^{(5)}=\sum_{\text{A}}^{N}M_{\text{A}}^{(5)}.$$

(2.6.1)

This is essential for the correct lattice sum calculation to be carried out. However, to perform a lattice sum for the pairwise coupling that exists in the nonlocalised mechanism [AAABB] requires a subtle analysis to correctly account for interaction over a system of optical centres where $N>2$. It transpires that (see Appendix 2.1) the correct form of the matrix element for the pairwise AB interactions takes for form

$$M_{\text{AB}}^{(5)}=\left(N-1\right)^{-1}\sum_{\text{A}}^{N}\sum_{\text{B}\neq\text{A}}^{N-1}M_{\text{AB}}^{(5)}.$$

(2.6.2)

For the following quantitative analysis, we neglect the [AAAAA] contributions, and all other high-order mechanisms in fact, for reasons outlined above in Section 2.4.

The position of the optical centre A is chosen to be the origin $\left(r_A = 0\right)$ of our spatial coordinate system. Therefore, the positional displacement vector of site B from site A is $\Delta r = r_B - r_A \equiv r_B$. Combining the localised (2.3.5) and nonlocalised (2.5.2) quantum amplitudes for SPDC, along with the correct lattice sum factors that are present in (2.6.1) and (2.6.2), gives the overall rate of SPDC for an optical medium containing N optical centres as

$$
\Gamma = S \left| e_i \, \bar{e}_k' \, \chi_{i(jk)}^{(2)} \left(-\omega, -\omega; 2\omega\right) \right.
$$
$$
\left. \times \left(\bar{e}_j' + \bar{e}_m' \chi_{lm}^{(1)} \left(-\omega, \omega\right) \frac{\varepsilon_0}{n^2 N'(N-1)} \sum_{B}^{N-1} e^{-ik' \cdot r_B} V_{jl}\left(n, k', r_B\right) \right) \right|^2 .
$$
$$(2.6.3)$$

From here on in, the tensor functions will be written without their arguments for brevity. All scalar pre-multiplicative factors common to both terms are consolidated in (2.6.3) into the constant of proportionality S

$$
S = -\frac{2\pi}{\hbar} \rho_f \left(\frac{\hbar\omega}{n^2}\right)^3 \left(\frac{q}{\varepsilon_0 V}\right) N^2 ,
$$
$$(2.6.4)$$

where ρ_f is the density of final states – in this case the appropriate choice is of the radiation, due to the final state of the material component being in the ground state. Because the quantum amplitude has the same form for every site A, the sum over all positions of A becomes a factor of N^2 in the rate due to the coherent nature of the vector-matching $\left(k = 2k'\right)$ that is implicit within SPDC.

The total SPDC rate is calculated by performing a global sum over all sites B, including every possible interacting optical centre in the medium other than the chosen origin A. In a solid nonlinear medium larger than a few micrometres, the calculation requires an unfeasible

number of terms to include, and therefore to facilitate an indicative lattice simulation only sites that lie within a certain cutoff distance from the point A are included. Each active site of the medium is only included in the summation over B if $r_B \leq C$, such that C is the cutoff radius of a spherical region centred on A. It is within these spherical shells that nonlocalisation is accounted for, and by calculating the rate as a function of C, a picture of how the relative delocalised contributions from B can be determined at various distances from A.

The following tensor can be introduced to enable the formulation of the global summation of B with (N - 1) terms as a function of C

$$\sigma_{jl}\left(C\right) \equiv \sum_{B}^{N_C} e^{-i\mathbf{k}'\cdot\mathbf{r}_B} V_{jl},$$ (2.6.5)

where the (N - 1) normalisation integer becomes N_C, which is the integer number of centres B obeying $r_B \leq C$. Therefore, expressing the overall SPDC rate (2.6.3) as a function of C gives

$$\Gamma_C = S \left| e_i \, \overline{e}'_k \, \chi^{(2)}_{i(jk)} \left(\overline{e}'_j + \frac{\varepsilon_0}{n^2 N'} \overline{e}'_m \chi^{(1)}_{lm} \frac{\sigma_{jl}}{N_C} \right) \right|^2.$$ (2.6.6)

In the expansion of the system from a single centre to a spherical region of radial cutoff C, the interpretation of the overall rate of observed pair emission needs revising: the observable rate is increased by the cross-section area of the active region. That is, the rate equation (2.6.6) is measuring the down-conversion from the individual centre A, but as we are allowing the emission of the second photon from any B within the sphere, we must measure the emission over this cross sectional area to secure a rate that is indicative of the observable amount of SPDC. Therefore, the effective observable rate, Γ'_C, is given by multiplying the second term in (2.6.6) by the cross-sectional area of the sphere, πC^2 - as this represents the

transverse area from within which a pair of photons can emerge when delocalisation is accounted for:

$$\Gamma'_C = S \left| e_i \, \bar{e}'_k \, \chi^{(2)}_{i(jk)} \left(\bar{e}'_j + \frac{\varepsilon_0}{n^2 N'} \bar{e}'_m \chi^{(1)}_{lm} \frac{\pi C^2 \sigma_{jl}}{N_C} \right) \right|^2 . \tag{2.6.7}$$

Evidently as C becomes smaller and smaller until a point where no centres B are included, $N_C = 0$ and therefore $\sigma = 0$. This in turn leads the nonlocalised contribution to vanish upon setting the indeterminate 0/0 as zero, collapsing the rate equation into the single centre rate

$$\Gamma'_0 = S \left| M_A \right|^2 = S \left| e_i \, \bar{e}'_k \bar{e}'_j \, \chi^{(2)}_{i(jk)} \right|^2 . \tag{2.6.8}$$

2.7 RATE COMPUTATION

To secure a figure for the potential enhancement or diminution of the rate of SPDC that occurs due to the delocalised mechanism, a lattice sum calculation has to be carried out. Numerical calculations of this kind require real information about the physical properties of the material within which the optical process takes place, along with the beam parameters.

To approximate the optical medium in a computational analysis, it is efficient to model it as a primitive cubic lattice. The location of the optical centre A is an appropriate coordinate origin, and an optical centre B is placed at every site that has integer values for the x, y, and z coordinates in units of the unit-cell length u, such that $V^{-1} = N' = u^{-3}$. The length of u is chosen to be approximately one-tenth of the wavelength for the output mode $\lambda' = 2\pi/k'$. The total number of positions that are occupied by an optical centre B for this calculation is 101^3.

The necessary calculations can be broken into two parts, the first involves the computation of values of $\sigma_{jl}(C)$, using equation (2.6.5), for all values of C up to $50u$ (in increments of $0.1u$). The results of carrying out these calculations are presented in Figure 2.7.1.

To proceed in calculating the total rate, we require indicative figures of the physical parameters in equation (2.6.7). Firstly, on the assumption of an isotropic medium, the linear susceptibility may be cast in a scalar form $\delta_{lm}\chi^{(1)}_{lm} = \chi^{(1)}$, enabling the use of the relationship $|n|^2 - 1 = \chi^{(1)}$ to provide a useful estimate for the values of $\chi^{(1)}$. The values for the nonlinear-susceptibility tensor $\chi^{(2)}_{i(jk)}$ need not be subjected to such approximations. A suitable choice for the nonlinear medium is beta-barium borate (BBO), a crystal that is routinely used to create down-converted photon pairs [23]. If the plane of each BBO unit is aligned to the lattice xy plane, then only four components of $\chi^{(2)}_{i(jk)}$ are significant: $\chi^{(2)}_{x(xx)} = \chi^{(2)}_{y(yy)}$; $\chi^{(2)}_{z(xx)} = \chi^{(2)}_{z(yy)}$, with the other 14 components being negligible.

The second part of the calculation uses the computed values of $\sigma_{jl}(C)$ and N_C to implement (2.6.7), and the ensuing data allows a plot of the normalised rate of SPDC as a function of the cutoff radius C from zero to $50u$ – the results exhibited in Figure 2.7.2.

In Figure 2.7.2, the first nine data points correspond to $C < 1.0u$ and describes the limit $\Gamma'_C = \Gamma'_0$ according to (2.6.8). The opposite limit Γ'_∞ is found at the convergence of Γ'_C in the region of $C > 4\lambda'$, a range of where delocalisation over more than 300 000 B centres are accounted for. The physically sensible convergence is only secured through the correct form of the multicentre sums (2.6.2). Comparing the overall long-range delocalised result to the standard single-centre rate gives the ratio $\Gamma'_\infty / \Gamma'_0 = 1.022$, meaning that the contribution to the rate of degenerate down-conversion from the delocalised mechanism accounts for 2.2% of the correlated photons produced – or, 1 pair in every 50 pairs of correlated photons produced can be attributed to the delocalised mechanism.
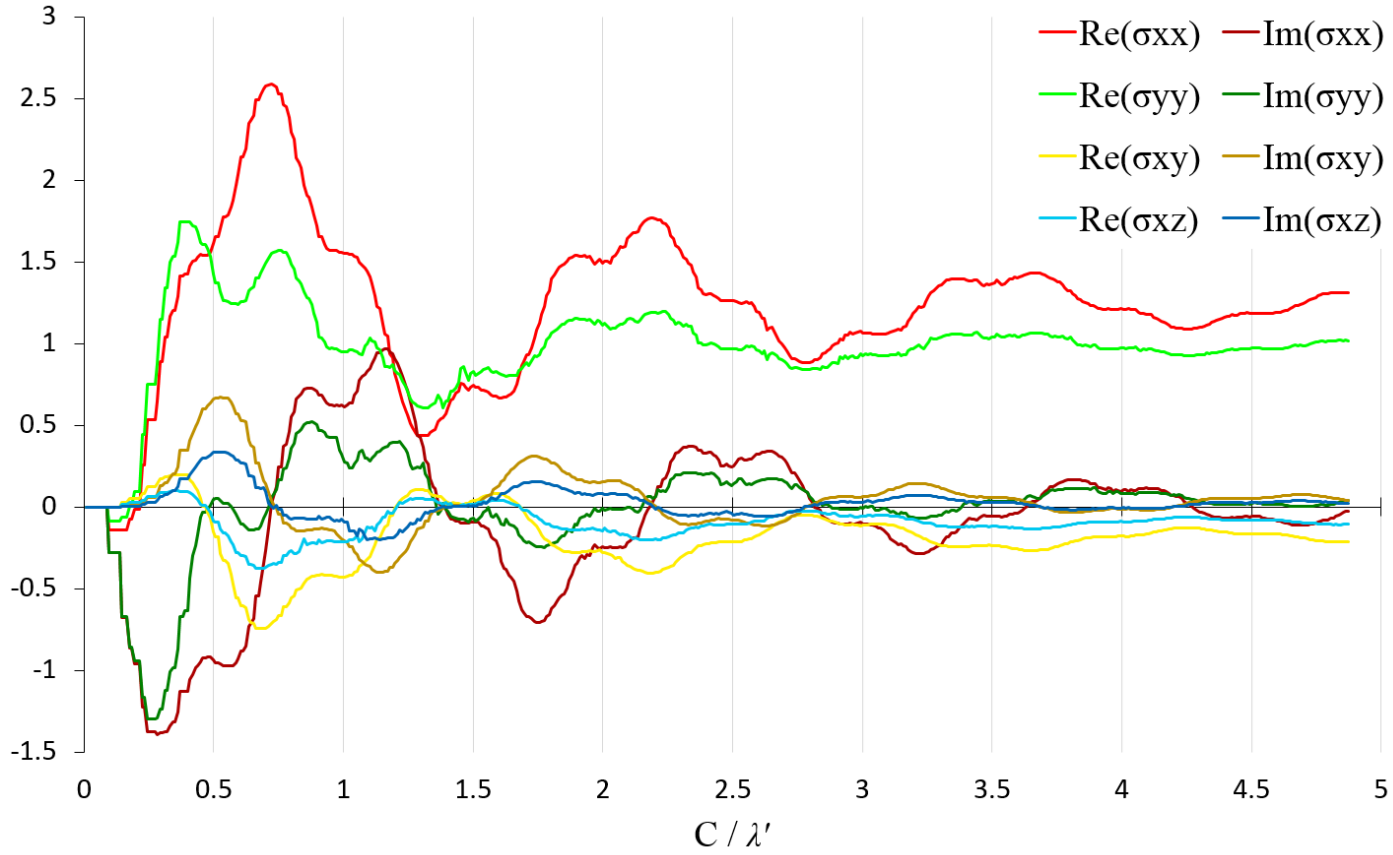
Figure 2.7.1. The four independent components of the tensor $\sigma_{jl}(C)$, computed according to Equation (2.6.5) in our virtual cubic lattice of 101^3 positions. In order to avoid alignments that might influence the sum over positions, the direction of the radiation mode is chosen to be misaligned with the Cartesian unit vectors - in a standard basis, $\boldsymbol{k}' = 0.25u^{-1}\hat{\mathbf{i}} + 0.5u^{-1}\hat{\mathbf{j}} + 0.25u^{-1}\hat{\mathbf{k}}$. The index-symmetry of V_{ij} leads to $\sigma_{jl} = \sigma_{lj}$, and the equality $k_x = k_z$ in our choice of $\boldsymbol{k}'$ leads to $\sigma_{xx} = \sigma_{zz}$ and $\sigma_{xy} = \sigma_{yz}$.
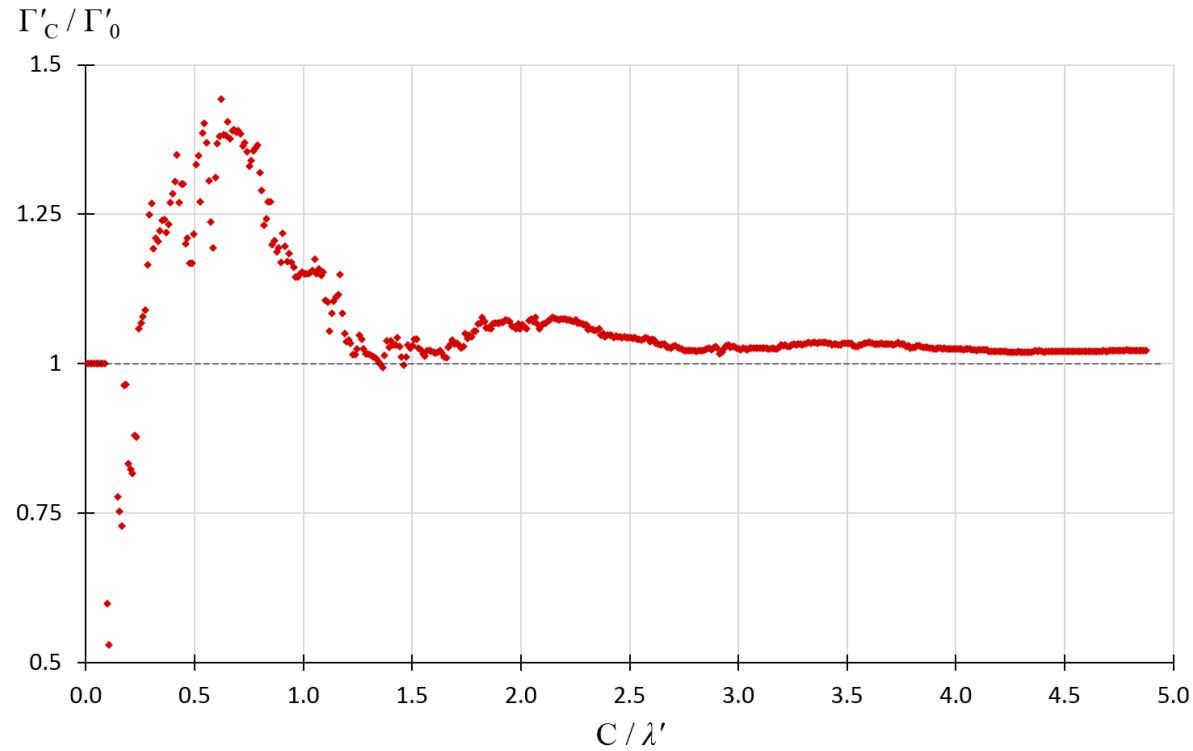
The observable rate of SPDC, Γ'_C , computed according to Equation (2.6.7) using the σ results shown in Figure 2.7.1, and normalised against the

C=0 rate given by Equation (2.6.8). Values for the material parameters are chosen to approximately match BBO: $n \cong 1.7 + 0.1i$; $\chi^{(2)}_{x(xx)} = 5.8$ and

$\chi^{(2)}_{z(xx)} = 0.29$ (manufacturer reported values relative to standard KDP reference).[1]

---

[1] http://www.redoptronics.com/BBO-crystal.html

2.8 SECOND-HARMONIC GENERATION

The delocalised mechanism highlighted in this chapter for the specific case of SDPC can in fact be applied in a more general sense to other suitable optical processes. One such process that is immediately amenable to the same form of analysis is another nonlinear optical process: second-harmonic generation (SHG). In coherent SHG, two pump photons of wave vector $\boldsymbol{k}$ are converted into a single output photon $\boldsymbol{k}'$, where photon momentum is conserved such that $2\boldsymbol{k} = \boldsymbol{k}'$. Clearly then, SHG is seen to be the time-inverse process of SPDC (see Figure 2.8.1), and it is for this reason that general analysis on SPDC is easily implemented to SHG.
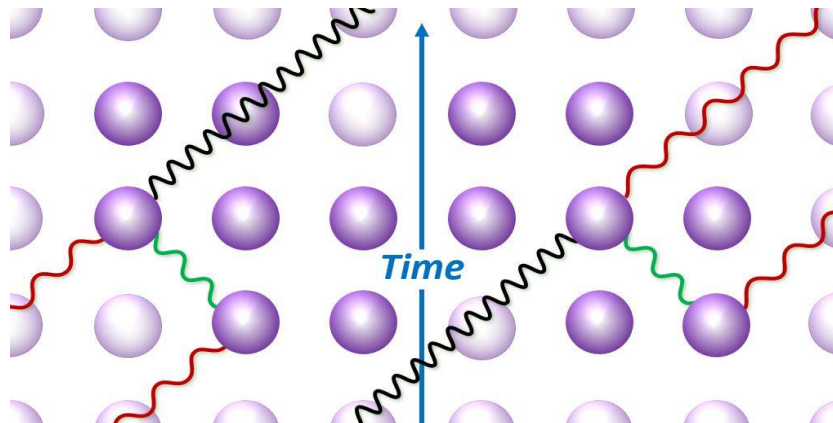
Figure 2.8.1 A schematic depiction highlighting the time-symmetry relationship between the delocalised mechanisms of SHG (left) and SPDC (right).

Using the same methods as in Section 2.3 and with the aid of the time-ordered diagrams for SHG in Figure 2.8.2, the localised rate of coherent SHG is seen take the form

$$M_{(A)}^{SHG} = -\frac{i}{2}\left(\frac{\hbar\omega}{\varepsilon_0 V n^2}\right)^{3/2}\left(\frac{n^2+2}{3}\right)^3 \{(q+1)q\}^{1/2}\, \vec{e}_i' e_j e_k \beta_{i(jk)}(\omega,\omega;-2\omega) e^{i(2k-k')\cdot r_A}$$

$$= -\frac{i}{2}\left(\frac{\hbar\omega}{n^2}\right)^{3/2}\left(\frac{(q+1)q}{\varepsilon_0 V}\right)^{1/2}\, \vec{e}_i' e_j e_k \chi_{i(jk)}^{(2)}(\omega,\omega;-2\omega) e^{i(2k-k')\cdot r_A} . \tag{2.8.1}$$
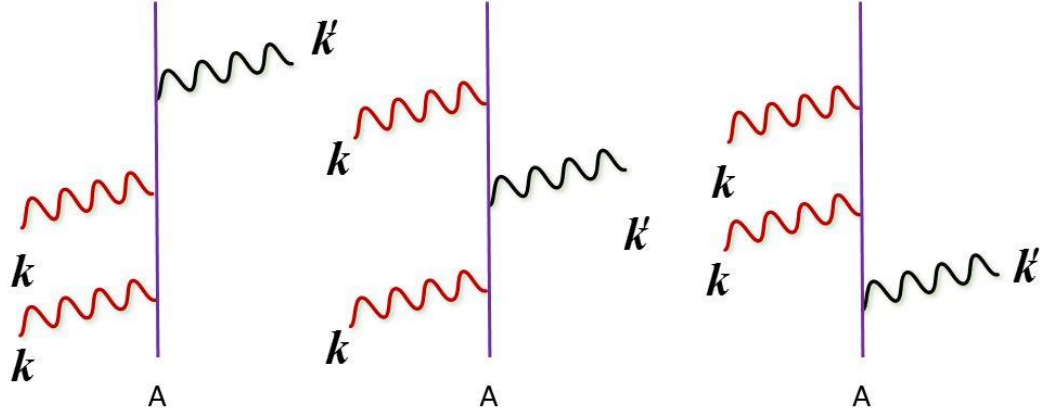
Figure 2.8.2 The three topologically distinct Feynman diagrams for localised SHG.

Whilst the nonlocalised quantum amplitude for SHG when the two input photons are annihilated at two distinct centres A and B, producing a harmonic from site B is [24]

$$M_{AB}^{SHG} = -\frac{i}{2N'}\left(\frac{\hbar\omega}{n^2}\right)^{\frac{3}{2}}\left(\frac{\{(q+1)q\}\varepsilon_0}{V}\right)^{\frac{1}{2}}\frac{1}{n^2}e^{-ik'\cdot r_B}$$

$$\times \vec{e}_i' e_k e_m \chi_{i(jk)}^{(2)}(\omega,\omega;-2\omega)\,\chi_{lm}^{(1)}(-\omega;\omega)\,V_{jl}(n,k,r_B). \tag{2.8.2}$$

One of the single indicative Feynman diagrams used when calculating the amplitude (2.8.2) is shown in Figure 2.8.3.
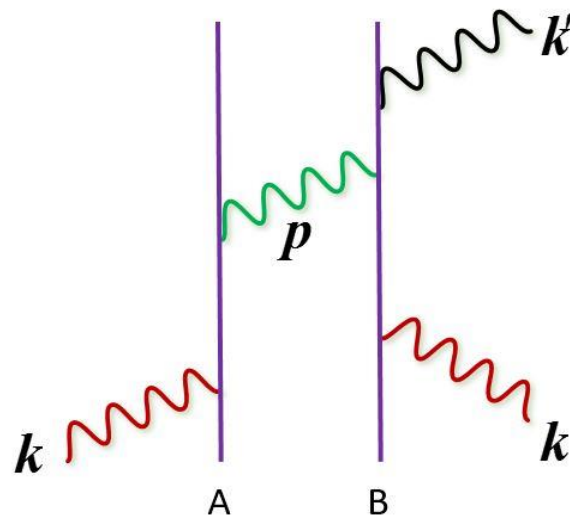
Figure 2.8.3 1 of 120 representative Feynman diagrams for the nonlocalised mechanism

for SHG.

Within the constraints of which the theory was derived, the detailed results and simulations secured for SPDC are readily applicable to SHG due to the highlighted symmetry between the two processes. The rate equations deliver a result that has exactly the same form for both SHG and SPDC – subject to factors connected with the input mode intensities: SHG has a nonlinear (quadratic) dependence on the input irradiance, whereas SPDC has a strictly linear dependence.

2.9 DISCUSSION

The first physical consequence that can be drawn from the analysis on delocalised contributions to the nonlinear optical processes of SPDC and SHG concern the effect that particle and optical crystal size has on the output rate. Although the graph in Figure 2.7.2 is

only applicable within the context of a rectangular lattice upon which it models, the dampened oscillatory behaviour exhibited leads to an obvious distance-dependent efficiency. It is important to realise that the graph displays a normalised rate of SPDC whose form is already integrated in the sense that each individual point C accounts for all local and non-local SPDC up to that particular distance: the area under the curve does not represent the rate, the individual points do. Aside from the local fluctuations, the most important behaviour is associated with the sharp rise in efficiency that runs out to about half of the longer of the two wavelengths (input for SHG and output for SPDC). Beyond this point, a gradual decline occurs leading to an eventual convergence on a rate that is slightly enhanced (compared to the normalised localised rate) to approximately 2%. These results are tabulated in Table 2.9.1.

Radius / λ	<0.2	1.0	1.33	2.0	3.0	4.0	5.0	6.0	∞
Enhancement %	0	+33	+40	+15	+3	+6	+4	+2	+2

Table 2.9.1 Tabulated data extracted from Figure 2.7.2: Extent of conversion efficiency enhancement in nanoparticles of dimensions comparative to the wavelength of input (for SHG) and output (SPDC).

Therefore, by controlling the size of nanoparticles (a particle built up of many optical centres) or nonlinear crystals, the conversion efficiency of SPDC and SHG can be fine-tuned to exhibit an enhanced propensity of nonlinear activity per unit volume relative to that for a bulk of the same material. It can be envisaged that a collection of compact, suitably-sized nanoparticles would lead to a markedly large increase in optical nonlinearity. This is suggestive of a significant design criterion when synthesising the appropriate nonlinear mediums – an artistic representation of what might be created is presented in Figure 2.9.1.
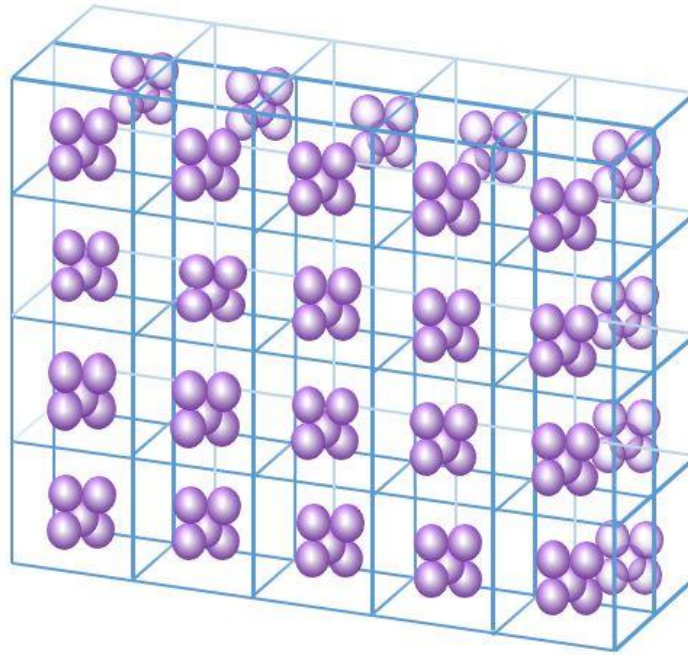
Figure 2.9.1 Impression of an engineered nanomaterial consisting of compact, suitably sized nanoparticles (purple spheres) placed in an array, taking advantage of the size-dependent enhancement of nonlinear processes identified from Table 2.9.1.

The physical origin of this size-dependent effect stems from the local effects of constructive optical interference within the nonlinear medium. Interestingly, a similar effect has been observed in SHG within nanomaterials [25, 26]. Evidently, as the sample size grows beyond a couple of wavelengths it starts to trail off to an asymptotic limit and any such advantages from particle-size effects are quickly lost. This is down to additional contributions causing destructive interferences and eventually any individual particle becomes more and more representative of the bulk phase.

Several features of nonlocal origin are anticipated to be detectable in the output. Firstly, in the case of SPDC, one can expect a degree of temporal broadening associated with some down-converted photon pairs being emitted from positions that are separated by a wavelength or so in advance of, or behind, each other with respect to the forward emission direction.

The corresponding lateral broadening of the photonic output has implications for both SPDC and SHG. The delocalised emission of photon pairs in SPDC signifies that in applications such as ghost imaging [27-30], the resolution of the image [31] will be to some extent

jeopardised by an insurmountable phenomenon of quantum origin (notwithstanding the experimental limitations when dealing with physical optics). This is due to the fact that perfect imaging would require each correlated pair to originate from the same spatial origin. This effect, if the nonlocal mechanism had not been identified, might be interpreted as simply a position-momentum quantum uncertainty with respect to directions perpendicular to the down-converted photon propagation. On a similar note, two photons arriving at distinct and well-separated locations producing the output harmonic SHG (as in the delocalised mechanism) can be anticipated to have implications on the resolution of SHG microscopy [32, 33]: perfect imaging would require each photon to annihilate at precisely the same optical centre.

The delocalised production of correlated photon pairs may also have some significance in the field of quantum entanglement [13, 14, 34]. The issue of whether the delocalised photon pair retains its entanglement fidelity is a reasonable question. However, it is to be recognised that the resonance coupling tensor which permits the energy mediation and photon transfer to the site 'B', in its derivation accounts for all possible polarisation states through the sum over polarisation states. Therefore, the entangled polarisation state fidelity is clearly maintained.

Further interesting considerations of entanglement fidelity arise when one permits the use of light endowed with orbital angular momentum to produce down-converted photon pairs. It has been verified that photon pairs produced in SPDC with Laguerre-Gaussian beams have entangled OAM states [35]. Combined with the fact that multipole transitions do not convey well-defined values of angular momentum through the resonant multipole-multipole coupling tensor [36, 37], adds weight to the assertion that correlated photon pairs produced through the nonlocalised mechanism retain the fidelity of their entangled states.

APPENDIX 2.1

As noted in Section 2.7, the convergence of the delocalised contribution to SPDC can only be secured by implementation of the correct optical centre sums. At the quantum electrodynamical level, to this point there are no known attempts to tackle such multicentre sums. The largest body of such calculations are limited two-centre interactions, associated with specifically *pairwise* interactions between the nearest individual molecules of the bulk [3, 18, 38-40]. There does exist a limited number of reports where three-centre interactions are entertained, but no lattice sums were required in the analyses [41, 42].

To show how the correct $(N-1)^{-1}$ factor arises in multi-centre lattice sums of the type studied in this Chapter, we begin with the foundational equations for the quantum amplitude M_{fi}:

$$M_{fi} = \sum_{s=0} \langle f | (H_{\text{int}} T_0)^s H_{\text{int}} | i \rangle, \tag{A2.1}$$

where

$$T_0 \approx (E_i - H_0)^{-1}, \tag{A2.2}$$

is the expression for the propagator T_0 is based on the eigenstates of the full Hamiltonian H being similar to those of H_0. Equation A2.1 represents a coupling that propagates from an initial system state i into a final state f, where $s+1$ is the order of perturbation theory based on the eigenstates of H_0. In both these equations, all states, energies and operators relate to the system as a whole. For a wave-vector matched process such as SPDC, the optical centre sums that feature in the quantum amplitude A2.1 will be phase-coherent and therefore directly additive. Noting that only even values of $s \geq 2$ can contribute to the sum in Equation A2.1, then on implementing the optical centre sums we obtain a result expressible as;

$$M_{fi} = \sum_{p=0} \langle f_{rad} | \prod_{j=1}^{N} \langle 0(\xi_j) | \left(\sum_{k=1}^{N} H_{int}(\xi_k) T_0 \right)^{2(p+1)} \sum_{m=1}^{N} H_{int}(\xi_m) \prod_{l=1}^{N} | 0(\xi_l) \rangle | i_{rad} \rangle. \tag{A2.3}$$

The leading term, $p = 0$, delivers interactions that are third order in H_{int}, comprising a sum of N terms, each signifying single-centre SPDC. To this order, it is readily established that all terms for which the three operations of H_{int} are not effected at the same centre vanish.

With the use of the completeness relation

$$1 = \sum_r | r(\xi_q) \rangle \langle r(\xi_q) | \tag{A2.4}$$

for any individual centre ξ_q, the leading term to emerge from Equation A2.3 takes the form

$$M_{fi}^{(3)} = \sum_{r^{(2)}, r^{(1)}} \frac{\langle f | H_{int} | r^{(2)} \rangle \langle r^{(2)} | H_{int} | r^{(1)} \rangle \langle r^{(1)} | H_{int} | i \rangle}{\left(E_i - E_{r^{(2)}} \right) \left(E_i - E_{r^{(1)}} \right)}, \tag{A2.5}$$

where it is implicit that the entire expression relates to a single, representative centre. Equation A2.5 thus relates to all N conventional SPDC interactions of type [AAA] identified in this Chapter. The next order, $p = 1$ in Equation A2.3, delivers the leading corrections, of the form [AAAAA] and [AAABB]. By similar arguments to those used above, the following emerges as a representative of the former;

$$M_{fi}^{(5)} = \sum_{\substack{r^{(4)}, r^{(3)} \\ r^{(2)}, r^{(1)}}} \frac{\langle f | H_{int} | r^{(4)} \rangle \langle r^{(4)} | H_{int} | r^{(3)} \rangle \langle r^{(3)} | H_{int} | r^{(2)} \rangle \langle r^{(2)} | H_{int} | r^{(1)} \rangle \langle r^{(1)} | H_{int} | i \rangle}{\left(E_i - E_{r^{(4)}} \right) \left(E_i - E_{r^{(3)}} \right) \left(E_i - E_{r^{(2)}} \right) \left(E_i - E_{r^{(1)}} \right)}. \tag{A2.6}$$

The expression signifies a self-energy [AAAAA] correction to single-centre SPDC, all interactions once again occurring at the same centre. However, the $p = 1$ term in Equation A2.3 can also deliver non-vanishing results when two distinct centres are involved. Then, the completeness relation of Equation A2.4 is to be implemented not only for any centre taking the role of A, but also in each case for the full set of (N-1) centres that can act as component B. Accordingly

$$1 = (N-1)^{-1} \sum_{q \neq A}^{N-1} \sum_{r} \left| r(\xi_q) \right\rangle \left\langle r(\xi_q) \right|. \tag{A2.7}$$

This signifies that a normalisation factor of $1/(N$-1) has to be included in implementing a global sum over all centres that can take the role of B. This factor will arise once in each state sequence pathway or Feynman diagram, at the point where the operation of H_{int} is first effected at centre B. To summarise, we can thus write

$$M_{fi} = \sum_{\xi}^{N} M_{fi}^{(3)}(\xi) + \sum_{\xi}^{N} M_{fi}^{(5)}(\xi) + (N-1)^{-1} \sum_{\xi}^{N} \sum_{\xi'}^{N-1} M_{fi}^{(5)}(\xi, \xi') + \ldots, \tag{A2.8}$$

where the three successive terms represent explicit calculations for quantum amplitude contributions of the form [AAA], [AAAAA] and [AAABB].

REFERENCES

[1]   D. L. Andrews and P. Allcock, *Optical Harmonics in Molecular Systems* (Wiley-VCH, Weinheim, 2002).

[2]   R. W. Boyd, *Nonlinear Optics* (Academic Press, New York, 2003).

[3]   A. Salam, *Molecular Quantum Electrodynamics. Long-Range Intermolecular Interactions* (Wiley, Hoboken, NJ, 2010).

[4]   D. L. Andrews and D. S. Bradshaw, *The role of virtual photons in nanoscale photonics*, Ann. Phys. (Berlin) **526**, 173 (2014).

[5]   A. Salam, *Molecular Quantum Electrodynamics of Radiation-Induced Intermolecular Forces*, Adv. Quant. Chem. **62**, 1 (2011).

[6]   G. J. Daniels, R. D. Jenkins, D. S. Bradshaw, and D. L. Andrews, *Resonance energy transfer: The unified theory revisited*, J. Chem. Phys. **119**, 2264 (2003).

[7]   G. Grynberg, A. Aspect, and C. Fabre, *Introduction to Quantum Optics: From the Semi-Classical Approach to Quantized Light* (Cambridge University Press, Cambridge, UK, 2010).

[8]   P. D. Drummond and M. Hillery, *The Quantum Theory of Nonlinear Optics* (Cambridge University Press, 2014).

[9]   G. Juzeliūnas. and D. L. Andrews, *Quantum electrodynamics of resonant energy-transfer in condensed matter*, Phys. Rev. B **49**, 8751 (1994).

[10]   G. Juzeliūnas. and D. L. Andrews, *Quantum electrodynamics of resonant energy-transfer in condensed matter. II. dynamical aspects*, Phys. Rev. B **50**, 13371 (1994).

[11]   G. Juzeliūnas., *Microscopic theory of quantization of radiation in molecular dielectrics: Normal-mode representation of operators for local and averaged (macroscopic) fields*, Phys. Rev. A **53**, 3543 (1996).

[12]   G. Juzeliūnas., *Microscopic theory of quantization of radiation in molecular dielectrics. II. Analysis of microscopic field operators*, Phys. Rev. A **55**, 929 (1997).

[13]   K. Edamatsu, *Entangled photons: generation, observation, and characterization*, Jpn. J. App. Phys. **46**, 7175 (2007).

[14] R. Horodecki, P. Horodecki, M. Horodecki, and K. Horodecki, *Quantum entanglement*, Rev. Mod. Phys. **81**, 865 (2009).

[15] R. D. Jenkins, D. L. Andrews, and L. C. Dávila Romero, *A new diagrammatic methodology for non-relativistic quantum electrodynamics*, J. Phys. B: At. Mol. Opt. Phys. **35**, 445 (2002).

[16] K. A. Forbes, J. S. Ford, and D. L. Andrews, *Nonlocalized generation of correlated photon pairs in degenerate down-conversion*, Phys. Rev. Lett. **118**, 133602 (2017).

[17] K. A. Forbes, J. S. Ford, G. A. Jones, and D. L. Andrews, *Quantum delocalization in photon-pair generation*, Phys. Rev. A **96**, 023850 (2017).

[18] D. P. Craig and T. Thirunamachandran, *Molecular Quantum Electrodynamics: An Introduction to Radiation-Molecule Interactions* (Dover Publications, Mineola, NY, 1998).

[19] K. A. Forbes, M. D. Williams, and D. L. Andrews, *Quantum theory for the nanoscale propagation of light through stacked thin film layers*, Proc. SPIE **9884**, 988434 (2016).

[20] G. D. Scholes and D. L. Andrews, *Damping and higher multipole effects in the quantum electrodynamical model for electronic energy transfer in the condensed phase*, J. Chem. Phys. **107**, 5374 (1997).

[21] A. Salam, *A general formula for the rate of resonant transfer of energy between two electric multipole moments of arbitrary order using molecular quantum electrodynamics*, J. Chem. Phys. **122**, 044112 (2005).

[22] D. L. Andrews and A. A. Demidov, *Resonance Energy Transfer* (Wiley, Chichester, 1999).

[23] R. Rangarajan, M. Goggin, and P. Kwiat, *Optimizing type-I polarization-entangled photons*, Opt. Express **17**, 18920 (2009).

[24] K. A. Forbes, J. S. Ford, and D. L. Andrews, *Quantum localization issues in nonlinear frequency conversion and harmonic generation*, Proc. SPIE **10359**, 1035908 (2017).

[25] P. Allcock, D. L. Andrews, S. R. Meech, and A. J. Wigman, *Doubly forbidden second-harmonic generation from isotropic suspensions: Studies on the purple membrane of Halobacterium halobium*, Phys. Rev. A **53**, 2788 (1996).

[26] D. L. Andrews and L. C. Dávila Romero, *Local coherence and the temporal development of second harmonic emission*, J. Phys. B: At. Mol. Opt. Phys. **34**, 2177 (2001).

[27] T. Pittman, Y. Shih, D. Strekalov, and A. Sergienko, *Optical imaging by means of two-photon quantum entanglement*, Phys. Rev. A **52**, R3429 (1995).

[28] P. A. Morris, R. S. Aspden, J. E. Bell, R. W. Boyd, and M. J. Padgett, *Imaging with a small number of photons*, Nat. Commun. **6** (2015).

[29] J. Cheng, *Theory of ghost scattering with biphoton states*, Photonics Research **5**, 41 (2017).

[30] P. A. Moreau, E. Toninelli, T. Gregory, and M. J. Padgett, *Ghost Imaging Using Optical Correlations*, Laser & Photon. Rev. (2017).

[31] M. H. Rubin and Y. Shih, *Resolution of ghost imaging for nondegenerate spontaneous parametric down-conversion*, Phys. Rev. A **78**, 033836 (2008).

[32] T. Verbiest, K. Clays, and V. Rodriguez, *Second-order nonlinear optical characterization techniques: an introduction* (CRC press, Boca Raton, FL, 2009).

[33] P. J. Campagnola and C. Y. Dong, *Second harmonic generation microscopy: principles and applications to disease diagnosis*, Laser & Photon. Rev. **5**, 13 (2011).

[34] D. S. Simon, G. Jaeger, and A. V. Sergienko, *Quantum Metrology, Imaging, and Communication* (Springer, Berlin, 2017).

[35] R. Fickler, R. Lapkiewicz, W. N. Plick, M. Krenn, C. Schaeff, S. Ramelow, and A. Zeilinger, *Quantum entanglement of high angular momenta*, Science **338**, 640 (2012).

[36] D. L. Andrews, *Optical angular momentum: Multipole transitions and photonics*, Phys. Rev. A **81**, 033825 (2010).

[37] D. L. Andrews, *On the conveyance of angular momentum in electronic energy transfer*, Phys. Chem. Chem. Phys. **12**, 7409 (2010).

[38] E. Power and T. Thirunamachandran, *Casimir-Polder potential as an interaction between induced dipoles*, Phys. Rev. A **48**, 4761 (1993).

[39] D. S. Bradshaw and D. L. Andrews, in *Phys. Rev. A*2005), p. 033816.

[40] D. L. Andrews and J. S. Ford, *Resonance energy transfer: Influence of neighboring matter absorbing in the wavelength region of the acceptor*, J. Chem. Phys. **139**, 014107 (2013).

[41] R. Passante, E. A. Power, and T. Thirunamachandran, *Radiation-molecule coupling using dynamic polarizabilities: Application to many-body forces*, Phys. Lett. A **249**, 77 (1998).

[42] A. Salam, *Dispersion potential between three-bodies with arbitrary electric multipole polarizabilities: Molecular QED theory*, J. Chem. Phys. **140**, 244105 (2014).

3

DIAMAGNETIC INTERACTIONS IN SCATTERING AND NONLINEAR OPTICS

3.1 INTRODUCTION

In Chapter 1 the derivation of the multipolar Hamiltonian for a closed system of radiation interacting with matter led to a result cast in the familiar electric and magnetic multipole moments, alongside the less well-known diamagnetic terms. The contribution of the latter to optical processes is rarely discussed. However, as will be shown here, it has highly unique characteristics and is more than worthy of inclusion when studying interactions between light and matter. Indeed, for any multiphoton process, it *has* to be included for a fully correct result.

In general, the spatial variation of the vector potential across molecular centres can be neglected and the lowest order form of electromagnetic coupling, namely electric dipole E1, is sufficient to account for most optical phenomena. This approximation being known as the 'electric-dipole approximation', and is widely utilised throughout molecular optics as in general it gives the most important physical results for a large number of optical processes, and higher-order terms often deliver no new physics, but only minor corrections to the calculated magnitude. Indeed, in Chapter 2 the E1 contributions to the localised and delocalised mechanisms in nonlinear optics were sufficient to produce the relevant physics. However, in certain circumstances and special systems, higher order interaction such as E2 and M1 are the dominant form of couplings and their inclusion is requisite. Indeed, M1 couplings are the signature hallmark of optical activity [1] and chiral discriminations [2] in molecules that possesses low symmetry, the subject of the final two chapters. Importantly,

these higher order M1 and E2 terms are necessary to explain the physics of special phenomena, however they also warrant inclusion when E1 couplings are either small or zero – one such example being an electronic transition that is electric dipole forbidden [3]. Particular examples of where higher-order couplings play a significant role include light-harvesting complexes [4], nanomaterials [5-8], metamaterials [9, 10], the optics of lanthanides [11, 12], optical forces [13, 14], and numerous other theoretical studies [15, 16].

Evidently, E1 interactions are the most well-studied of the couplings between light and matter, and the higher order E*n* and M*n* multipole couplings are also widely utilised in explaining special optical phenomena. However, as was shown in Section 1, there is another form of coupling which is known as diamagnetic coupling (which is given the notation D*n*) that is needed to be included for a fully rigorous treatment of optical interactions. It is interesting to speculate on why the term has received such little interest, seeing as it possesses the unique property of being quadratically dependent on the magnetic field and electric charge. As we shall see, this leads to some interesting and unique properties. The lowest-order D1 interactions are also produced at the same level of multipolar expansion in the PZW Hamiltonian as the much more widely studied E2 and M1 moments. Another important point is that it can only play a role in optical processes that involve 2 or more photons: thus, it plays no role in one photon processes.

The physical significance of the diamagnetic term has its origins in correctly accounting for the overall magnetic susceptibility response of a molecule [17]. The magnetic susceptibility is a gauge invariant property that manifests itself in two-photon interactions and is always measureable. The diamagnetic susceptibility, as well as the paramagnetic susceptibility are not independent of the gauge, and therefore have little meaning in a general sense [18]. However, in the Coulomb gauge they are legitimately separable physical quantities, so long as it is understood that only when they are combined do they give useful gauge invariant physical predictions. This is the main reason for why diamagnetic couplings should always be included in multiphoton processes. At the lowest-order diamagnetic D1 and magnetic dipole coupling M1 for two-photon processes, we produce the leading terms to the diamagnetic susceptibilities and paramagnetic susceptibilities. It is worth pointing out, however, that molecular QED is a non-relativistic theory and as such takes no account of spin [19]. Therefore, when we discuss paramagnetic susceptibilities in molecular QED, we are implicitly discussing the temperature-independent form. The spin-only paramagnetic

term can be added on in a phenomenological manner because a spin interaction term can be included in the Hamiltonian in an analogously ad-hoc way [20]. Dn and Mn couplings where $n>2$ give rise to higher-order corrections to these susceptibilities, but are so small in magnitude they stimulate very little motivation for their inclusion.

Once computed, the D1 and M1^2 terms are combined to give the overall magnetic susceptibility contribution to the specified multiphoton process. If the D1 contribution is larger than the M1^2, then the molecule is said to be diamagnetic: the other way around, then it is paramagnetic. The vast majority of molecules are diamagnetic and therein lays another reason that in molecular QED it is extremely important to include the diamagnetic couplings terms. Indeed, it has been shown that a particular example where diamagnetic couplings become important and prominent is in the Casimir-Polder dispersion forces between ground-state molecules [21].

This chapter begins by outlining the general interaction Hamiltonian needed to compute D1-couplings with matter, followed by calculating the D1 contributions to the rate of two-photon absorption and Rayleigh scattering. Comparisons between the E1 and D1 contributions to both the rate of two-photon absorption and scattering are made, highlighting the uniquely different spectroscopic properties of D1 couplings.

3.2 D1 INTERACTION HAMILTONIAN

The lowest order D1 contribution to the multipolar interaction Hamiltonian derived in Chapter 1 (Equation 1.16.15) is given as

$$H_{\text{int}}^{\text{mult(D1)}} = \frac{e^2}{8m} \sum_{\xi,\alpha} \left\{ \left[\boldsymbol{q}_\alpha(\xi) - \boldsymbol{R}_\xi \right] \times \boldsymbol{b}\left(\boldsymbol{R}_\xi \right) \right\}^2, \tag{3.2.1}$$

where $\boldsymbol{b}$ is the standard mode expansion for the magnetic field

$$b(r) = i \sum_{k,\eta} \left(\frac{\hbar k}{2\varepsilon_0 cV} \right)^{1/2} \left[b^{(\eta)}(k) a^{(\eta)}(k) e^{ik \cdot r} + \bar{b}^{(\eta)}(k) a^{\dagger(\eta)}(k) e^{-ik \cdot r} \right]. \tag{3.2.2}$$

For the purpose of calculations, (3.2.1) is more easily implemented when written in its expanded form

$$H_{\text{int}}^{\text{mult(D1)}} = \frac{e^2}{8m} \varepsilon_{pij} \varepsilon_{pkl} \sum_{\substack{k,\eta \\ k',\eta'}} \sum_{\xi,\alpha} \left(\frac{\hbar}{2\varepsilon_0 cV} \right) (kk')^{1/2} \left[q_\alpha(\xi) - R_\xi \right]_i \left[q_\alpha(\xi) - R_\xi \right]_k$$

$$\times \left(b_j a\, e^{ik \cdot R_\xi} - \bar{b}_j a^\dagger\, e^{-ik \cdot R_\xi} \right) \left(b_l' a'\, e^{ik' \cdot R_\xi} - \bar{b}_l' a'^\dagger\, e^{-ik' \cdot R_\xi} \right), \tag{3.2.3}$$

where the vector calculus result $(a \times b)_i = \varepsilon_{ijk} a_j b_k$ enables the vector cross products to be expressed using Levi-Civita tensors. For further clarity, the photon modes are now suppressed. On the standard assumption that photon annihilation and creation events occur at single electrons, its wave function is therefore to a first approximation exactly separable from those of the other charged particles in the molecules. This allows us to characterise the molecular interactions through transition dipole moments, namely we can write

$$-e \sum_\alpha \left[q_\alpha(\xi) - R_\xi \right]_i = \mu_i(\xi). \tag{3.2.4}$$

By invoking the completeness relation, we can introduce a sum over intermediate states $|r\rangle$ that connect the initial $|i\rangle$ and final $|f\rangle$ states through

$$\left(\mu_i\mu_k\right)^{f0} = \langle f|\mu_i\mu_k|0\rangle = \sum_r \langle f|\mu_i|r\rangle\langle r|\mu_k|0\rangle = \sum_r \mu_i^{fr}\mu_k^{r0}. \tag{3.2.5}$$

With the general mathematical toolkit of D1 interactions outlined, the following sections in this chapter will look at implementing them by calculating the D1 contribution to the rate of firstly two-photon absorption, followed by Rayleigh scattering.

3.3   TWO-PHOTON ABSORPTION

This section will calculate the lowest-order diamagnetic contribution to two-photon absorption (TPA). In contrast to conventional one-photon absorption, multiphoton absorption processes involve the concerted absorption of two or more photons at a single chromophore centre, where the first photon absorbed puts the optical centre into a virtual state that isn't an eigenstate of the molecule, which is *simultaneously* promoted to the final state through absorption of the second photon – (i) in Figure 3.3.1 [22, 23]. TPA has become a widely utilised method within nonlinear spectroscopy [24]. Such nonlinear processes require the use of intense sources of radiation: ideally suited to pass this constraint are pulsed lasers [25]. The calculation is carried out assuming the absorption of both photons occurs at a single electron, and that the origin of both photons is from a single monochromatic beam.

In contrast to standard E*n* or M*n* multipole TPA, diamagnetic interactions D*n* occur through a single interaction vertex (ii) in Figure 3.3.1. The consequence is that the first-order perturbation theory is required for the lowest order diamagnetic contribution D1 to TPA - in contrast to the second-order interaction term necessary for computing the electric and magnetic multipole contributions. It is therefore interesting to note there are no diamagnetic contributions to single-photon absorption.
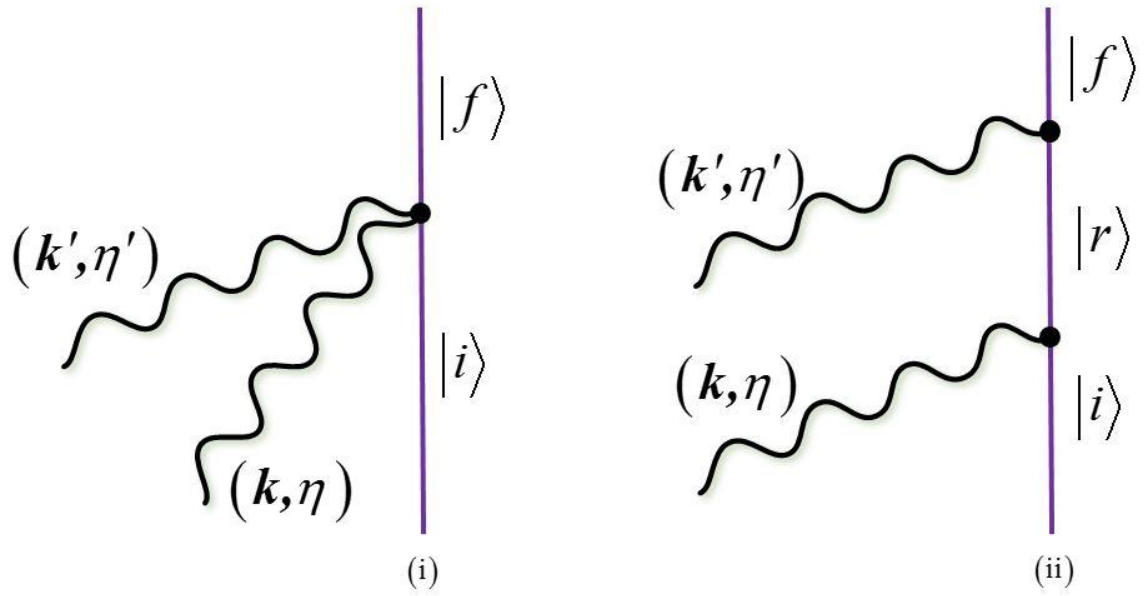
Figure 3.3.1 (i) Feynman diagram for the diamagnetic two-photon absorption, where the molecule transitions from an initial state i to a final state f. (ii) A conventional and representative Feynman graph for two-photon absorption, where in contrast to (i), the molecule progresses through a virtual intermediate state r.

A single beam of n photons of mode $(\boldsymbol{k}, \eta)$ is incident upon N molecules in their ground state energy level E_0. The quantum amplitude for the diamagnetic interaction is given by

$$M_{fi} = \langle f | H_{\text{int}} | i \rangle, \tag{3.3.1}$$

where the initial state of the radiation-matter system is given by $|i\rangle = |n(\boldsymbol{k}, \eta)\rangle |E_0\rangle$ and the final state by $\langle f| = \langle n - 2(\boldsymbol{k}, \eta)| \langle E_f|$. Inserting (3.2.3) for H_{int} and carrying out the radiation part of the calculation

$$\langle n-2(\mathbf{k},\eta)|aa|n(\mathbf{k},\eta)\rangle = \sqrt{n}\,\langle n-2(\mathbf{k},\eta)|a|n-1(\mathbf{k},\eta)\rangle$$
$$= \sqrt{n}\sqrt{n-1}\,\langle n-2(\mathbf{k},\eta)|n-2(\mathbf{k},\eta)\rangle$$
$$= \{n(n-1)\}^{1/2}. \tag{3.3.2}$$

Calculating the material part of the matrix element, with the aid of (3.2.4) and (3.2.5), yields the overall quantum amplitude as

$$M_{fi} = \varepsilon_{pij}\varepsilon_{pkl}\left(\frac{\hbar k}{16m\varepsilon_0 cV}\right)\{n(n-1)\}^{1/2}\sum_r \mu_i^{fr}\mu_k^{r0}b_j b_l\, \mathrm{e}^{i\mathbf{k}\cdot\mathbf{R}_\xi}\, \mathrm{e}^{i\mathbf{k}\cdot\mathbf{R}_\xi}. \tag{3.3.3}$$

In two-photon absorption, the molecule being in a discrete state initially, ends up in an excited continuum of states. Also, it is clear that there is a difference between the initial and final state of the radiation field. Being an optical process, we require the use of the Fermi rule $\Gamma = (2\pi/\hbar)|M_{fi}|^2 N\rho_f$. It is worth noting that the correct choice for the density of states ρ_f^{molecule} in multiphoton absorption processes is that of the molecule. This makes the result dependent on the line shape of the molecular states only. Of course, in actual fact, any process will have a dependence on the density of states of both the molecule and the radiation. However, it is the factor that delivers the highest overall number of states per unit frequency, momentum, or energy interval that will have largest influence upon the overall rate. It is therefore appropriate to use the density of final molecule states rather than that of the radiation, especially since multiphoton absorption and other nonlinear excitation processes are studied with narrow-linewidth laser light.

Inserting (3.3.3) into the Fermi rule gives

$$\Gamma = \left(\frac{2\pi N}{\hbar}\right)\left(\frac{\hbar k}{16m\varepsilon_0 cV}\right)^2 \rho_f\, n(n-1)\,\varepsilon_{pij}\varepsilon_{pkl}\varepsilon_{uqr}\varepsilon_{ust}\sum_r \mu_i^{fr}\mu_k^{r0}\bar{\mu}_q^{fr}\bar{\mu}_s^{r0}b_j b_l \bar{b}_r \bar{b}_t. \tag{3.3.4}$$

To progress, we require the use of the identity for the product of Levi-Civita tensors

$$\varepsilon_{pij}\varepsilon_{mkl} = \delta_{pm}\delta_{ik}\delta_{jl} + \delta_{pk}\delta_{il}\delta_{jm} + \delta_{pl}\delta_{im}\delta_{jk} - \delta_{pk}\delta_{im}\delta_{jl} - \delta_{pm}\delta_{il}\delta_{jk} - \delta_{pl}\delta_{ik}\delta_{jm}. \tag{3.3.5}$$

In the above, all six indices differ, however we require the result when $p = m$ which is easily secured from (3.3.5)

$$\begin{aligned}
\varepsilon_{pij}\varepsilon_{pkl} &= \delta_{pp}\delta_{ik}\delta_{jl} + \delta_{pk}\delta_{il}\delta_{jp} + \delta_{pl}\delta_{ip}\delta_{jk} - \delta_{pk}\delta_{ip}\delta_{jl} - \delta_{pp}\delta_{il}\delta_{jk} - \delta_{pl}\delta_{ik}\delta_{jp} \\
&= \delta_{ik}\delta_{jl} + \delta_{il}\delta_{jk} + \delta_{il}\delta_{jk} - \delta_{il}\delta_{jk} - \delta_{ik}\delta_{jl} - \delta_{ik}\delta_{jl} \\
&= \delta_{il}\delta_{jk} - \delta_{ik}\delta_{jl},
\end{aligned} \tag{3.3.6}$$

which leads to

$$\begin{aligned}
\varepsilon_{pij}\varepsilon_{pkl}\varepsilon_{uqr}\varepsilon_{ust} &= \left(\delta_{ik}\delta_{jl} - \delta_{il}\delta_{jk}\right)\left(\delta_{qs}\delta_{rt} - \delta_{qt}\delta_{rs}\right) \\
&= \delta_{ik}\delta_{jl}\delta_{qs}\delta_{rt} + \delta_{il}\delta_{jk}\delta_{qt}\delta_{rs} - \delta_{ik}\delta_{jl}\delta_{qt}\delta_{rs} - \delta_{il}\delta_{jk}\delta_{qs}\delta_{rt}.
\end{aligned} \tag{3.3.7}$$

Taking the result (3.3.7) and inserting into (3.3.4)

$$\Gamma = \left(\frac{2\pi N}{\hbar}\right)\left(\frac{\hbar k}{16m\varepsilon_0 cV}\right)^2 \rho_f n(n-1)$$

$$\times \sum_r \mu_i^{fr}\mu_k^{r0}\bar{\mu}_q^{fr}\bar{\mu}_s^{r0}b_j b_l \bar{b}_r \bar{b}_t \left(\delta_{ik}\delta_{jl}\delta_{qs}\delta_{rt} + \delta_{il}\delta_{jk}\delta_{qt}\delta_{rs} - \delta_{ik}\delta_{jl}\delta_{qt}\delta_{rs} - \delta_{il}\delta_{jk}\delta_{qs}\delta_{rt}\right)$$

$$= \left(\frac{2\pi N}{\hbar}\right)\left(\frac{\hbar k}{16m\varepsilon_0 cV}\right)^2 \rho_f n(n-1)\sum_r \left(\mu_i^{fr}\mu_i^{r0}\bar{\mu}_q^{fr}\bar{\mu}_q^{r0}|\boldsymbol{b}\cdot\boldsymbol{b}|^2\right.$$

$$\left.-\mu_i^{fr}\mu_i^{r0}\bar{\mu}_q^{fr}\bar{\mu}_s^{r0}(\boldsymbol{b}\cdot\boldsymbol{b})\bar{b}_q\bar{b}_s - \mu_i^{fr}\mu_k^{r0}\bar{\mu}_q^{fr}\bar{\mu}_q^{r0}(\bar{\boldsymbol{b}}\cdot\bar{\boldsymbol{b}})b_i b_k + \mu_i^{fr}\mu_k^{r0}\bar{\mu}_q^{fr}\bar{\mu}_s^{r0}b_i b_k \bar{b}_q \bar{b}_s\right). \tag{3.3.8}$$

The result (3.3.8) is applicable to oriented systems such as molecular solids or liquids with some form of order. However, for liquids and gases the orientations of the absorbing molecules are usually random, and therefore an appropriate averaging scheme needs to be applied to the rate (3.3.8) for it to apply in these cases. With the aid of standard techniques [26], a rotational average can be applied to each of the different rank tensors in (3.3.8), namely zeroth, 2nd , and 4th rank tensors. It is instructive to explicitly show the averaging technique to each individual tensor, they are given as:

$$\left\langle \mu_i^{fr}\mu_i^{r0}\bar{\mu}_q^{fr}\bar{\mu}_q^{r0}\right\rangle|\boldsymbol{b}\cdot\boldsymbol{b}|^2 = \mu_\lambda^{fr}\mu_\lambda^{r0}\bar{\mu}_\pi^{fr}\bar{\mu}_\pi^{r0}|\boldsymbol{b}\cdot\boldsymbol{b}|^2 , \tag{3.3.9}$$

$$-\left\langle \mu_i^{fr}\mu_i^{r0}\right\rangle\boldsymbol{b}\cdot\boldsymbol{b}\left\langle \bar{\mu}_q^{fr}\bar{\mu}_s^{r0}\right\rangle\bar{b}_q\bar{b}_s = -\frac{1}{3}\mu_\lambda^{fr}\mu_\lambda^{r0}\bar{\mu}_\pi^{fr}\bar{\mu}_\pi^{r0}|\boldsymbol{b}\cdot\boldsymbol{b}|^2 , \tag{3.3.10}$$

$$-\left\langle \bar{\mu}_q^{fr}\bar{\mu}_q^{r0}\right\rangle\bar{\boldsymbol{b}}\cdot\bar{\boldsymbol{b}}\left\langle \mu_i^{fr}\mu_k^{r0}\right\rangle b_i b_k = -\frac{1}{3}\mu_\lambda^{fr}\mu_\lambda^{r0}\bar{\mu}_\pi^{fr}\bar{\mu}_\pi^{r0}|\boldsymbol{b}\cdot\boldsymbol{b}|^2 . \tag{3.3.11}$$

The final term in brackets of (3.3.8) is a fourth-rank tensor, whose rotational averaging scheme is more complicated than the zeroth and two 2nd rank tensors secured in (3.3.9)-(3.3.11). The more complicated procedure for the fourth-rank tensor is shown below:

$$\left\langle \mu_i^{fr}\mu_k^{r0}\overline{\mu}_q^{fr}\overline{\mu}_s^{r0}\right\rangle b_ib_k\overline{b}_q\overline{b}_s = b_ib_k\overline{b}_q\overline{b}_s \frac{1}{30}\Big[\delta_{ik}\delta_{qs}\left(4\delta_{\lambda\pi}\delta_{\nu\varphi}-\delta_{\lambda\nu}\delta_{\pi\varphi}-\delta_{\lambda\varphi}\delta_{\pi\nu}\right)$$

$$+\delta_{iq}\delta_{ks}\left(-\delta_{\lambda\pi}\delta_{\nu\varphi}+4\delta_{\lambda\nu}\delta_{\pi\varphi}-\delta_{\lambda\varphi}\delta_{\pi\nu}\right)$$

$$+\delta_{is}\delta_{kq}\left(-\delta_{\lambda\pi}\delta_{\nu\varphi}-\delta_{\lambda\nu}\delta_{\pi\varphi}+4\delta_{\lambda\varphi}\delta_{\pi\nu}\right)\Big]\mu_\lambda^{fr}\mu_\pi^{r0}\overline{\mu}_\nu^{fr}\overline{\mu}_\varphi^{r0}, \qquad (3.3.12)$$

contracting the Greek indices gives

$$\left\langle \mu_i^{fr}\mu_k^{r0}\overline{\mu}_q^{fr}\overline{\mu}_s^{r0}\right\rangle b_ib_k\overline{b}_q\overline{b}_s = b_ib_k\overline{b}_q\overline{b}_s \frac{1}{30}\Bigg[\delta_{ik}\delta_{qs}\begin{Bmatrix}4\mu_\lambda^{fr}\mu_\lambda^{r0}\overline{\mu}_\pi^{fr}\overline{\mu}_\pi^{r0}-\\ \mu_\lambda^{fr}\mu_\pi^{r0}\overline{\mu}_\lambda^{fr}\overline{\mu}_\pi^{r0}-\mu_\lambda^{fr}\mu_\pi^{r0}\overline{\mu}_\pi^{fr}\overline{\mu}_\lambda^{r0}\end{Bmatrix}$$

$$+\delta_{iq}\delta_{ks}\begin{Bmatrix}-\mu_\lambda^{fr}\mu_\lambda^{r0}\overline{\mu}_\pi^{fr}\overline{\mu}_\pi^{r0}\\ +4\mu_\lambda^{fr}\mu_\pi^{r0}\overline{\mu}_\lambda^{fr}\overline{\mu}_\pi^{r0}-\mu_\lambda^{fr}\mu_\pi^{r0}\overline{\mu}_\pi^{fr}\overline{\mu}_\lambda^{r0}\end{Bmatrix}$$

$$+\delta_{is}\delta_{kq}\begin{Bmatrix}-\mu_\lambda^{fr}\mu_\lambda^{r0}\overline{\mu}_\pi^{fr}\overline{\mu}_\pi^{r0}\\ -\mu_\lambda^{fr}\mu_\pi^{r0}\overline{\mu}_\lambda^{fr}\overline{\mu}_\pi^{r0}+4\mu_\lambda^{fr}\mu_\pi^{r0}\overline{\mu}_\pi^{fr}\overline{\mu}_\lambda^{r0}\end{Bmatrix}\Bigg]. \qquad (3.3.13)$$

In all of the above, Latin indices refer to the laboratory-fixed frame and the Greek indices to the molecule-fixed frame. To finally secure the result, the Latin indices in (3.3.13) are contracted to give

$$\left\langle \mu_i^{fr}\mu_k^{r0}\overline{\mu}_q^{fr}\overline{\mu}_s^{r0}\right\rangle b_ib_k\overline{b}_q\overline{b}_s = \frac{1}{15}\Big[\left(2|\boldsymbol{b}\cdot\boldsymbol{b}|^2-1\right)\mu_\lambda^{fr}\mu_\lambda^{r0}\overline{\mu}_\pi^{fr}\overline{\mu}_\pi^{r0}$$

$$-\left(|\boldsymbol{b}\cdot\boldsymbol{b}|^2-3\right)\mu_\lambda^{fr}\mu_\pi^{r0}\overline{\mu}_\lambda^{fr}\overline{\mu}_\pi^{r0}\Big], \qquad (3.3.14)$$

where $\boldsymbol{b}\cdot\overline{\boldsymbol{b}}=1$ for photons in the same mode has been implemented and the fact that the transition dipole moment product is index symmetric.

Inserting (3.3.9)-(3.3.11) and (3.3.14) into the rate equation (3.3.8) yields the fully rotationally averaged result as

$$
\langle \Gamma \rangle = \left(\frac{\pi N}{15\hbar} \right) \left(\frac{\hbar k}{16 m \varepsilon_0 cV} \right)^2 \rho_f n(n-1)
$$
$$
\times \sum_r \left[\left(7|\boldsymbol{b} \cdot \boldsymbol{b}|^2 - 1 \right) \mu_\lambda^{fr} \mu_\lambda^{r0} \bar{\mu}_\pi^{fr} \bar{\mu}_\pi^{r0} - \left(|\boldsymbol{b} \cdot \boldsymbol{b}|^2 - 3 \right) \left(\mu_\lambda^{fr} \mu_\pi^{r0} \bar{\mu}_\lambda^{fr} \bar{\mu}_\pi^{r0} \right) \right].
$$

(3.3.15)

This result is secured upon the summing of (3.3.9)-(3.3.11) and (3.3.14):

$$
\sum = \mu_\lambda^{fr} \mu_\lambda^{r0} \bar{\mu}_\pi^{fr} \bar{\mu}_\pi^{r0} |\boldsymbol{b} \cdot \boldsymbol{b}|^2 - \frac{1}{3} \mu_\lambda^{fr} \mu_\lambda^{r0} \bar{\mu}_\pi^{fr} \bar{\mu}_\pi^{r0} |\boldsymbol{b} \cdot \boldsymbol{b}|^2 - \frac{1}{3} \mu_\lambda^{fr} \mu_\lambda^{r0} \bar{\mu}_\pi^{fr} \bar{\mu}_\pi^{r0} |\boldsymbol{b} \cdot \boldsymbol{b}|^2
$$
$$
+ \frac{1}{15} \left[\left(2|\boldsymbol{b} \cdot \boldsymbol{b}|^2 - 1 \right) \mu_\lambda^{fr} \mu_\lambda^{r0} \bar{\mu}_\pi^{fr} \bar{\mu}_\pi^{r0} - \left(|\boldsymbol{b} \cdot \boldsymbol{b}|^2 - 3 \right) \mu_\lambda^{fr} \mu_\pi^{r0} \bar{\mu}_\lambda^{fr} \bar{\mu}_\pi^{r0} \right]
$$

$$
= \frac{1}{3} \mu_\lambda^{fr} \mu_\lambda^{r0} \bar{\mu}_\pi^{fr} \bar{\mu}_\pi^{r0} |\boldsymbol{b} \cdot \boldsymbol{b}|^2 + \frac{1}{15} \left[\left(2|\boldsymbol{b} \cdot \boldsymbol{b}|^2 - 1 \right) \mu_\lambda^{fr} \mu_\lambda^{r0} \bar{\mu}_\pi^{fr} \bar{\mu}_\pi^{r0} \right.
$$
$$
\left. - \left(|\boldsymbol{b} \cdot \boldsymbol{b}|^2 - 3 \right) \mu_\lambda^{fr} \mu_\pi^{r0} \bar{\mu}_\lambda^{fr} \bar{\mu}_\pi^{r0} \right]
$$

$$
= \frac{5}{15} \mu_\lambda^{fr} \mu_\lambda^{r0} \bar{\mu}_\pi^{fr} \bar{\mu}_\pi^{r0} |\boldsymbol{b} \cdot \boldsymbol{b}|^2 + \frac{1}{15} \left[\left(2|\boldsymbol{b} \cdot \boldsymbol{b}|^2 - 1 \right) \mu_\lambda^{fr} \mu_\lambda^{r0} \bar{\mu}_\pi^{fr} \bar{\mu}_\pi^{r0} \right.
$$
$$
\left. - \left(|\boldsymbol{b} \cdot \boldsymbol{b}|^2 - 3 \right) \mu_\lambda^{fr} \mu_\pi^{r0} \bar{\mu}_\lambda^{fr} \bar{\mu}_\pi^{r0} \right]
$$

$$
= \frac{1}{15} \left[\left(7|\boldsymbol{b} \cdot \boldsymbol{b}|^2 - 1 \right) \mu_\lambda^{fr} \mu_\lambda^{r0} \bar{\mu}_\pi^{fr} \bar{\mu}_\pi^{r0} - \left(|\boldsymbol{b} \cdot \boldsymbol{b}|^2 - 3 \right) \mu_\lambda^{fr} \mu_\pi^{r0} \bar{\mu}_\lambda^{fr} \bar{\mu}_\pi^{r0} \right].
$$

(3.3.16)

The pre-multiplier present in (3.3.15) can be manipulated in a way as to be written in a more succinct form:

$$\left(\frac{2\pi N}{15\hbar}\right)\left(\frac{\hbar k}{16m\varepsilon_0 cV}\right)^2 \rho_f n(n-1) = \frac{\pi N\hbar^2 k^2}{1920m^2 c^2 \hbar \varepsilon_0^2 V^2}\rho_f n(n-1)$$

$$= \frac{c^4}{c^4}\frac{\pi N\hbar^2 k^2}{1920m^2 c^2 \hbar \varepsilon_0^2 V^2}\frac{\langle n\rangle^2}{\langle n\rangle^2}\langle n(n-1)\rangle$$

$$= \left(\frac{\langle n\rangle c\hbar ck}{V}\right)^2 \frac{\langle n(n-1)\rangle}{\langle n\rangle^2} N \frac{\pi\rho_f}{1920m^2 c^6 \hbar \varepsilon_0^2}$$

$$= \bar{I}^2 g^{(2)} N \frac{\pi\rho_f}{1920m^2 c^6 \hbar \varepsilon_0^2}, \tag{3.3.17}$$

where firstly taking into account the degree of second-order coherence $g^{(2)}$, which is given by [27]

$$g^{(2)} = \frac{\langle n(n-1)\rangle}{\langle n\rangle^2}, \tag{3.3.18}$$

and secondly by noting that the beam intensity can be given as the mean irradiance

$$\bar{I} = \frac{\langle n\rangle c\hbar\omega}{V}, \tag{3.3.19}$$

with $\omega = ck$, gives the overall rate expressible as [28]

$$\langle\Gamma\rangle = N\bar{I}^2 g^{(2)} B^{DI}, \tag{3.3.20}$$

with

$$B^{\text{D1}} = \frac{\pi\rho_f}{1920m^2c^6\hbar\varepsilon_0^2}\sum_r \left[\left(7|\boldsymbol{b}\cdot\boldsymbol{b}|^2 - 2\right)\mu_\lambda^{fr}\mu_\lambda^{r0}\bar{\mu}_\pi^{fr}\bar{\mu}_\pi^{r0} - \left(|\boldsymbol{b}\cdot\boldsymbol{b}|^2 - 3\right)\left(\mu_\lambda^{fr}\mu_\pi^{r0}\bar{\mu}_\lambda^{fr}\bar{\mu}_\pi^{r0}\right)\right]. \quad (3.3.21)$$

The absorption rate (3.3.20) depends on the polarisation of the incident photons through the scalar product $\boldsymbol{b}\cdot\boldsymbol{b}$, which is unity for a linearly polarised beam. For both left and right circularly polarised photons, the factor becomes zero via $\boldsymbol{b}^{\text{L/R}} = \left(-i/\sqrt{2}\right)\left(\hat{\boldsymbol{i}}\pm\hat{i}\hat{\boldsymbol{j}}\right)$, but evidently the overall result doesn't vanish.

Further insight into the physical properties of diamagnetic interactions can be obtained by comparing the rate (3.3.20) with that of electric dipole E1 contributions to TPA

$$\langle\Gamma\rangle = N\bar{I}^2 g^{(2)}B^{\text{E1}}, \quad (3.3.22)$$

where

$$B^{\text{E1}} = \frac{\pi\rho_f}{120\varepsilon_0^2\hbar}$$
$$\times\left[\left(2|\boldsymbol{e}\cdot\boldsymbol{e}|^2 - 1\right)\alpha_{\lambda\lambda}^{f0}(\omega,\omega)\bar{\alpha}_{\pi\pi}^{f0}(\omega,\omega) - \left(|\boldsymbol{e}\cdot\boldsymbol{e}|^2 - 3\right)\alpha_{\lambda\pi}^{f0}(\omega,\omega)\bar{\alpha}_{\lambda\pi}^{f0}(\omega,\omega)\right]. \quad (3.3.23)$$

A minor difference from the result reported by Craig and Thirunamachandran [2] is that our results are written in a form with quadratic dependence on the input irradiance, which is a reflection of our more appropriate choice of density of states factor for reasons explained

above. It also correctly gives a rate that has a quadratic dependence on the input beam intensity.

There are spectroscopic properties of TPA which differ markedly from conventional E1 one-photon absorption. One important difference is the fact that the selection rules are not the same, and therefore two-photon transitions can produce states that could otherwise not have been produced. It can be shown that the standard TPA selection rules for E1 are the same as the selection rules for D1 contributions to TPA. Because the two photons absorbed in D1-TPA come from the same mode, the dyadic $\mu_\lambda^{fr}\mu_\pi^{r0}$ effectively becomes index-symmetric due to its tensor contraction with the magnetic polarisation vectors. Since the selection rules for D1-TPA are determined by the properties of $\mu_\lambda^{fr}\mu_\pi^{r0}$, they are the same as those of E1 which are determined by the index symmetric $\alpha_{\lambda\pi}^{f0}(\omega,\omega)$. As stated earlier, the D1 interactions are of a similar magnitude as that of the M1 couplings, being in the order of the fine-structure constant smaller than the dominant E1 terms. Therefore, one can expect the typical quantum amplitude the D1 couplings to be around 10^{-3}-10^{-2} times smaller relative to those of E1.

3.4 RAYLEIGH SCATTERING

Rayleigh scattering is a two-photon process involving a single photon annihilation and creation event, where the final molecular state is equal to the initial state and therefore the incident and scattered photon energies are equal (an elastic process). This is in contrast to Raman scattering, where the energy of the molecule can either be increased or decreased via coupling to the radiation field, leading to Stokes and anti-Stokes shifts in the output photon (inelastic scattering) respectively. Both are multiphoton processes, and therefore D1 couplings will make a contribution to the overall rates of the scattering mechanisms. In both cases, the scattering can be either forward or non-forward, depending on the direction of the output wave vector. The theory presented will concentrate on elastic scattering, but the mechanism developed for D1 scattering can readily be extended to inelastic scattering.

For the same reasons as discussed for two-photon absorption, the D1 contributions to two-photon scattering processes are calculated using first-order perturbation theory (3.3.1) whereas non-diamagnetic contributions are second order in the interaction.
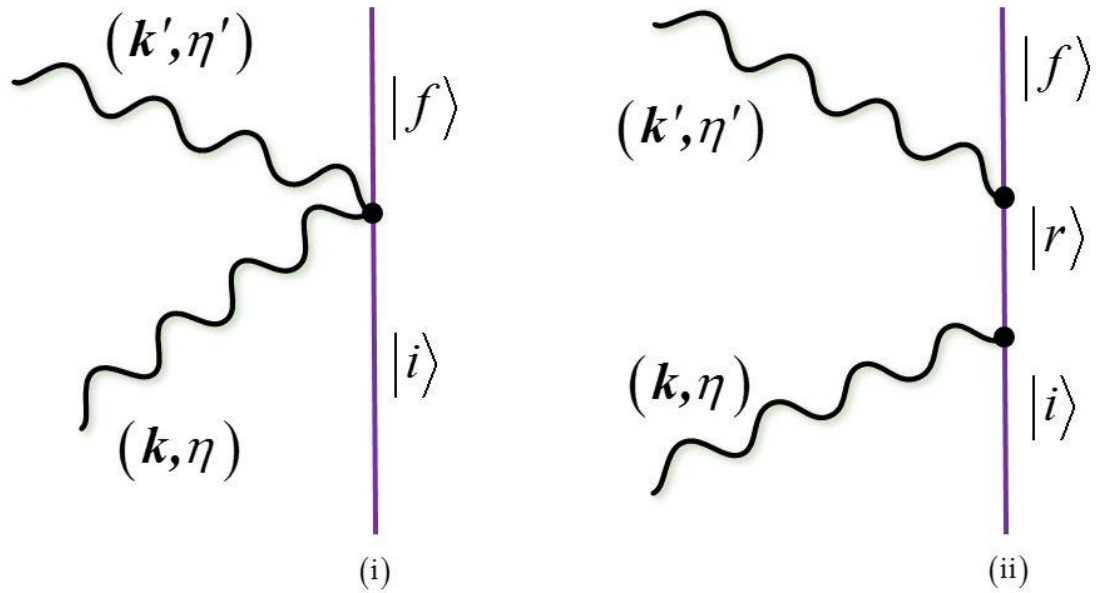
Figure 3.4.1 (i) Time-ordered diagram for the diamagnetic contribution to Rayleigh scattering. (ii) Representative Feynman graph for conventional Rayleigh scattering.

Let the incident beam be in an initial state of n photons of mode $(\mathbf{k}, \eta)$, whilst the scattered photon (whose quantities are labelled with a prime) state is initially unoccupied; inserting H_{int} into (3.3.1) leads to the radiation part of the matrix element taking the form

$$\left\langle 1(k',\eta'),n-1(k,\eta)\middle|a'^{\dagger}a\middle|n(k,\eta),0(k',\eta')\right\rangle$$

$$=\sqrt{n}\left\langle 1(k',\eta'),n-1(k,\eta)\middle|a'^{\dagger}\middle|n-1(k,\eta),0(k',\eta')\right\rangle$$

$$=\sqrt{n}\sqrt{1}\left\langle 1(k',\eta')\middle|1(k',\eta')\right\rangle\left\langle n-1(k,\eta)\middle|n-1(k,\eta)\right\rangle$$

$$=\sqrt{n}. \tag{3.4.1}$$

Assuming the molecule is in its ground state E_0 the rest of the calculation can be carried out, yielding the quantum amplitude

$$M_{fi}=\varepsilon_{pij}\varepsilon_{pkl}\left(\frac{\hbar}{16m\varepsilon_0 cV}\right)\sqrt{nkk'}\sum_r\mu_i^{fr}\mu_k^{r0}b_j\bar{b}_l'e^{i(k-k')\cdot R}. \tag{3.4.2}$$

To proceed we once again use the Fermi rule. In contrast to two-photon absorption, for Rayleigh scattering we make the judicious choice that the density of final states is that for the emitted radiation, which is due to the uncertainty associated with the axis of emission (the molecular state is the ground state and is therefore well defined) [29]

$$\rho_f^{\text{emission}}=\frac{k'^2 d\Omega' V}{(2\pi)^3\hbar c}, \tag{3.4.3}$$

where $d\Omega'$ represents the solid angle centred in the output k' direction. Using (3.4.3) for the density of final states in the Fermi rule, and inserting the matrix element as (3.4.2) gives for collection of N molecules ξ

$$d\Gamma = \left(\frac{2\pi}{\hbar}\right)\left(\frac{\hbar}{16m\varepsilon_0 cV}\right)^2 \frac{nkk'^3 d\Omega' V}{\left(2\pi\right)^3 \hbar c} \left|\varepsilon_{pij}\varepsilon_{pkl}\sum_r \sum_\xi^N \mu_i^{fr}\left(\xi\right)\mu_k^{r0}\left(\xi\right)b_j \bar{b}_l' e^{i(k-k')\cdot R_\xi}\right|^2,$$

(3.4.4)

which is the infinitesimal scattering rate into the element of solid angle $d\Omega'$. Division by the photon flux number $\left(nc/V\right)$ converts (3.4.4) into an infinitesimal cross section $d\sigma$:

$$d\sigma = \frac{kk'^3 d\Omega'}{256m^2\varepsilon_0^2\left(2\pi\right)^2 c^4} \left|\varepsilon_{pij}\varepsilon_{pkl}\sum_r \sum_\xi^N \mu_i^{fr}\left(\xi\right)\mu_k^{r0}\left(\xi\right)b_j \bar{b}_l' e^{i(k-k')\cdot R_\xi}\right|^2,$$

(3.4.5)

where the differential cross section $d\sigma/d\Omega'$ follows immediately, securing an analogous diamagnetic form of the Kramers-Heisenberg dispersion formula.

Due to the presence of the phase factor in (3.4.5), to proceed requires the distinction between non-forward scattering $k \neq k'$ and forward scattering $k = k'$. Of course, for Rayleigh scattering $|k| = |k'|$. The forward scattering term is responsible for optical trapping forces and takes the form of

$$\Delta E^{D1} = \frac{I}{16m\varepsilon_0 c^3}\sum_r \left(\mu_i^{0r}\left(\xi\right)\mu_i^{r0}\left(\xi\right)b_j \bar{b}_j - \mu_i^{0r}\left(\xi\right)\mu_j^{r0}\left(\xi\right)\bar{b}_i b_j\right).$$

(3.4.6)

For non-forward scattering, the modulus square of the phase factor introduces off-diagonal terms

$$\left|\sum_\xi^N e^{i(k-k')\cdot R_\xi}\right|^2 = \sum_\xi^N + \sum_\xi^N \sum_{\substack{\xi' \\ \xi' \neq \xi}}^N e^{i(k-k')\cdot(R_\xi - R_{\xi'})}.$$

(3.4.7)

The second term clearly depends on the positions of pairs of molecules, whilst the first term depends on a single molecular centre. For an elastic process we can set $k = k'$ and the one centre terms are therefore

$$d\Gamma = \left(\frac{2\pi}{\hbar}\right)\left(\frac{\hbar}{16m\varepsilon_0 cV}\right)^2 \frac{nk'^4 d\Omega' V}{(2\pi)^3 \hbar c}$$

$$\times \sum_r^N \sum_\xi \varepsilon_{pij}\varepsilon_{pkl}\varepsilon_{uqr}\varepsilon_{ust}\mu_i^{fr}(\xi)\mu_k^{r0}(\xi)\bar{\mu}_q^{fr}(\xi)\bar{\mu}_s^{r0}(\xi)b_j\bar{b}_l'\bar{b}_r b_t', \qquad (3.4.8)$$

with the two centre terms as

$$d\Gamma = \left(\frac{2\pi}{\hbar}\right)\left(\frac{\hbar}{16m\varepsilon_0 cV}\right)^2 \frac{nk'^4 d\Omega' V}{(2\pi)^3 \hbar c}$$

$$\times \sum_r^N \sum_\xi^N \sum_{\xi' \neq \xi}^N \varepsilon_{pij}\varepsilon_{pkl}\varepsilon_{uqr}\varepsilon_{ust}\mu_i^{fr}(\xi)\mu_k^{r0}(\xi)\bar{\mu}_q^{fr}(\xi')\bar{\mu}_s^{r0}(\xi')b_j\bar{b}_l'\bar{b}_r b_t' e^{i(k-k')\cdot(R_\xi - R_{\xi'})}. \qquad (3.4.9)$$

The single centre term (3.4.8) represents the incoherent contribution, whilst (3.4.9) embodies the coherent mechanism of scattering. In the rotational averaging to follow, the coherent term vanishes for non-forward scattering, and so can be ignored. Thus, using the same rotational averaging technique from section 3.2, the non-forward infinitesimal scattering rate of an assembly of randomly orientated molecules is

$$d\Gamma = \frac{Nd\Omega' nk'^4}{3840m^2\varepsilon_0^2(2\pi)^2 Vc^3}\sum_r\left[\left(14|b\cdot\bar{b}'|^2 - |b\cdot b'|^2 - 1\right)\mu_\lambda^{fr}\mu_\lambda^{r0}\bar{\mu}_\pi^{fr}\bar{\mu}_\pi^{r0}\right.$$

$$\left. +\left(4 - |b\cdot\bar{b}'|^2 - |b\cdot b'|^2\right)\mu_\lambda^{fr}\mu_\pi^{r0}\bar{\mu}_\lambda^{fr}\bar{\mu}_\pi^{r0} + \left(4|b\cdot b'|^2 - |b\cdot\bar{b}'|^2 - 1\right)\mu_\lambda^{fr}\mu_\pi^{r0}\bar{\mu}_\pi^{fr}\bar{\mu}_\lambda^{r0}\right]. \qquad (3.4.10)$$

Writing the result (3.4.10), with recourse to (3.4.4), in terms of the scattered intensity $I(\mathbf{k}')$

$$I(\mathbf{k}') = \frac{NIk'^4}{30720m^2\varepsilon_0^2\pi^2c^4} \sum_r \left[\left(14|\mathbf{b}\cdot\bar{\mathbf{b}}'|^2 - |\mathbf{b}\cdot\mathbf{b}'|^2 - 1\right)\mu_\lambda^{fr}\mu_\lambda^{r0}\bar{\mu}_\pi^{fr}\bar{\mu}_\pi^{r0} \right.$$
$$\left. + \left(4 - |\mathbf{b}\cdot\bar{\mathbf{b}}'|^2 - |\mathbf{b}\cdot\mathbf{b}'|^2\right)\mu_\lambda^{fr}\mu_\pi^{r0}\bar{\mu}_\lambda^{fr}\bar{\mu}_\pi^{r0} + \left(4|\mathbf{b}\cdot\mathbf{b}'|^2 - |\mathbf{b}\cdot\bar{\mathbf{b}}'|^2 - 1\right)\mu_\lambda^{fr}\mu_\pi^{r0}\bar{\mu}_\pi^{fr}\bar{\mu}_\lambda^{r0} \right], \quad (3.4.11)$$

via $I(\mathbf{k}') = (\mathrm{d}\Gamma/\mathrm{d}\Omega')\hbar c k'$. Finally, due to the transition dipole moment products being index symmetric, the final two terms in square brackets of (3.4.11) can be summed to give [28]

$$I(\mathbf{k}') = \frac{NIk'^4}{30720m^2\varepsilon_0^2\pi^2c^4} \sum_r \left[\left(14|\mathbf{b}\cdot\bar{\mathbf{b}}'|^2 - |\mathbf{b}\cdot\mathbf{b}'|^2 - 1\right)\mu_\lambda^{fr}\mu_\lambda^{r0}\bar{\mu}_\pi^{fr}\bar{\mu}_\pi^{r0} \right.$$
$$\left. + \left(3 - 2|\mathbf{b}\cdot\bar{\mathbf{b}}'|^2 + 3|\mathbf{b}\cdot\mathbf{b}'|^2\right)\mu_\lambda^{fr}\mu_\pi^{r0}\bar{\mu}_\lambda^{fr}\bar{\mu}_\pi^{r0} \right], \quad (3.4.12)$$

Once again, it is worth comparing the D1 result (3.4.12) to the standard E1 result for non-forward Rayleigh scattering, namely

$$I(\mathbf{k}') = \frac{NIk'^4}{16\varepsilon_0^2\pi^2} \bar{e}'_i e_j e'_k \bar{e}_l \left\langle \alpha_{ij}^{f0}(\omega,-\omega)\bar{\alpha}_{kl}^{f0}(\omega,-\omega) \right\rangle, \quad (3.4.13)$$

where $\alpha_{ij}^{f0}(\omega,-\omega)$ is the frequency-dependent polarisability

$$\alpha_{ij}^{f0}(\omega,-\omega) = \sum_r \frac{\mu_i^{fr}\mu_j^{r0}}{E_{r0} - \hbar\omega} + \frac{\mu_j^{fr}\mu_i^{r0}}{E_{r0} + \hbar\omega} \qquad (3.4.14)$$

In both cases of D1 and E1 scattering there exists the fourth power dependence on the frequency (inverse fourth power of wavelength) that is characteristic of scattering intensities. However, there also exists dispersion character from the E1 (indeed, all En/Mn multipole contributions) term through two dipole interactions, manifest in the dynamic molecular polarisability (3.4.14). Clearly, no such dispersion character is present in D1 scattering, making this contribution to scattering especially striking and unique. It is worth speculating on a potential way to observe this dispersion-free behavior. In principle, a study of scattering wavelength dependence, over a region of significant dispersion, should enable the specific identification, verification, and quantification of the diamagnetisation effect. By best-fitting the dispersion curve to a suitable line-shape function, running the residuals into a log-log plot against wavelength and observing a -4 gradient (which has its origin on the wavelength dependence present in the premuliplier in (3.4.12)) would verify the dispersion-free characteristic of the scattering and therefore verify the D1 diamagnetisation coupling.

REFERENCES

[1] L. D. Barron, *Molecular Light Scattering and Optical Activity* (Cambridge University Press Cambridge, UK, 2004), Vol. 2.

[2] D. P. Craig and T. Thirunamachandran, *Molecular Quantum Electrodynamics: An Introduction to Radiation-Molecule Interactions* (Dover Publications, Mineola, NY, 1998).

[3] D. L. Andrews and J. M. Leeder, *Resonance energy transfer: When a dipole fails*, J. Chem. Phys. **130**, 184504 (2009).

[4] B. P. Krueger, G. D. Scholes, and G. R. Fleming, *Calculation of couplings and energy-transfer pathways between the pigments of LH2 by the ab initio transition density cube method*, J. Phys. Chem. B **102**, 5378 (1998).

[5] N. Tate, H. Sugiyama, M. Naruse, W. Nomura, T. Yatsui, T. Kawazoe, and M. Ohtsu, *Quadrupole–dipole transform based on optical near-field interactions in engineered nanostructures*, Opt. Express **17**, 11113 (2009).

[6] M. Burresi, T. Kampfrath, D. van Oosten, J. Prangsma, B. Song, S. Noda, and L. Kuipers, *Magnetic light-matter interactions in a photonic crystal nanocavity*, Phys. Rev. Lett. **105**, 123901 (2010).

[7] P. Grahn, A. Shevchenko, and M. Kaivola, *Electromagnetic multipole theory for optical nanomaterials*, New J. Phys. **14**, 093033 (2012).

[8] A. G. Curto, T. H. Taminiau, G. Volpe, M. P. Kreuzer, R. Quidant, and N. F. van Hulst, *Multipolar radiation of quantum emitters with nanowire optical antennas*, Nat. Commun. **4**, 1750 (2013).

[9] D. J. Cho, F. Wang, X. Zhang, and Y. R. Shen, *Contribution of the electric quadrupole resonance in optical metamaterials*, Phys. Rev. B **78**, 121101 (2008).

[10] J. Petschulat, C. Rockstuhl, C. Menzel, A. Chipouline, A. Tünnermann, F. Lederer, and T. Pertsch, in *Plasmonics and Plasmonic Metamaterials*, edited by G. Shvets, and I. Tsukerman (World Scientific, Singapore, 2012), pp. 67.

[11] C. M. Dodson and R. Zia, *Magnetic dipole and electric quadrupole transitions in the trivalent lanthanide series: Calculated emission rates and oscillator strengths*, Phys. Rev. B **86**, 125102 (2012).

[12] T. H. Taminiau, S. Karaveli, N. F. Van Hulst, and R. Zia, *Quantifying the magnetic nature of light emission*, Nat. Commun. **3**, 979 (2012).

[13] N. Moiseyev, M. Šindelka, and L. S. Cederbaum, *Trapping of cold atoms in optical lattices by the quadrupole force*, Phys. Lett. A **362**, 215 (2007).

[14] D. S. Bradshaw, K. A. Forbes, J. M. Leeder, and D. L. Andrews, *Chirality in optical trapping and optical binding*, Photonics **2**, 483 (2015).

[15] D. L. Andrews, *Optical angular momentum: Multipole transitions and photonics*, Phys. Rev. A **81**, 033825 (2010).

[16] S. Karaveli and R. Zia, *Spectral tuning by selective enhancement of electric and magnetic dipole emission*, Phys. Rev. Lett. **106**, 193004 (2011).

[17] A. Hinchliffe and R. W. Munn, *Molecular Electromagnetism* (John Wiley & Sons, 1985).

[18] P. W. Atkins and R. S. Friedman, *Molecular Quantum Mechanics* (Oxford University Press, 2011).

[19] R. Woolley, *The electrodynamics of atoms and molecules*, Adv. Chem. Phys **33**, 153 (1975).

[20] R. E. Moss, *Advanced Molecular Quantum Mechanics* (Chapman and Hall London, 1973).

[21] A. Salam, *On the contribution of the diamagnetic coupling term to the two-body retarded dispersion interaction*, J. Phys. B: At. Mol. Opt. Phys. **33**, 2181 (2000).

[22] M. Göppert-Mayer, *Über elementarakte mit zwei quantensprüngen*, Ann. Phys. (Berlin) **401**, 273 (1931).

[23] W. M. McClain, *Two-photon molecular spectroscopy*, Acc. Chem. Res. **7**, 129 (1974).

[24] M. Pawlicki, H. A. Collins, R. G. Denning, and H. L. Anderson, *Two‑photon absorption and the design of two‑photon dyes*, Angew. Chem. Int. Ed. **48**, 3244 (2009).

[25] D. L. Andrews, *Lasers in Chemistry* (Springer-Verlag, Berlin ; New York, 1997).

[26] D. L. Andrews and T. Thirunamachandran, *On three-dimensional rotational averages*, J. Chem. Phys. **67**, 5026 (1977).

[27] R. Loudon, *The Quantum Theory of Light* (Oxford University Press, Oxford, 2000).

[28] K. A. Forbes, D. S. Bradshaw, and D. L. Andrews, *Identifying diamagnetic interactions in scattering and nonlinear optics*, Phys. Rev. A **94**, 033837 (2016).

[29] E. A. Power, *Introductory Quantum Electrodynamics* (American Elsevier Pub. Co., New York, 1965).

4

OPTICAL ORBITAL ANGULAR MOMENTUM: TWISTED LIGHT AND CHIRALITY

4.1 INTRODUCTION

Radiation fields consist of massless photons which possess and convey energy, and therefore according to Einstein's relativistic energy-momentum relation, photons must also possess linear momentum. This association of linear momentum and energy has long been understood in physics, and is manifest in phenomena such as radiation pressure [1]. However, light can also exhibit an angular momentum [2]. Total angular momentum consists of a spin and an orbital part: with regards to light, the associated intrinsic spin angular momentum has been known for some time and is established in terms of circularly polarised photons carrying a spin angular momentum of $\pm\hbar$. The fact that light can possess an orbital angular momentum is not a new concept either. Darwin [3], during the early development of modern quantum theory, realised that in radiative quadrupole transitions the photon must carry away not only spin but also an orbital angular momentum. However, the realisation that intense beams of laser light could be prepared in the laboratory with a well-defined orbital angular momentum of $\pm\ell\hbar$ about the axis of propagation is relatively recent [4].

The fact light beams and photons can possess an intrinsic orbital angular momentum has found wide application, and the optical orbital angular momentum of light has become a substantial and ever-growing field of research in its own right [5, 6]. One of the most striking

and physically gratifying studies of the angular momentum of light to date was the demonstration that spin angular momentum would induce a trapped particle to rotate on its axis, and the orbital angular momentum causes the particle to orbit around the beam axis [7]. Another key advancement in the field was the utilisation of spontaneous parametric down-conversion (the process that is the subject of Chapter 2) to prove that quantised orbital angular momentum existed at the single-photon level [8].

This chapter aims to resolve the issues surrounding if, and how, the orbital angular momentum of structured light plays a role in chiroptical interactions with matter. Such discriminatory effects that are sensitive to the material and/or the radiation components of the system have been long understood in terms of the spin angular momentum of light, which is manifest through circular polarisation handedness [9, 10]. The work begins with a review of chirality in the general sense, through fundamental symmetry analysis; this is followed by a short introduction to Laguerre-Gaussian beams, the most widely used and studied form of structure/twisted/vortex light; then a full QED analysis of one-photon absorption by chiral molecules possessing E1, M1, and E2 multipole transition moments is carried out to determine whether the orbital angular momentum of the input light can engage with chiral matter.

4.2 CHIRALITY

Molecules are said to be chiral if they belong to point groups which include no improper axis of rotation, and can either be right- or left-handed; light can also possesses a handedness through circularly polarised photons, and/or the direction the vortex twists in a beam possessing OAM. In a chemical sense, a molecule's handedness can have drastic effects when interacting with other molecules in chemical processes. However, the interplay between the handedness of light and matter is exclusively manifest in *chiroptical* interactions. That is to say, chiral molecules and chiral light can exhibit discriminatory effects, where the magnitudes of optical processes and phenomena are dependent on the handedness of the light and/or molecules [11].

Quantum electrodynamics, like nearly all physical theories and laws, is invariant to the universal symmetry operations of spatial parity inversion P, and time reversal T (charge

conjugation *C* does not concern us in non-relativistic QED). That is to say, any equation describing an optical process does not change if the system coordinates are inverted through the coordinate origin; or if all the motions of the fields and particles are reversed. The origin of this invariance is that the laws underlying electrodynamics are the Maxwell equations and the Lorentz force, all of which can easily be shown to be invariant to the symmetry operations, and consequently any interaction that involves electromagnetic fields must conserve these symmetry elements.

Fully accounting for these simple laws of symmetry invariance allows the determination of whether any known or conjectured light-matter interaction is going to be observable or not. This form of symmetry analysis is particularly well-suited for scrutinising the interplay of optical and intrinsic material chirality. Indeed, it will be shown that looking at the individual matter or radiation part of the system allows for the determination of whether a particular chiral discrimination is allowed or disallowed [10].

The first point that needs to be made if one is to successfully utilise symmetry operations to make predictions of the legitimacy of any chiroptical processes is that any symmetry law applies to the total system: radiation and matter. For example, a spatial parity operation *P* on the material components may give a different result which appears to violate the symmetry invariance, however, the same operation applied to the radiation part will always recover the same initial physical result if the optical process is allowed. In fact, it is this ability to partition the material and radiation components of a total system that enables the prediction of whether specific chiroptical interactions are observable.

The appropriate physical quantities to apply the symmetry considerations to in the photon-molecule interactions that this work is concerned with are the electric and magnetic multipole moments E*n* and M*n*, along with the electric and magnetic fields. We will concentrate on the operations of *P*, rather than *T,* as an even or odd character to *P* for any quantity necessarily requires the same parity for *T* in any legitimate light-matter interaction in order to conserve overall *PT* symmetry.

 The determination of the spatial parity of any transition electric multipole or magnetic multipole moment is simply given by

$$P\{\mathrm{E}n\} = (-1)^n \qquad ; P\{\mathrm{M}n\} = (-1)^{n-1},$$

(4.2.1)

where n is a positive integer. From these two simple relations, the spatial parity eigenvalues of any combination of electric and magnetic multipole transitions, their interferences, and respective molecular response tensors can be determined.

For the radiation part, the analysis is not as straightforward because a single axis becomes the symmetry element, and not the coordinate centre of a physical entity such as a molecule. This has its origins in retaining the right-hand rule and the correct sign of the Poynting vector. To account for this, use is made of the following polarisation vector identity [12]:

$$\bar{e}^{(\eta)}\left(\boldsymbol{k}\right) = -e^{(\eta)}\left(-\boldsymbol{k}\right);$$

(4.2.2)

and the resultant operations of P on circularly polarised states of light are found to be

$$P\left(e^{(\mathrm{L/R})}\left(\boldsymbol{k}\right)\right) = -e^{(\mathrm{L/R})}\left(-\boldsymbol{k}\right),$$

$$P\left(b^{(\mathrm{L/R})}\left(\boldsymbol{k}\right)\right) = P\left(\hat{\boldsymbol{k}} \times e^{(\mathrm{L/R})}\left(\boldsymbol{k}\right)\right) = -\hat{\boldsymbol{k}} \times -e^{(\mathrm{L/R})}\left(-\boldsymbol{k}\right) = b^{(\mathrm{L/R})}\left(-\boldsymbol{k}\right).$$

(4.2.3)

Therefore, spatial inversion changes the sign of the electric, but not the magnetic polarisation vectors. This agrees with the well-known fact that the electric field is a true or polar vector, and the magnetic field is an axial or pseudovector. However, it is worth highlighting the fact that the symmetry assertions for the electromagnetic fields are true only for the fields as a whole, and do not necessarily apply when considering specific modes.

For the purposes of the analysis in this Chapter, we require the simple results from the above considerations that the operation of the spatial parity P on a chiral molecule results in a swapping of molecular handedness. And for the radiation, the two parts that have the capacity to carry a sense of handedness, namely the circular polarisation state and the sense of direction of the twisted beam manifest through the sign of the topological charge, will also be a swapping of the handedness.

4.3 OPTICAL ORBITAL ANGULAR MOMENTUM

It has been shown in Chapter 1 that Maxwell's equations, although generally given in terms of the electric and magnetic fields, can be cast in terms of the vector $\boldsymbol{a}$ and scalar ϕ potentials, and implementing this yields the wave equation (1.6.5). Throughout this chapter, and indeed most experimental and theoretical work in the field of optical orbital angular momentum, we restrict the equations to the *paraxial approximation* [13]. This is a justified simplification due to the fact that in general, during laser beam propagation, the wave vectors of the field fall within a narrow cone with a small inclination to the optical axis, which is conventionally defined as being the z-axis. This restricts beam propagation to the z-axis, and that the component of $\boldsymbol{k}$ in the xy-plane is small compared to the z-component: $k_z \approx k = \omega/c$. Thus, in the paraxial regime, an ansatz for the vector field $\boldsymbol{a}$ is

$$\boldsymbol{a}(\boldsymbol{r},t) = \boldsymbol{e}u(x,y,z)\mathrm{e}^{(ikz-i\omega t)}, \tag{4.3.1}$$

where $\boldsymbol{e}$ is a polarisation vector normal to $\hat{z}$ and $u(x,y,z)$ is the transverse amplitude.

It follows that $u(x,y,z)$ must satisfy the paraxial scalar Helmholtz equation:

$$\left(\frac{\partial^2}{\partial x^2} + \frac{\partial^2}{\partial x^2}\right)u(x,y,z) + 2ik\frac{\partial}{\partial z}u(x,y,z) = 0. \tag{4.3.2}$$

There exists many light beams which are solutions to the paraxial equation (4.3.2). Examples include Hermite-Gaussian beams and Bessel beams. It is worth mentioning, however, that non-paraxial wave solutions do exist for the full Helmholtz equation. For reasons outlined above, however, we will restrict ourselves to paraxial light beams. One such solution that is widely utilised to describe laser fields possessing an orbital angular momentum are the

Laguerre-Gaussian modes.[4] These LG modes have a cylindrical symmetry and therefore are more conveniently expressed in cylindrical coordinates, consisting of an off-axis radial distance r, axial position z and azimuthal angle ϕ. As a consequence, LG beams are solutions to (4.3.2) when it is expressed in cylindrical coordinates

$$\left(\frac{1}{r}\frac{\partial}{\partial r} + \frac{\partial^2}{\partial r^2} + \frac{1}{r^2}\frac{\partial^2}{\partial \phi^2} + 2ik\frac{\partial}{\partial z} \right) u_{\ell,p}^{\mathrm{LG}}(r,\phi,z) = 0,$$ (4.3.3)

where the normalised solution for the amplitude $u_{\ell,p}^{\mathrm{LG}}(r,\phi,z)$ is

$$u_{\ell,p}^{\mathrm{LG}}(r,\phi,z) = \frac{C_p^{|\ell|}}{w(z)}\left[\frac{\sqrt{2}r}{w(z)} \right]^{|\ell|} \mathrm{e}^{\left(-r^2/w^2(z)\right)} L_p^{|\ell|}\left(\frac{2r^2}{w^2(z)} \right)$$

$$\times \exp\left[-i\frac{kr^2 z}{2\left(z^2 + z_R^2\right)} - i\ell\phi + i\left(2p + \ell + 1\right)\arctan\left(\frac{z}{z_R} \right) \right],$$ (4.3.4)

with the normalisation constant taking the form $C_p^{|\ell|} = \sqrt{2^{|\ell|+1} p!\big/\left[\pi\left(p+|\ell|\right)! \right]}$; $w(z) = w_0\sqrt{1+\left(z\right)^2\big/\left(z_R\right)^2}$ is the radius of the beam at z, with w_0 the Gaussian beam-waist at $z = 0$; $\left(2p+\ell+1\right)\arctan\left(z/z_R\right)$ is known as the Gouy phase; z_R is the Rayleigh range (a measure of the focal region of the beam); and finally $L_p^{|\ell|}$ is the generalised Laguerre polynomial of order p, which for a given argument x are found using

$$L_p^{\ell}(x) = \sum_{n=0}^{p}(-1)^n \binom{p+\ell}{p-n}\frac{1}{n}x^n.$$ (4.3.5)

The Rayleigh range is a measure of how sustained the collimation of the beam is over z, and experimentally for LG beams it can be in the order of several metres. In considering beam

interactions with particles it is therefore reasonable to assume $z_R \gg z$. In the long Rayleigh range, we have

$$w(z) = w_0, \tag{4.3.6}$$

$$\frac{kr^2 z}{2(z^2 + z_R^2)} \to 0, \tag{4.3.7}$$

and

$$(2p + \ell + 1)\arctan\left(\frac{z}{z_R}\right) \to 0. \tag{4.3.8}$$

These allow the amplitude $u_{\ell,p}^{\mathrm{LG}}(r, \phi, z)$ to take the form of

$$u_{\ell,p}^{\mathrm{LG}}(r, \phi, z) \equiv u_{\ell,p}^{\mathrm{LG}}(r, \phi) = f_{\ell,p}(r)\mathrm{e}^{-i\ell\phi}, \tag{4.3.9}$$

where the radial distribution function $f_{\ell,p}(r)$ is given by

$$f_{\ell,p}(r) = \frac{C_p^{|\ell|}}{w_0}\left[\frac{\sqrt{2}r}{w_0}\right]^{|\ell|}\mathrm{e}^{(-r^2/w_0^2)}L_p^{|\ell|}\left(\frac{2r^2}{w_0^2}\right). \tag{4.3.10}$$

Transitioning to the quantum theory, the electric displacement and magnetic field expansions for Laguerre-Gaussian beams in the paraxial approximation emerge as functions of the

cylindrical coordinates [14, 15]: the off-axis radial distance r, axial position z and azimuthal angle ϕ

$$
\begin{aligned}
\boldsymbol{d}^{\perp}\left(\boldsymbol{r}\right) = i \sum_{\boldsymbol{k},\eta,\ell,p} & \left(\frac{\hbar c k \varepsilon_0}{2V}\right)^{1/2} \left[\boldsymbol{e}_{\ell,p}^{(\eta)}\left(\boldsymbol{k}\right) a_{\ell,p}^{(\eta)}\left(\boldsymbol{k}\right) f_{\ell,p}\left(r\right) \mathrm{e}^{(ikz+i\ell\phi)} \right. \\
& \left. -\overline{\boldsymbol{e}}_{\ell,p}^{(\eta)}\left(\boldsymbol{k}\right) a_{\ell,p}^{\dagger(\eta)}\left(\boldsymbol{k}\right) \overline{f}_{\ell,p}\left(r\right) \mathrm{e}^{-(ikz+i\ell\phi)} \right],
\end{aligned}
$$

(4.3.11)

and

$$
\begin{aligned}
\boldsymbol{b}\left(\boldsymbol{r}\right) = i \sum_{\boldsymbol{k},\eta,\ell,p} & \left(\frac{\hbar k}{2\varepsilon_0 c V}\right)^{1/2} \left[\boldsymbol{b}_{\ell,p}^{(\eta)}\left(\boldsymbol{k}\right) a_{\ell,p}^{(\eta)}\left(\boldsymbol{k}\right) f_{\ell,p}\left(r\right) \mathrm{e}^{(ikz+i\ell\phi)} \right. \\
& \left. -\overline{\boldsymbol{b}}_{\ell,p}^{(\eta)}\left(\boldsymbol{k}\right) a_{\ell,p}^{\dagger(\eta)}\left(\boldsymbol{k}\right) \overline{f}_{\ell,p}\left(r\right) \mathrm{e}^{-(ikz+i\ell\phi)} \right],
\end{aligned}
$$

(4.3.12)

where $a_{\ell,p}^{(\eta)}\left(\boldsymbol{k}\right)$ and $a_{\ell,p}^{\dagger(\eta)}\left(\boldsymbol{k}\right)$ are the annihilation and creation operators for a photon of mode $\left(\boldsymbol{k},\eta,\ell,p\right)$. The most significant part of (4.3.11) and (4.3.12) is the azimuthal angular dependence contained in the term $\mathrm{e}^{-i\ell\phi}$. This azimuthal phase structure is what gives Laguerre-Gaussian modes their OAM. This term gives rise to $|\ell|$ intertwined helical wave-fronts, and these wave-fronts can twist either clockwise or anticlockwise as they propagate. This twist direction, determined by the sign of ℓ, gives the helices their handedness: by definition, for $\ell > 0$, beams twist to the left and for $\ell < 0$, to the right. Therefore, light propagating with any form of helical wavefront is inherently chiral. It is for this reason that it would be reasonable to anticipate chiroptical interactions with respect to the orbital angular momentum, in an analogous way to how chirally discriminant effects are manifest through spin orbital angular momentum and circular polarised light.

4.4   TWISTED LIGHT INTERACTING WITH CHIRAL MATTER

There exist a multitude of optical processes and phenomena that are ideally suited for carrying out an explicit analysis looking at whether the handedness of twisted light can play a role in chiroptical interactions. The optical rates or energy shifts of all such discriminatory interactions are sensitive to the handedness of the molecules and/or the handedness of the light. Well-known optical processes and phenomena that are explicitly chiroptical in their nature are circular dichroism [16-18], optical rotation [19], differential Raman and Rayleigh scattering [20, 21], and induced circular dichroism [22]. There also exists the case of discriminatory absorption of left- and right-handed photons by achiral molecules, known as magnetic circular dichroism [23], and chiroptical interactions in intermolecular forces as outlined in Chapter 5, as well as chiral discriminatory forces in optical trapping.

The most elementary of these chiroptical interactions is arguably circular dichroism – which is simply a difference in the rate of one-photon absorption of circularly polarised photons by chiral molecules. For this reason, in the first instance, it seems logical to focus the analysis of how twisted beam handedness interacting with molecules could potentially exhibit a chiroptical influence on one-photon absorption. Indeed, previous work looking at OAM and chirality in light-matter interactions has focused on E1 and M1 couplings in one-photon absorption [24]. These analyses concluded that wavefront handedness should, up to the order of multipole interaction studied, provide no chiroptical influence in optical processes. Their prediction was then met with experimental verification [25, 26]. However, the following analysis will highlight that due consideration of electric quadrupole (E2) moments and the degree of orientational order of the matter will indeed reveal a basis for the helicity associated with photon OAM to exhibit a chiroptical influence in one-photon absorption: the rate of absorption will depend on which direction the vortex beam is twisting and therefore the sign of the topological charge. To elucidate all the physics and produce a fully rigorous result up to the chosen multipolar level, we will also include M1 interactions in our analysis. We need not include diamagnetic D1 couplings as this is a single-photon interaction (see Chapter 3).

Once again, the Power-Zienau-Woolley Hamiltonian is adopted (Equation 1.16.15). The quantum amplitude of one-photon absorption by a molecule ξ in its ground state, subjected to an incident LG beam of n photons in a single mode (k, η, ℓ, p), is

$$M_{fi} = \langle \text{final} | H_{\text{int}} | \text{initial} \rangle = \langle f | -\varepsilon_0^{-1} \mu_i(\xi) d_i^\perp - m_i(\xi) b_i - \varepsilon_0^{-1} Q_{ij}(\xi) \nabla_j d_i^\perp | 0 \rangle$$

$$= -\varepsilon_0^{-1} \langle E_f | \mu_i(\xi) | E_0 \rangle \langle (n-1) | d_i^\perp(\boldsymbol{r}) | n \rangle - \langle E_f | m_i(\xi) | E_0 \rangle \langle (n-1) | b_i(\boldsymbol{r}) | n \rangle$$
$$- \varepsilon_0^{-1} \langle E_f | Q_{ij}(\xi) | E_0 \rangle \langle (n-1) | \nabla_j d_i^\perp(\boldsymbol{r}) | n \rangle$$

$$= -\varepsilon_0^{-1} \mu_i^{f0}(\xi) \langle (n-1) | d_i^\perp(\boldsymbol{r}) | n \rangle - m_i^{f0}(\xi) \langle (n-1) | b_i(\boldsymbol{r}) | n \rangle$$
$$- \varepsilon_0^{-1} Q_{ij}^{f0}(\xi) \langle (n-1) | \nabla_j d_i^\perp(\boldsymbol{r}) | n \rangle. \tag{4.4.1}$$

For clarity, all photon mode dependence will be assumed rather than explicitly stated throughout the analysis, and we can also drop the ξ label for the same reason. It is also easier to explicitly calculate each of the three terms in (4.4.1) on a term by term basis, where we use the mode expansions given in (4.3.11) and (4.3.12)

$$-\varepsilon_0^{-1} \mu_i^{f0} \langle (n-1) | d_i^\perp(\boldsymbol{r}) | n \rangle = -i \left(\frac{n\hbar c k}{2\varepsilon_0 V} \right)^{1/2} f_{\ell,p}(r) e_i \mu_i^{f0} e^{(ikz + i\ell\phi)}, \tag{4.4.2}$$

$$-m_i^{f0} \langle (n-1) | b_i(\boldsymbol{r}) | n \rangle = -i \left(\frac{n\hbar k}{2\varepsilon_0 c V} \right)^{1/2} f_{\ell,p}(r) b_i m_i^{f0} e^{(ikz + i\ell\phi)}, \tag{4.4.3}$$

$$-\varepsilon_0^{-1} Q_{ij}^{f0} \langle (n-1) | \nabla_j d_i^\perp(\boldsymbol{r}) | n \rangle = -i \left(\frac{n\hbar c k}{2\varepsilon_0 V} \right)^{1/2} f_{\ell,p}(r) e_i Q_{ij}^{f0} \nabla_j e^{(ikz + i\ell\phi)}. \tag{4.4.4}$$

To move towards calculating a rate with the aid of the Fermi rule, it is necessary to carry out the gradient operation present in (4.4.4). The operator is, in cylindrical coordinates

$$\nabla_j = \frac{\partial}{\partial r}\hat{r}_j + \frac{1}{r}\frac{\partial}{\partial \phi}\hat{\phi}_j + \frac{\partial}{\partial z}\hat{z}_j,$$

(4.4.5)

where

$$\hat{r} = \cos\phi\,\hat{x} + \sin\phi\,\hat{y}$$
$$\hat{\phi} = -\sin\phi\,\hat{x} + \cos\phi\,\hat{y}$$
$$\hat{z} = \hat{z}.$$

(4.4.6)

In Cartesian coordinates, $\dfrac{\partial \hat{i}}{\partial i} = 0$ (where $i = x,\ y,$ or z), however this is not necessarily the case for the corresponding cylindrical coordinates as can be seen from (4.4.6):

$$\frac{\partial \hat{\phi}}{\partial \phi} = \frac{\partial}{\partial \phi}\left(-\sin\phi\,\hat{x} + \cos\phi\,\hat{y}\right) = -\cos\phi\,\hat{x} - \sin\phi\,\hat{y} = -\hat{r}.$$

(4.4.7)

With the characteristics of the gradient operator outlined above, it can now be implemented and used to evaluate the E2 contribution to the matrix element (4.4.4),

$$\nabla_j f_{\ell,p}(r) e^{(ikz+i\ell\phi)} = f_{\ell,p}(r)\frac{\partial}{\partial r}\hat{r}_j e^{(ikz+i\ell\phi)} + f_{\ell,p}(r)\frac{1}{r}\frac{\partial}{\partial\phi}\hat{\phi}_j e^{(ikz+i\ell\phi)} + f_{\ell,p}(r)\frac{\partial}{\partial z}\hat{z}_j e^{(ikz+i\ell\phi)}$$

$$= e^{(ikz+i\ell\phi)}\left[f_{\ell,p}(r)\frac{\partial\hat{r}_j}{\partial r} + \hat{r}_j\frac{\partial f_{\ell,p}(r)}{\partial r}\right] + f_{\ell,p}(r)\frac{1}{r}\left[\frac{\partial\hat{\phi}_j}{\partial\phi}e^{i\ell\varphi} + \hat{\phi}_j\frac{\partial e^{i\ell\phi}}{\partial\phi}\right]e^{ikz}$$

$$+ f_{\ell,p}(r)\left[\frac{\partial\hat{z}_j}{\partial z}e^{ikz} + \hat{z}_j\frac{\partial e^{ikz}}{\partial z}\right]e^{i\ell\phi}$$

$$= \hat{r}_j\frac{\partial f_{\ell,p}(r)}{\partial r}e^{(ikz+i\ell\phi)} + f_{\ell,p}(r)\frac{1}{r}\left(i\ell\hat{\phi}_j - \hat{r}_j\right)e^{(ikz+i\ell\phi)}$$

$$+ f_{\ell,p}(r)ik\hat{z}_j e^{(ikz+i\ell\phi)}.$$

$$(4.4.8)$$

This result allows (4.4.4) to be written in a form where the gradient operation has been carried out

$$-\varepsilon_0^{-1}Q_{ij}^{f0}\left\langle(n-1)\middle|\nabla_j d_i^\perp(r)\middle|n\right\rangle = -i\left(\frac{n\hbar ck}{2\varepsilon_0 V}\right)^{1/2}f_{\ell,p}(r)e_i Q_{ij}^{f0}$$

$$\times\left[\frac{1}{f_{\ell,p}(r)}\frac{\partial f_{\ell,p}(r)}{\partial r}\hat{r}_j + \frac{1}{r}\left(i\ell\hat{\phi}_j - \hat{r}_j\right) + ik\hat{z}_j\right]e^{(ikz+i\ell\phi)}. \qquad (4.4.9)$$

Using (4.4.2), (4.4.3), and (4.4.9) gives the total quantum amplitude as

$$M_{fi} = -i\left(\frac{n\hbar ck}{2\varepsilon_o V}\right)^{1/2}f_{\ell,p}(r)$$

$$\times\left(\underbrace{e_i\mu_i^{f0}}_{E1} + \underbrace{\frac{1}{c}b_i m_i^{f0}}_{M1} + \underbrace{e_i Q_{ij}^{f0}\left(\hat{r}_j\frac{1}{f_{\ell,p}(r)}\frac{\partial f_{\ell,p}(r)}{\partial r} + \frac{1}{r}\left(i\ell\hat{\phi}_j - \hat{r}_j\right) + ik\hat{z}_j\right)}_{E2}\right)e^{(ikz+i\ell\hat{\phi})}. \quad (4.4.10)$$

The matrix element is now in a suitable form to secure the rate of one-photon absorption, with the aid of the Fermi rule, where $\Gamma \sim \left| M_{fi} \right|^2$, and taking term by term:

$$\mathrm{E1\bar{E}1} = \left(\frac{n\hbar ck}{2\varepsilon_o V} \right) f_{\ell,p}{}^2(r) e_i \bar{e}_k \mu_i^{f0} \bar{\mu}_k^{f0}, \tag{4.4.11}$$

$$\mathrm{M1\bar{M}1} = \left(\frac{n\hbar k}{2c\varepsilon_o V} \right) f_{\ell,p}{}^2(r) b_i \bar{b}_k m_i^{f0} \bar{m}_k^{f0}, \tag{4.4.12}$$

$$\mathrm{E1\bar{M}1} = \left(\frac{n\hbar k}{2\varepsilon_o V} \right) f_{\ell,p}{}^2(r) e_i \bar{b}_k \mu_i^{f0} \bar{m}_k^{f0}, \tag{4.4.13}$$

$$\mathrm{\bar{E}1M1} = \left(\frac{n\hbar k}{2\varepsilon_o V} \right) f_{\ell,p}{}^2(r) \bar{e}_k b_i \bar{\mu}_k^{f0} m_i^{f0}, \tag{4.4.14}$$

$$\mathrm{M1\bar{E}2} = \left(\frac{n\hbar k}{2\varepsilon_o V} \right) f_{\ell,p}{}^2(r) b_i \bar{e}_k m_i^{f0} \bar{Q}_{kj}^{f0} \left(\hat{r}_j \frac{1}{f_{\ell,p}(r)} \frac{\partial f_{\ell,p}(r)}{\partial r} + \frac{1}{r} \left(-i\ell \hat{\phi}_j - \hat{r}_j \right) - ik\hat{z}_j \right), \tag{4.4.15}$$

$$\mathrm{\bar{M}1E2} = \left(\frac{n\hbar k}{2\varepsilon_o V} \right) f_{\ell,p}{}^2(r) \bar{b}_k e_i \bar{m}_k^{f0} Q_{ij}^{f0} \left(\hat{r}_j \frac{1}{f_{\ell,p}(r)} \frac{\partial f_{\ell,p}(r)}{\partial r} + \frac{1}{r} \left(i\ell \hat{\phi}_j - \hat{r}_j \right) + ik\hat{z}_j \right), \tag{4.4.16}$$

$$\mathrm{E1\bar{E}2} = \left(\frac{n\hbar ck}{2\varepsilon_o V} \right) f_{\ell,p}{}^2(r) e_i \bar{e}_k \mu_i^{f0} \bar{Q}_{kj}^{f0} \left(\hat{r}_j \frac{1}{f_{\ell,p}(r)} \frac{\partial f_{\ell,p}(r)}{\partial r} + \frac{1}{r} \left(-i\ell \hat{\phi}_j - \hat{r}_j \right) - ik\hat{z}_j \right), \tag{4.4.17}$$

$$\bar{E}1E2 = \left(\frac{n\hbar ck}{2\varepsilon_o V}\right) f_{\ell,p}{}^2(r) e_i \bar{e}_k \bar{\mu}_k^{f0} Q_{ij}^{f0} \left(\hat{r}_j \frac{1}{f_{\ell,p}(r)} \frac{\partial f_{\ell,p}(r)}{\partial r} + \frac{1}{r}\left(i\ell\hat{\phi}_j - \hat{r}_j\right) + ik\hat{z}_j\right), \qquad (4.4.18)$$

$$E2\bar{E}2 = \left(\frac{n\hbar ck}{2\varepsilon_o V}\right) f_{\ell,p}{}^2(r) e_i \bar{e}_k Q_{ij}^{f0} \bar{Q}_{kl}^{f0} \left(\hat{r}_j \frac{1}{f_{\ell,p}(r)} \frac{\partial f_{\ell,p}(r)}{\partial r} + \frac{1}{r}\left(i\ell\hat{\phi}_j - \hat{r}_j\right) + ik\hat{z}_j\right)$$
$$\times \left(\hat{r}_l \frac{1}{f_{\ell,p}(r)} \frac{\partial f_{\ell,p}(r)}{\partial r} + \frac{1}{r}\left(-i\ell\hat{\phi}_l - \hat{r}_l\right) - ik\hat{z}_l\right). \qquad (4.4.19)$$

Clearly, the terms that depend on the handedness of the vortex beam through a linear dependence on ℓ include the E1E2, M1E2, and E2E2 contributions (notice that all involve the quadrupole E2 moment). The E1E1 term is the standard result for one-photon absorption in the electric dipole approximation and is not influenced by the chirality of either the molecules or the radiation; the M1M1 is the magnetic dipole contribution to the one-photon absorption rate, smaller than the E1E1 by about 10^{-6}, and it too is not discriminatory; the E1M1 terms are discriminatory, being the leading order contributions to circular dichroism (CD), in which the one-photon absorption rate is dependent on the helicity of the input circularly polarised photons and the handedness of the molecules − but the handedness of a vortex beam has no influence upon the rate of CD.

With recourse to Section 4.2, it is appropriate to remind ourselves of the space parity of the multipole moments; E1 (-1), M1 (+1), and E2 (+1). Therefore, the M1E2 and E2E2 multipole moment products have even space parity, and therefore replacing one chiral molecule with its corresponding enantiomer of opposite handedness (equivalent to parity inversion) leaves these multipole moment products invariant. It can be therefore be concluded that M1E2 and E2E2 have no chiroptical sensitivity with regards to the material component of the system. This doesn't rule out the possibility of discriminatory effects with regards to the helicity of the radiation part of the system − we return to this issue in the Appendix 4.1. In contrast to the M1E2 and E2E2, the E1E2 multipole couplings will change sign under parity inversion, and therefore E1E2 contributions to the overall rate of one-photon absorption will be sensitive to the particular handedness of the molecules and the sign of ℓ. Therefore, collecting these terms which have chiroptical sensitivity to both the material and vortex twist, and invoking the all the components of the Fermi rule, yields the modified rate

$$\Gamma'(\ell) = \frac{2\pi}{\hbar} \frac{n\hbar ck}{2\varepsilon_0 V} N\rho_f \frac{1}{r} f_{\ell,p}^{\ 2}(r) e_i \bar{e}_k i\ell\hat{\phi}_j \left(\bar{\mu}_k^{f0} Q_{ij}^{f0} - \mu_i^{f0} \bar{Q}_{kj}^{f0} \right), \tag{4.4.20}$$

where N is the number of absorbers. Writing the density of final states in terms of the irradiance per unit frequency interval $I(\omega)$ (of which integration over the frequency gives the beam intensity)

$$\rho_f = \frac{I(\omega)V}{2\pi nc\hbar^2\omega}, \tag{4.4.21}$$

allows the modified rate to be written as

$$\Gamma'(\ell) = \frac{I(\omega)N}{2c\hbar^2\varepsilon_o} \frac{1}{r} f_{\ell,p}^{\ 2}(r) e_i \bar{e}_k i\ell\hat{\phi}_j \left(\bar{\mu}_k^{f0} Q_{ij}^{f0} - \mu_i^{f0} \bar{Q}_{kj}^{f0} \right). \tag{4.4.22}$$

Evidently, since all the other parameters in (4.4.22) are real, the polarisation vectors must be complex quantities to produce a non-zero real result. Therefore, at the most significant order of E1E2, we would only expect a chiroptical response if the incident photons are circularly polarised. This has the interesting and somewhat unique property that to this order, the orbital angular momentum of light alone cannot produce chiroptical effects, and that only in conjunction with spin angular momentum is it possible to engage the handedness of vortex beams in discriminatory interactions with chiral molecules. In this sense, the process is an analogue of circular dichroism but with beams carrying a topological charge, a chiroptical effect that can be termed circular-vortex dichroism (CVD).

Recently, there has been experimentally verified discriminatory effects with vortex beams involving linear polarisation of states, termed 'helical dichroism' [27]. This is made possible when molecular responses are modified through plasmonic resonance [28-30]. The possibility of dichroism depending only on the twisted wavefront and molecule handedness

are not ruled out in the analysis here, but they do not arise in the leading E1E2 level of multipolar interaction of molecules in the paraxial approximation, which this analysis is concerned with. Nor is theory employed here suitable to study light interacting with matter that has an extensively delocalised electron structure.

To proceed, we make use of the following identity

$$e_i^{\mathrm{L}} \overline{e}_k^{\mathrm{L}} = \frac{1}{2}\left[\left(\delta_{ik} - \hat{k}_i \hat{k}_k\right) - i\varepsilon_{ikm}\hat{k}_m\right],$$

$$(4.4.23)$$

$$e_i^{\mathrm{R}} \overline{e}_k^{\mathrm{R}} = \frac{1}{2}\left[\left(\delta_{ik} - \hat{k}_i \hat{k}_k\right) + i\varepsilon_{ikm}\hat{k}_m\right].$$

Therefore, retaining only the real terms

$$\Gamma'^{(\mathrm{L/R})}\left(\ell\right) = \pm \frac{I\left(\omega\right)N}{4c\hbar^2 \varepsilon_o}\frac{1}{r}f_{\ell,p}{}^2\left(r\right)\varepsilon_{ikm}\hat{k}_m\ell\hat{\phi}_j\left(\overline{\mu}_k^{f0}Q_{ij}^{f0} - \mu_i^{f0}\overline{Q}_{kj}^{f0}\right). \qquad (4.4.24)$$

The result can also be written in terms of the absolute difference in absorption rates between left- and right-handed circularly polarised photons [31, 32]

$$\Gamma^{(\mathrm{L})} - \Gamma^{(\mathrm{R})} = \Delta\Gamma_{\mathrm{CD}} + \frac{I\left(\omega\right)N}{2c\hbar^2 \varepsilon_0}\frac{1}{r}f_{\ell,p}^2\left(r\right)\varepsilon_{ikm}\hat{k}_m\hat{\phi}_j\ell\left(\mu_k^{f0}Q_{ij}^{f0} + \mu_i^{f0}Q_{kj}^{f0}\right), \qquad (4.4.25)$$

where $\Delta\Gamma_{\mathrm{CD}}$ has been included and represents all of the terms that no dependence on the sign of the topological charge ℓ. These terms are seen to be:

$$\Delta\Gamma_{CD} = \Gamma^{(L)} - \Gamma^{(R)}$$

$$= \frac{2\pi N}{\hbar}\left(\frac{n\hbar ck}{2\varepsilon_0 V}\right)\rho_f f_{\ell,p}{}^2(r)\left[\frac{1}{c}\left(\delta_{ik} - \hat{k}_i\hat{k}_k\right)\left(\mu_i^{f0}\overline{m}_k'^{f0} - \overline{\mu}_k^{f0}m_i'^{f0}\right)\right.$$
$$\left. -\varepsilon_{ikm}\hat{k}_m k\hat{z}_j\left(\mu_i^{f0}Q_{kj}^{f0} - \mu_k^{f0}Q_{ij}^{f0}\right)\right], \tag{4.4.26}$$

where $m_i'^{f0} = im_i^{f0}$. The above result is simply the sum of the E1E2 and E1M1 contributions which have no dependence on the sign or magnitude of ℓ from (4.4.13), (4.4.14), (4.4.17), and (4.4.18). They represent a form for LG beams that is in full agreement with the well-known results for standard CD with non-vortex light reported by Craig and Thirunamachandran [9]. It is important to retain these terms as when $\ell = 0$, the total rate (4.4.25) reduces to the standard result for conventional CD.

It is interesting to comment on the magnitude of the CVD contributions, particularly in comparison with the CD rate. When all E1, E2 and M1 couplings are accounted for, and since E2 and M1 interactions with the field are approximately equal in strength, it is expected that the strength of CVD will be approximately the same as CD. It is worth remembering, however, that CVD does scale linearly ℓ. This also agrees with the fact that both the spin angular momentum and orbital angular momentum contribute on the same level of magnitude to the overall angular momentum flux.

As it stands, (4.4.25) applies to one or more molecules with a fixed orientation in any point in the LG beams (it is a local effect). The $\hat{\phi}_j$ term contracts with an index of the quadrupole transition moment (which itself has a fixed orientation within the molecule) and therefore the magnitude and sign of the CVD differential will in general vary around the beam axis. Specifically, for any given sign of ℓ, the CVD rate will vary between a maximum and minimum of opposite sign across the beam profile: the angular variation of CVD intensity exhibits a simple sinusoidal dependence. This is due to the different directions of phase gradient around each intensity ring that are experienced by chiral molecules with a common orientation. Therefore, for a system of molecules that possess a degree of orientational order, the observed differential will be enhanced on one side of the beam and equally diminished on the other (as compared to the standard CD value along the singular core). One way to fully verify this mechanism would be to conduct experiments with varying values of ℓ and

plot the measured differential $\Gamma^{(L)} - \Gamma^{(R)}$, necessarily taking account of the differences in intensity distribution associated with the corresponding radial distribution functions $f_{\ell,p}(r)$. It is worth bearing in mind, however, that due to the radial and azimuthal components being symmetrical about the z axis, any integration over the beam profile will only leave terms that are dependent solely on z: namely, the standard CD terms (4.4.26). This means that the net result of CVD will be zero if looking at the whole beam profile. Most experiments do not resolve the extent of absorption at different locations within the beam profile, but this is what would be needed to observe the effect of CVD.

To complete the analysis, we now consider the case where the molecules possess no sense of orientational order. Such a randomly orientated distribution of optical centres occurs in molecular fluids. To elucidate the effect that random orientation has on the rate of CVD we have to perform an isotropic rotational average [33] of the expression (4.4.25). This requires the E1-E2 and E2-E1 terms to be contracted with the corresponding third rank Levi-Civita isotropic tensor. However, since the electric quadrupole moment is fully index symmetric, and the Levi-Civita is antisymmetric in its indices, the resulting molecular average is zero. Therefore, it can be concluded that the rate of CVD is zero for fully randomly oriented molecules. Differential one-photon absorption with a circularly polarised vortex beam is therefore only non-zero for systems that possess a degree of ordering.

4.5 DISCUSSION

In light of the analysis of the previous section on molecular orientational averaging, it is worth discussing the possibility of specially designed systems for introducing molecular order. Although molecular fluids are generally isotropic, there are potential ways to engineer special systems for chiral effects using twisted light. Such systems are routinely employed in nonlinear optics [34], where the generation of second harmonics is usually precluded in isotropic fluids, and allow normally forbidden transitions to occur. One potential method involves exploiting the degree of molecular ordering that is present at the boundaries of isotropic systems [35]. Other ways would be introducing molecular alignment using optical methods [36], or introducing a magnetic field to induce symmetry breaking [37]. Another interesting point is that although E2 moments usually generate small contributions to the

overall amplitude of an optical process due to their dependence on the gradient of the electromagnetic field, in vortex beams the gradient of the field becomes increasingly significant as the topological charge increases. Indeed, this is manifest in (4.4.25) through the linear dependence on ℓ . This enhanced role of E2 moments is already recognised with vortex beams interacting with atoms and molecules [38-41].

The aim of this Chapter was to consider whether the orbital angular momentum of light could produce chiroptical interactions with chiral molecules. Previous work has correctly concluded that in neither E1 nor M1 interactions could the vortex handedness play any role in chiroptical interactions. However, it has now been clearly demonstrated to the leading order that any potential discriminatory process with respect to the topological charge of vortex beams must engage with the quadrupole E2 moment of the material component. For the most generally significant order whereby these effects are anticipated - the interference term E1E2 - it was found that for one-photon absorption the material component must possesses a degree of molecular ordering, and the beam must also possesses circular polarisation. This process was termed circular-vortex dichroism (CVD), due to its similarity to regular circular dichroism. Clearly, for any optical process the E2 moment must be engaged for any anticipation of OAM-dependent chiroptical interactions, beyond this, however, any detailed conclusions about the polarisation state and/or molecular orientation requires specific analysis.

The idea of whether vortex handedness can play a role in chiroptical interactions has been subject to much uncertainty since twisted light was discovered, and the many viewpoints on the issue are in a constant flux. However, it is hoped that the analysis presented here progresses the field further and will provide a broader basis and further stimulus for experimental and theoretical work on the potentially significant role that vortex handedness can now be anticipated to play in chiroptical interactions.

APPENDIX 4.1

Calculating the full rate of one-photon absorption using the Fermi rule with the total matrix element given by (4.4.10), produces a rate which includes all E1, E2 and M1 multipole couplings and their interference terms:

$$
\Gamma = \frac{2\pi}{\hbar} \rho_f \left(\frac{n\hbar ck}{2\varepsilon_o V} \right) f_{\ell,p}{}^2(r)
$$

$$
\sum_{\xi} \left\{ e_i \bar{e}_k \left[\underbrace{\mu_i^{f0} \bar{\mu}_k^{f0}}_{\text{E1E1}} + \mu_i^{f0} \bar{Q}_{kl}^{f0} \underbrace{\left(\hat{r}_l \frac{1}{f_{\ell,p}(r)} \frac{\partial f_{\ell,p}(r)}{\partial r} + \frac{1}{r}\left(-i\ell\hat{\varphi}_l - \hat{r}_l\right) - ik\hat{z}_l \right)}_{\text{E1}\bar{\text{E}}2} \right. \right.
$$

$$
\left. + \underbrace{\bar{\mu}_k^{f0} Q_{ij}^{f0} \left(\hat{r}_j \frac{1}{f_{\ell,p}(r)} \frac{\partial f_{\ell,p}(r)}{\partial r} + \frac{1}{r}\left(i\ell\hat{\varphi}_j - \hat{r}_j\right) + ik\hat{z}_j \right)}_{\bar{\text{E}}1\text{E}2} \right.
$$

$$
\left. + \underbrace{\begin{array}{l} Q_{ij}^{f0} \bar{Q}_{kl}^{f0} \left(\hat{r}_j \frac{1}{f_{\ell,p}(r)} \frac{\partial f_{\ell,p}(r)}{\partial r} + \frac{1}{r}\left(i\ell\hat{\varphi}_j - \hat{r}_j\right) + ik\hat{z}_j \right) \\ \times \left(\hat{r}_l \frac{1}{f_{\ell,p}(r)} \frac{\partial f_{\ell,p}(r)}{\partial r} + \frac{1}{r}\left(-i\ell\hat{\varphi}_l - \hat{r}_l\right) - ik\hat{z}_l \right) \end{array}}_{\text{E2}\bar{\text{E}}2} \right]
$$

$$
+ \frac{1}{c} \left[\underbrace{e_i \bar{b}_k \mu_i^{f0} \bar{m}_k^{f0}}_{\text{E1}\bar{\text{M}}1} + \underbrace{\bar{e}_k b_i \bar{\mu}_k^{f0} m_i^{f0}}_{\bar{\text{E}}1\text{M}1} \right.
$$

$$
+ \underbrace{b_i \bar{e}_k m_i^{f0} \bar{Q}_{kl}^{f0} \left(\hat{r}_l \frac{1}{f_{\ell,p}(r)} \frac{\partial f_{\ell,p}(r)}{\partial r} + \frac{1}{r}\left(-i\ell\hat{\varphi}_l - \hat{r}_l\right) - ik\hat{z}_l \right)}_{\text{M}1\bar{\text{Q}}2}
$$

$$
\left. + \underbrace{\bar{b}_k e_i \bar{m}_k^{f0} Q_{ij}^{f0} \left(\hat{r}_j \frac{1}{f_{\ell,p}(r)} \frac{\partial f_{\ell,p}(r)}{\partial r} + \frac{1}{r}\left(i\ell\hat{\varphi}_j - \hat{r}_j\right) + ik\hat{z}_j \right)}_{\bar{\text{M}}1\text{Q}2} \right]
$$

$$
+ \frac{1}{c^2} \underbrace{b_i \bar{b}_k m_i^{f0} \bar{m}_k^{f0}}_{\text{M}1\bar{\text{M}}1} \Bigg\}.
\tag{A4.1}
$$

In the main body of work in the Chapter, we specifically identified those leading-order terms that were dependent on the sign of the handedness of the vortex beam through the sign of the topological charge and the handedness of the molecules. However, the full-derivation also produces other terms that are interesting. We have discussed the E1E1, M1M1, and E1E2 and E1M1 terms explicitly above. We will now concentrate on the remaining terms.

All the terms that have either a quadratic or linear dependence on the electric quadrupole moment (E2E2 and M1E2) are accompanied by a plethora of further physical quantities. Nearly all of these terms represent position-dependent effects, due to the nature of the LG beam structure and the interaction of the quadrupole moment with the variation of the vector potential. These contributions are local and therefore their net contribution is anticipated to be zero across the whole beam profile. Terms that depend on only $\hat{z}$ clearly survive a beam average, and represent higher-order contributions to standard one-photon absorption. For example, the term

$$\Gamma' = \frac{2\pi}{\hbar}\left(\frac{n\hbar ck}{2\varepsilon_o V}\right)N\rho_f f_{\ell,p}{}^2(r)k^2 e_i \bar{e}_k Q_{ij}^{f0}\bar{Q}_{kl}^{f0}\hat{z}_j\hat{z}_l, \tag{A4.2}$$

is in precise agreement with the standard electric quadrupole contribution to one-photon absorption, if the intensity distribution of an LG beam is taken account of [9]. There are then other terms, which will also survive a beam average, which represent the influence of the vortex structure on the E2E2 contribution to one-photon absorption:

$$\Gamma'' = \frac{2\pi}{\hbar}\left(\frac{n\hbar ck}{2\varepsilon_o V}\right)N\rho_f f_{\ell,p}{}^2(r)\frac{\ell^2}{r^2} e_i \bar{e}_k Q_{ij}^{f0}\bar{Q}_{kl}^{f0}\hat{\varphi}_j\hat{\varphi}_l. \tag{A4.3}$$

With regards to the multipole moments, the E2E2 and M1E2 couplings are clearly invariant - and possess even parity signature with regards to - the operation of spatial inversion *P*. Therefore, they could not play any role in chiroptical effects that have chiral sensitivity with regards to intrinsic molecular chirality. However, it does not rule out the possibility of seemingly chiral effects if LG beams with circular polarisation states were used. This

'mixing' of handedness between vortex structure and polarisation state has yet to be specifically studied, and a physical interpretation of this mixing of helicity is yet to be elucidated, so any conclusions cannot not be made with regards to whether it is a legitimate chiroptical effect. It will represent a possible avenue for future work both at a level of interest for its application, but also at the fundamental symmetry level. It is anticipated to be involved in issues of spin-orbit coupling. As outlined in the Discussion section of the main text, this current work is in its infancy at present, leaving many exciting questions to be answered by people engaged in the study of the angular momentum of light.

REFERENCES

[1]   A. Ashkin, *Acceleration and trapping of particles by radiation pressure*, Phys. Rev. Lett. **24**, 156 (1970).

[2]   D. L. Andrews and M. Babiker, *The Angular Momentum of Light* (Cambridge University Press, Cambridge, UK, 2013).

[3]   C. Darwin, *Notes on the theory of radiation*, Proc. R. Soc. A **136**, 36 (1932).

[4]   L. Allen, M. W. Beijersbergen, R. J. C. Spreeuw, and J. P. Woerdman, *Orbital angular momentum of light and the transformation of Laguerre-Gaussian laser modes*, Phys. Rev. A **45**, 8185 (1992).

[5]   D. L. Andrews, *Structured Light and its Applications: An Introduction to Phase-Structured Beams and Nanoscale Optical Forces* (Academic, Amsterdam, Boston, 2008).

[6]   S. M. Barnett, M. Babiker, and M. J. Padgett, *Optical orbital angular momentum* (The Royal Society, 2017), Vol. 375.

[7]   V. Garcés-Chávez, D. McGloin, M. Padgett, W. Dultz, H. Schmitzer, and K. Dholakia, *Observation of the transfer of the local angular momentum density of a multiringed light beam to an optically trapped particle*, Phys. Rev. Lett. **91**, 093602 (2003).

[8]   A. Mair, A. Vaziri, G. Weihs, and A. Zeilinger, *Entanglement of the orbital angular momentum states of photons*, Nature **412**, 313 (2001).

[9]   D. P. Craig and T. Thirunamachandran, *Molecular Quantum Electrodynamics: An Introduction to Radiation-Molecule Interactions* (Dover Publications, Mineola, NY, 1998).

[10]   L. D. Barron, *Molecular Light Scattering and Optical Activity* (Cambridge University Press Cambridge, UK, 2004), Vol. 2.

[11]   D. L. Andrews, *Quantum formulation for nanoscale optical and material chirality: symmetry issues, space and time parity, and observables*, J. Opt. **20**, 033003 (2018).

[12]   S. Naguleswaran and G. Stedman, *Onsager relations and time-reversal symmetry in nonlinear optics*, J. Phys. B: At. Mol. Opt. Phys. **31**, 935 (1998).

[13]   A. E. Siegman, *Lasers* (Oxford University Press, Oxford, 1986).

[14]   L. C. Dávila Romero, D. L. Andrews, and M. Babiker, *A quantum electrodynamics framework for the nonlinear optics of twisted beams*, J. Opt. B: Quantum Semiclass. Opt. **4**, S66 (2002).

[15]   G. Nienhuis, in *Structured Light and Its Applications* (Academic Press, Burlington, 2008).

[16]   E. Power and T. Thirunamachandran, *Circular dichroism: A general theory based on quantum electrodynamics*, J. Chem. Phys. **60**, 3695 (1974).

[17]   J. Riehl and F. Richardson, *General theory of circularly polarized emission and magnetic circularly polarized emission from molecular systems*, J. Chem. Phys. **65**, 1011 (1976).

[18]   B. Nordén, *Circular Dichroism and Linear Dichroism* (Oxford University Press, USA, 1997), Vol. 1.

[19]   P. L. Polavarapu, *Optical rotation: Recent advances in determining the absolute configuration*, Chirality **14**, 768 (2002).

[20]   D. L. Andrews and T. Thirunamachandran, *A quantum electrodynamical theory of differential scattering based on a model with two chromophores. I. Differential Rayleigh-scattering of circularly polarized-light*, Proc. R. Soc. A **358**, 297 (1978).

[21]   D. L. Andrews and T. Thirunamachandran, *A quantum electrodynamical theory of differential scattering based on a model with two chromophores. II. Differential Raman-scattering of circularly polarized-light*, Proc. R. Soc. A **358**, 311 (1978).

[22]   S. Allenmark, *Induced circular dichroism by chiral molecular interaction*, Chirality **15**, 409 (2003).

[23]   P. Stephens, *Magnetic circular dichroism*, Adv. Chem. Phys **35**, 197 (1976).

[24]   D. L. Andrews, L. C. Dávila Romero, and M. Babiker, *On optical vortex interactions with chiral matter*, Opt. Commun. **237**, 133 (2004).

[25]   F. Araoka, T. Verbiest, K. Clays, and A. Persoons, *Interactions of twisted light with chiral molecules: an experimental investigation*, Phys. Rev. A **71**, 055401 (2005).

[26]   W. Löffler, D. Broer, and J. Woerdman, *Circular dichroism of cholesteric polymers and the orbital angular momentum of light*, Phys. Rev. A **83**, 065801 (2011).

[27]   W. Brullot, M. K. Vanbel, T. Swusten, and T. Verbiest, *Resolving enantiomers using the optical angular momentum of twisted light*, Science Advances **2**, e1501349 (2016).

[28]   V. Valev, A. Silhanek, N. Verellen, W. Gillijns, P. Van Dorpe, O. Aktsipetrov, G. Vandenbosch, V. Moshchalkov, and T. Verbiest, *Asymmetric optical second-harmonic generation from chiral G-shaped gold nanostructures*, Phys. Rev. Lett. **104**, 127401 (2010).

[29]   V. K. Valev, J. J. Baumberg, C. Sibilia, and T. Verbiest, *Chirality and chiroptical effects in plasmonic nanostructures: fundamentals, recent progress, and outlook*, Adv. Mater. **25**, 2517 (2013).

[30]   X.-T. Kong, L. Khosravi Khorashad, Z. Wang, and A. O. Govorov, *Photothermal Circular Dichroism Induced by Plasmon Resonances in Chiral Metamaterial Absorbers and Bolometers*, Nano Lett. **18**, 2001 (2018).

[31]   K. A. Forbes and D. L. Andrews, *Optical orbital angular momentum: twisted light and chirality*, Opt. Lett. **43**, 435 (2018).

[32]   K. A. Forbes and D. L. Andrews, *Chiroptical interactions between twisted light and chiral media*, Proc. SPIE **10549**, 1054915 (2018).

[33]   D. L. Andrews and T. Thirunamachandran, *On three-dimensional rotational averages*, J. Chem. Phys. **67**, 5026 (1977).

[34]   R. W. Boyd, *Nonlinear Optics* (Academic Press, New York, 2003).

[35]   Y. R. Shen, *Surface nonlinear optics*, JOSA B **28**, A56 (2011).

[36]   M. Lemeshko, R. V. Krems, J. M. Doyle, and S. Kais, *Manipulation of molecules with electromagnetic fields*, Mol. Phys. **111**, 1648 (2013).

[37]   W. R. Mason, *Magnetic Circular Dichroism Spectroscopy* (John Wiley & Sons, Hoboken, NJ, 2007).

[38]   V. Lembessis and M. Babiker, *Enhanced quadrupole effects for atoms in optical vortices*, Phys. Rev. Lett. **110**, 083002 (2013).

[39]   M. G. Mandujano and J. A. Maytorena, *Quadrupolar second-harmonic generation by helical beams and vectorial vortices with radial or azimuthal polarization*, Phys. Rev. A **88**, 023811 (2013).

[40]   A. Afanasev, C. E. Carlson, and A. Mukherjee, *High-multipole excitations of hydrogen-like atoms by twisted photons near a phase singularity*, J. Opt **18**, 074013 (2016).

[41]   T. Wu, W. Zhang, R. Wang, and X. Zhang, *A giant chiroptical effect caused by the electric quadrupole*, Nanoscale **9**, 5110 (2017).

5

CHIRAL DISCRIMINATION IN OPTICAL FORCES

5.1 INTRODUCTION

The capacity of electromagnetic fields to produce forces and torques on particles is well established [1, 2]. Indeed, the forces that arise from radiation pressure have been known since the formulation of Maxwell's equations [3, 4]. However, it was not until the invention of the laser that the magnitude and manipulation of these radiation forces became suitable for experimental investigation. In his pioneering work, Ashkin [5] showed how intense beams of laser light could manipulate and control small particles of matter through non-contact radiation forces. The nature of the work required narrow beam-width intense laser light, which in turn provided for sharp intensity gradients and differential forces across the beam. These *gradient forces* are completely distinct from the transfer of momentum associated with the *radiation force* due to the radiation pressure. In the QED description, the radiation force is due to one-photon absorption, whilst forward Rayleigh scattering produces the gradient force [6]. The latter of these forces provide the basis for the well-known optical tweezer technique [7], and both forces constitute the method of optical trapping [8].

The radiation and gradient forces are single-particle forces. However, *interparticle forces* are known to arise between two or more particles, and their origin is also due to electromagnetic fields. Indeed, in the absence of any applied optical source, vacuum field

fluctuations induce electric dipole moments, whose coupling produces the well-known Casimir-Polder interaction [9].

The associated fields due to the presence of a sufficiently intense laser beam can produce another kind of interparticle force. First predicted by Thirunamachandran using QED methods [10], the laser-induced intermolecular force is commonly known as optical binding. Completely distinct from the single-particle forces present in optical trapping, in optical binding the optically-induced dipoles couple *between* two (or more) distinct particles. A decade after the original QED analysis, Burns *et al*. [11] provided the first experimental studies of optical binding. Using the aforementioned optical tweezer technique to isolate a pair of micron-sized polystyrene spheres, their semi-classical analysis found that the spheres formed a bound structure with preferred distances of interparticle separation. Since then, optical binding has been realised as a significant optical method of manipulating both micro- and nanoparticle assemblies. To date, many theoretical and experimental investigations have been carried out [12, 13], with the most contemporary being occupied with the nanoscale regime [14-17].

In the following analysis, the issue of optical binding between chiral particles is addressed. In general, optical processes between chiral particles are dependent on the handedness of each material component and/or that of the radiation field. These chiral discriminations were the basis of the work in Chapter 4. The issue of discriminatory effects in optical binding has previously been studied using QED methods [18]. However, a different mechanism is highlighted in this Chapter, which leads to a discriminatory binding force typically several orders of magnitude larger than that of the earlier study. It also exhibits different physics, being chirally sensitive to both the handedness of the material and radiation components of the system. A full comparison between the two mechanisms is given in Section 5.7. First, however, the calculation method of induced multipole moments is outlined, followed by an implementation in deriving the optical binding energy shift between a pair of chiral molecules. Both molecular and phase-weighted pair orientational averages are carried out, along with a polarisation analysis, to give a set of results applicable to a plethora of experimental situations. To finish, the role that discriminatory binding forces could have in optical manipulation, and as a probe for identifying chirality in matter, is discussed.

5.2 INDUCED MULTIPOLE MOMENTS

Throughout this thesis the method of diagrammatic time-dependent perturbation theory was utilised when carrying out QED calculations. This is generally the most common method used in QED studies, with the diagrammatic part usually being fulfilled using Feynman time-ordered diagrams [19] for calculating matrix elements. There exists, however, a multitude of other methods which give further physical insight to optical processes and phenomena, and can also help circumvent the computational effort that comes with Feynman diagrams. Particular methods include state-sequence diagrams [20], response theory [21, 22], the retarded coupling approach [23], effective interaction "collapsed vertex" Hamiltonian [24-26], and the induced moments method [27-29]. Throughout this chapter it is the later technique which will be deployed for its added physical insight, but predominantly for its ease of implementation.

The method of induced moments is underpinned by the fact that multipole moments are induced in neutral polarisable bodies in the presence of electromagnetic fields, and these moments interact via the corresponding resonant multipole-multipole coupling tensor (which was discussed in Chapter 2). The expectation value of the appropriate matrix element over a radiation state with N photons, which combines the spatial variations of the radiation fields at two different points in space, then gives the required energy shift.

The $\left(i_1 ... i_n \right)$ component of the nth-order electric multipole moment induced by an incident electric displacement field in a polarisable body ξ is given by

$$P_{i_1 ... i_n}^{(n)\text{ind}} \left(\xi \right) = \varepsilon_0^{-1} \Xi_{(\text{E})i_1 ... i_n j_1 ... j_n}^{(n)} \left(\xi, \omega \right) \nabla_{j_2} ... \nabla_{j_n} d_{j_1}^{\perp} \left(\boldsymbol{R}_{\xi} \right), \tag{5.2.1}$$

with the nth-order magnetic multipole moment induced by an incident magnetic field is

$$M_{i_1 ... i_n}^{(n)\text{ind}} \left(\xi \right) = \Xi_{(\text{M})i_1 ... i_n j_1 ... j_n}^{(n)} \left(\xi, \omega \right) \nabla_{j_2} ... \nabla_{j_n} b_{j_1} \left(\boldsymbol{R}_{\xi} \right). \tag{5.2.2}$$

A generalised, frequency-dependent molecular polarisability $\Xi^{(p:q)}_{(E)i_1\ldots i_n j_1\ldots j_n}(\xi,\omega)$ is now introduced and defined by

$$\Xi^{(p:q)}_{(E)i_1\ldots i_n j_1\ldots j_n}(\xi,\omega) = \sum_r \left(\frac{\left[P^{(p)}_{i_1\ldots i_p}(\xi)\right]^{0r}\left[P^{(q)}_{j_1\ldots j_q}(\xi)\right]^{r0}}{\left(E^{(\xi)}_{r0} - \hbar\omega\right)} + \frac{\left[P^{(q)}_{j_1\ldots j_q}(\xi)\right]^{0r}\left[P^{(p)}_{i_1\ldots i_p}(\xi)\right]^{r0}}{\left(E^{(\xi)}_{r0} + \hbar\omega\right)} \right), \quad (5.2.3)$$

where $\left[P^{(n)}_{i_1\ldots i_p}(\xi)\right]^{ba}$ are components of the nth-order transition electric multipoles E_n for the transition from $b \leftarrow a$. The corresponding counterpart expression for a molecular polarisability cast in terms of magnetic multipoles Mn for $\Xi^{(p:q)}_{(M)i_1\ldots i_n j_1\ldots j_n}(\xi,\omega)$ has a form analogous to (5.2.3) involving on $\left[M^{(n)}_{i_1\ldots i_p}(\xi)\right]^{ba}$. There also exist mixed electric-multipole magnetic-multipole polarisabilities, which are dependent on both $\left[P^{(n)}_{i_1\ldots i_p}(\xi)\right]^{ba}$ and $\left[M^{(n)}_{i_1\ldots i_p}(\xi)\right]^{ba}$.

5.3 DERIVATION OF THE OPTICAL BINDING ENERGY FOR A PAIR OF CHIRAL MOLECLES

With the theory of induced moments outlined in the previous section, it is now employed in an analysis to determine the laser-induced intermolecular forces between chiral molecules. As has been outlined in Chapter 4, the source of chiroptical effects typically arise from E1-M1 coupling terms. Although small in comparison to E1 couplings, they possess unique characteristics that can be dependent on both molecular and radiation handedness.

Consider a pair of neutral polarisable chiral molecules (A, B) which are in mutual interaction within an optical trap. Any such species will possess electric-dipole polarisability $\alpha_{ij}(\omega)$

and mixed electric-magnetic polarisability $G_{ij}(\omega)$ tensors that have nonzero components. The two tensors are explicitly given by:

$$\alpha_{ij}(\omega) = \sum_r \left\{ \frac{\mu_i^{0r} \mu_j^{r0}}{E_{r0} - \hbar\omega} + \frac{\mu_j^{0r} \mu_i^{r0}}{E_{r0} + \hbar\omega} \right\}, \tag{5.3.1}$$

$$G_{ij}(\omega) = \sum_r \left\{ \frac{\mu_i^{0r} m_j^{r0}}{E_{r0} - \hbar\omega} + \frac{m_j^{0r} \mu_i^{r0}}{E_{r0} + \hbar\omega} \right\}. \tag{5.3.2}$$

The first of these represents the simplest and lowest order implementation of (5.2.3), namely the non-discriminatory $E1^2$ interaction – switching a molecule of one particular handedness to its respective enantiomer leaves the sign of this tensor unchanged. The second term is the E1M1 analogue, which clearly changes sign upon parity inversion through the product of E1 and M1 moments. This inversion physically corresponds to replacing one enantiomer by its corresponding partner of opposite handedness.

At this point, it is worth highlighting some of the properties of the molecular response tensors and transition moments. For real wave functions the transition moment $\boldsymbol{\mu}^{r0}$ is real and $\boldsymbol{m}^{r0}$ is imaginary. Therefore, provided the optical frequency is well away from any absorption band, $\alpha_{ij}(\omega)$ is a real quantity, whilst $G_{ij}(\omega)$ is imaginary. The reason is that transition electric dipoles are based on the displacement of charge, whilst transition magnetic dipole moments entail the circulation of charge, through an imaginary angular momentum operator.

To continue, in the presence of a radiation field, a chiral molecule ξ at position $\boldsymbol{R}_\xi$ experiences the induction of both an electric and magnetic dipole moment due to the $G_{ij}(\omega)$ tensor:

$$\mu_i^{\text{ind(G)}}(\xi) = G_{ij}(\xi, \omega) b_j(\boldsymbol{R}_\xi), \tag{5.3.3}$$

$$m_j^{\text{ind(G)}}(\xi) = \varepsilon_0^{-1} G_{ij}(\xi,\omega) d_i^\perp(\mathbf{R}_\xi). \tag{5.3.4}$$

As well as an induced electric-dipole moment due to the $\alpha_{ij}(\omega)$ tensor

$$\mu_i^{\text{ind}(\alpha)}(\xi) = \varepsilon_0^{-1} \alpha_{ij}(\xi,\omega) d_j^\perp(\mathbf{R}_\xi). \tag{5.3.5}$$

The incident field consists of n photons of any specific radiation mode $(\mathbf{k},\eta)$, and therefore we can assume that the process of photon annihilation and creation occurs in the same mode (since the emission is then stimulated and therefore the most favoured). This then allows the energy shift to be given as the expectation value of the following expression

$$\Delta E = \left[\mu_i^{\text{ind}(\alpha)}(A) \mu_j^{\text{ind(G)}}(B) + \mu_i^{\text{ind(G)}}(A) \mu_j^{\text{ind}(\alpha)}(B) \right] \text{Re} V_{ij}(k,\mathbf{R})$$
$$+ \left[\mu_i^{\text{ind}(\alpha)}(A) m_j^{\text{ind(G)}}(B) + m_i^{\text{ind(G)}}(A) \mu_j^{\text{ind}(\alpha)}(B) \right] \text{Im} U_{ij}(k,\mathbf{R}), \tag{5.3.6}$$

where $\mathbf{R}$ is the separation vector $\mathbf{R} = \mathbf{R}_B - \mathbf{R}_A$. It is therefore seen from (5.3.6) that electric dipoles induced at each centre couple through the tensor $V_{ij}(k,\mathbf{R})$, whilst an electric dipole induced at one centre couples to a magnetic dipole induced at the other through $U_{ij}(k,\mathbf{R})$; both retarded dipole-dipole coupling tensors are given explicitly as:

$$V_{ij}^\pm(k,\mathbf{R}) = \frac{1}{4\pi\varepsilon_0 R^3} \left[\left(\delta_{ij} - 3\hat{R}_i\hat{R}_j \right)(1 \pm ikR) - \left(\delta_{ij} - \hat{R}_i\hat{R}_j \right) k^2 R^2 \right] e^{\mp ikR}, \tag{5.3.7}$$

$$U_{ij}^\pm(k,\mathbf{R}) = \frac{1}{4\pi\varepsilon_0 c R^3} \varepsilon_{ijk} \hat{R}_k \left(ikR \mp k^2 R^2 \right) e^{\mp ikR}. \tag{5.3.8}$$

The first of these tensors (5.3.7) was discussed in Chapter 2, the second one (5.3.8) is similarly derived in the QED theory through a calculation based on virtual photons, and couples a magnetic transition dipole moment to an electric transition dipole moment.

To proceed, the induced moments from (5.3.3)-(5.3.5) are inserted into (5.3.6), producing a form of the energy shift that is cast in terms of the electric and magnetic radiation fields, along with the electric dipole polarisability (5.3.1) and mixed electric-magnetic dipole polarisability (5.3.2) of each of the two chiral molecules:

$$
\begin{aligned}
\Delta E = \varepsilon_0^{-1} \Big[& \alpha_{ik}\left(A,\omega\right) G'_{lj}\left(B,\omega\right) d_k^{\perp}\left(\boldsymbol{R}_A\right) b_l\left(\boldsymbol{R}_B\right) \\
& + G_{ki}\left(A,\omega\right) \alpha_{lj}\left(B,\omega\right) b_k\left(\boldsymbol{R}_A\right) d_l^{\perp}\left(\boldsymbol{R}_B\right) \Big] \times \mathrm{Re}\, V_{ij}\left(k,\boldsymbol{R}\right) \\
& + \varepsilon_0^{-2} \Big[\alpha_{ik}\left(A,\omega\right) G_{jl}\left(B,\omega\right) + G'_{ik}\left(A,\omega\right) \alpha_{lj}\left(B,\omega\right) \Big] \\
& \times d_k^{\perp}\left(\boldsymbol{R}_A\right) d_l^{\perp}\left(\boldsymbol{R}_B\right) \mathrm{Im}\, U_{ij}\left(k,\boldsymbol{R}\right).
\end{aligned}
\tag{5.3.9}
$$

In the above we have introduced the identity: $-G_{ij} = G'_{ji}$, which is manifested on the grounds that the magnetic-dipole operator is time-odd – magnetic transition dipoles therefore satisfy the relation $-m_i^{r0} = m_i^{0r}$ in the mixed electric-magnetic dipole polarisability tensor (5.3.2). The energy shift (5.3.9) is therefore clearly a result of the polarisability α of one chiral molecule, coupling to the G polarisability tensor of the other.
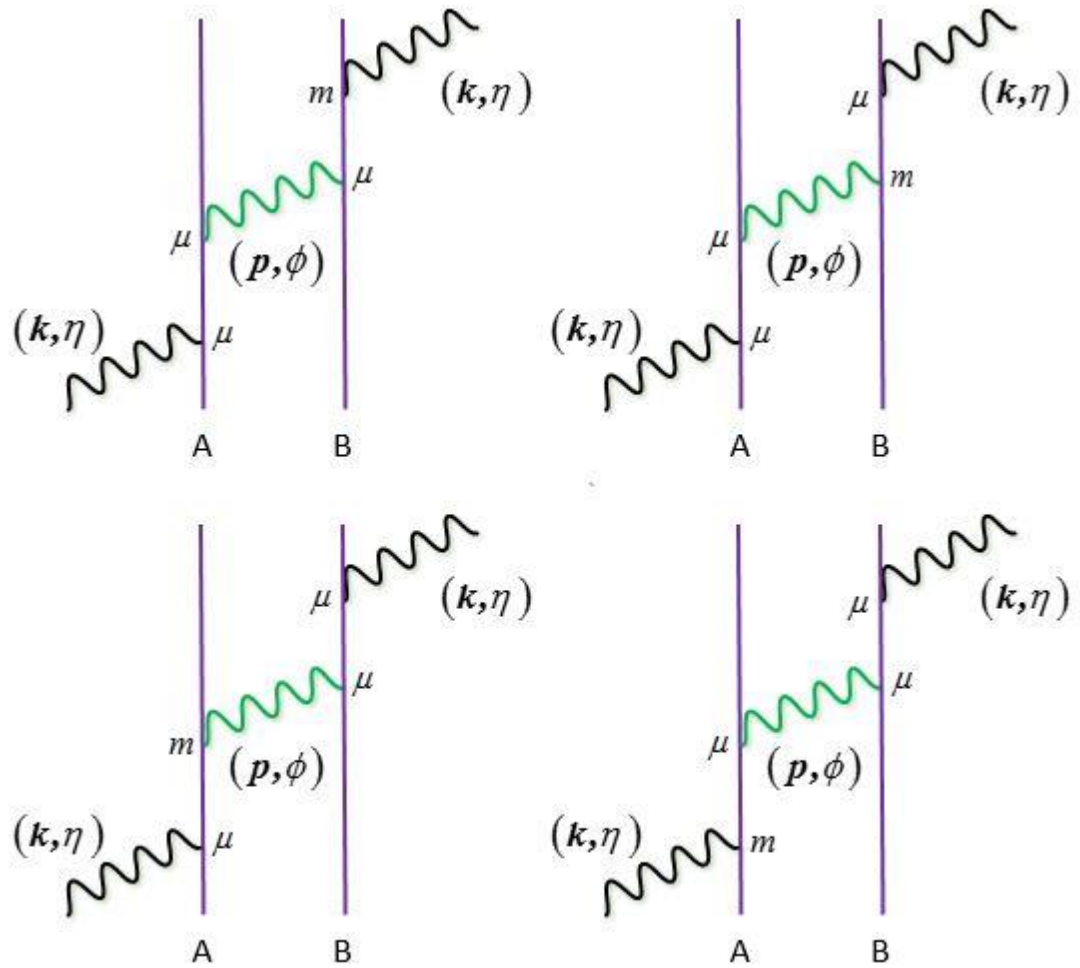
Figure 5.3.1 Four permutations of E1 and M1 interactions in '$\mu\mu\mu m$' contributions to the 48 topologically distinct Feynman time-ordered diagrams for optical binding, in one representative ordering.

The next step required is to calculate the expectation values for the system state $\left| E_0^A, E_0^B; n(k,\eta) \right\rangle$ for each of the four terms in (5.3.9). For all terms, the expectation values for the molecular parts yield the ground-state molecular polarisabilities. Focusing on the first term in (5.3.9), which we label $\mu\mu\mu m$ as it corresponds to the first representative time-ordered diagram in Figure 5.3.1, the expectation value over the radiation field is

$$\langle n(\boldsymbol{k},\eta)|d_k^\perp(\boldsymbol{R}_A)b_l(\boldsymbol{R}_B)|n(\boldsymbol{k},\eta)\rangle$$

$$= \left(\frac{\hbar k}{2V}\right)\left[(n+1)e_k^{(\eta)}(\boldsymbol{k})\bar{b}_l^{(\eta)}(\boldsymbol{k})e^{-i\boldsymbol{k}\cdot\boldsymbol{R}} + n\bar{e}_k^{(\eta)}(\mathbf{k})b_l^{(\eta)}(\mathbf{k})e^{i\boldsymbol{k}\cdot\boldsymbol{R}}\right]. \tag{5.3.10}$$

The numerical factors n and $(n+1)$ in (5.3.10) reflect the fact that two contributing terms have a different origin: in one, the throughput photon creation at one centre A or B features before the photon annihilation at the other centre B or A, whereas for the other term the opposite is true. The origins of this stem from the fact all possible pathways have to be summed over when calculating rates of processes and energy shifts in QED. However, on the valid assumption that for high intensity radiation, the mode occupation number is sufficiently large $(n+1) \sim n$, and therefore the two terms in (5.3.10) are complex conjugates, allows twice the real part to be taken. This then allows the energy shift to be expressed more concisely

$$\Delta E_{\mu\mu\mu m} = \frac{n\hbar k}{\varepsilon_0 V}\alpha_{ik}(A,\omega)G'_{lj}(B,\omega)e_k^{(\eta)}(\boldsymbol{k})\bar{b}_l^{(\eta)}(\boldsymbol{k})\mathrm{Re}V_{ij}(k,\boldsymbol{R})\cos(\boldsymbol{k}\cdot\boldsymbol{R}). \tag{5.3.11}$$

The three other remaining terms from (5.3.9), namely the $\mu\mu m\mu$, $\mu m\mu\mu$, and $m\mu\mu\mu$ (see Figure 5.3.1) terms can be calculated in a similar fashion with the use of the expectation values:

$$\langle n(\boldsymbol{k},\eta)|d_k^\perp(\boldsymbol{R}_A)d_l^\perp(\boldsymbol{R}_B)|n(\boldsymbol{k},\eta)\rangle$$

$$= \left(\frac{\hbar c k\varepsilon_0}{2V}\right)\left[(n+1)e_k^{(\eta)}(\boldsymbol{k})\bar{e}_l^{(\eta)}(\boldsymbol{k})e^{-i\boldsymbol{k}\cdot\boldsymbol{R}} + n\bar{e}_k^{(\eta)}(\mathbf{k})e_l^{(\eta)}(\mathbf{k})e^{i\boldsymbol{k}\cdot\boldsymbol{R}}\right], \tag{5.3.12}$$

$$\langle n(\boldsymbol{k},\eta)|d_k^\perp(\boldsymbol{R}_A)b_l(\boldsymbol{R}_B)|n(\boldsymbol{k},\eta)\rangle$$

$$= \left(\frac{\hbar k}{2V}\right)\left[(n+1)b_k^{(\eta)}(\boldsymbol{k})\bar{e}_l^{(\eta)}(\boldsymbol{k})e^{-i\boldsymbol{k}\cdot\boldsymbol{R}} + n\bar{b}_k^{(\eta)}(\mathbf{k})e_l^{(\eta)}(\mathbf{k})e^{i\boldsymbol{k}\cdot\boldsymbol{R}}\right]. \tag{5.3.13}$$

The corresponding energy shifts thus take the form of

$$\Delta E_{\mu\mu m\mu} = \frac{n\hbar ck}{\varepsilon_0 V}\alpha_{ik}(A,\omega)G'_{jl}(B,\omega)e_k^{(\eta)}(\boldsymbol{k})e_l^{(\eta)}(\boldsymbol{k})\operatorname{Im}U_{ij}(k,\boldsymbol{R})\cos(\boldsymbol{k}\cdot\boldsymbol{R}),$$ (5.3.14)

$$\Delta E_{\mu m\mu\mu} = \frac{n\hbar ck}{\varepsilon_0 V}G'_{ik}(A,\omega)\alpha_{lj}(B,\omega)e_k^{(\eta)}(\boldsymbol{k})\overline{e}_l^{(\eta)}(\boldsymbol{k})\operatorname{Im}U_{ij}(k,\boldsymbol{R})\cos(\boldsymbol{k}\cdot\boldsymbol{R}),$$ (5.3.15)

$$\Delta E_{m\mu\mu\mu} = \frac{n\hbar k}{\varepsilon_0 V}G_{ki}(A,\omega)\alpha_{lj}(B,\omega)b_k^{(\eta)}(\boldsymbol{k})\overline{e}_l^{(\eta)}(\boldsymbol{k})\operatorname{Re}V_{ij}(k,\boldsymbol{R})\cos(\boldsymbol{k}\cdot\boldsymbol{R}).$$ (5.3.16)

5.4 MOLECULAR ORIENTATION AVERAGING

The next step in the analysis is to perform an orientational average which will deliver results for the interaction of the molecules whose *relative* displacement $\boldsymbol{R}$ is in a fixed position with regards to the beam of throughput radiation, but whose individual orientations are random. We use the standard techniques [30] from previous chapters. Taking the $\mu\mu\mu m$ term (5.3.11) we find

$$\left\langle \alpha_{ik}(A,\omega)G'_{lj}(B,\omega)\right\rangle = \tfrac{1}{9}\delta_{ik}\delta_{lj}\alpha_{\lambda\mu}(A,\omega)G'_{\alpha\beta}(B,\omega)\delta_{\lambda\mu}\delta_{\alpha\beta},$$ (5.4.1)

where δ_{ij} is the symmetric Kronecker delta tensor. Inserting (5.4.1) into (5.3.11) gives the following energy shift

$$\Delta E_{\mu\mu\mu m} = \frac{n\hbar k}{\varepsilon_0 V} \alpha\left(A,\omega\right) G'\left(B,\omega\right) e_i^{(\eta)}\left(\boldsymbol{k}\right) \bar{b}_j^{(\eta)}\left(\boldsymbol{k}\right) \mathrm{Re}\, V_{ij}\left(k,\boldsymbol{R}\right) \cos\left(\boldsymbol{k}\cdot\boldsymbol{R}\right), \qquad (5.4.2)$$

where the numeral factor in (5.4.1) has been subsumed into the molecular tensors, allowing the result to be given in terms of polarisability scalars: $\alpha\left(\xi,\omega\right) = \tfrac{1}{3}\alpha_{\lambda\lambda}\left(\xi,\omega\right)$ and $G'\left(\xi,\omega\right) = \tfrac{1}{3}G'_{\alpha\alpha}\left(\xi,\omega\right)$.

Carrying out the same analysis on the three remaining terms (5.3.14)-(5.3.16) yields the total energy shift for mutually randomly oriented molecules as

$$
\begin{aligned}
\Delta E = \frac{n\hbar k}{\varepsilon_0 V} \Big\{ &\Big[\alpha\left(A,\omega\right) G'\left(B,\omega\right) e_i^{(\eta)}\left(\boldsymbol{k}\right) \bar{b}_j^{(\eta)}\left(\boldsymbol{k}\right) \\
&+ G\left(A,\omega\right)\alpha\left(B,\omega\right) b_i^{(\eta)}\left(\boldsymbol{k}\right)\bar{e}_j^{(\eta)}\left(\boldsymbol{k}\right) \Big] \times \mathrm{Re}\, V_{ij}\left(k,\boldsymbol{R}\right) \\
&+ c\Big[\alpha\left(A,\omega\right) G\left(B,\omega\right) + G'\left(A,\omega\right)\alpha\left(B,\omega\right) \Big] \\
&\times e_i^{(\eta)}\left(\boldsymbol{k}\right)\bar{e}_j^{(\eta)}\left(\boldsymbol{k}\right) \mathrm{Im}\, U_{ij}\left(k,\boldsymbol{R}\right) \Big\} \cos\left(\boldsymbol{k}\cdot\boldsymbol{R}\right).
\end{aligned}
\qquad (5.4.3)
$$

5.5 POLARISATION ANALYSIS

At this stage, it is appropriate to carry out a polarisation analysis. This allows us to ascertain if there is any difference in behaviour between using linearly polarised or circularly polarised input. We can also add further complexity to the analysis by defining the direction of propagation of the beam with respect to the interparticle displacement vector: the wave vector $\boldsymbol{k}$ can either be parallel $\parallel$ or perpendicular $\perp$ to $\boldsymbol{R}$.

When the input beam is linearly polarised, the result (5.4.3) is zero for both propagation configurations, $\boldsymbol{k} \parallel \boldsymbol{R}$ and $\boldsymbol{k} \perp \boldsymbol{R}$. This is anticipated on symmetry grounds alone: each term in (5.4.3) possesses only one constituent that is odd under parity inversion (the G tensor) and therefore one cannot expect a chiral response with achiral light. It is also evident from

expanding both $\operatorname{Re}V_{ij}(k,\boldsymbol{R})$ and $\operatorname{Im}U_{ij}(k,\boldsymbol{R})$ in (5.4.3) and using the following relations based on the transversality and real character of plane polarisation vectors

$$\delta_{ij}e_i^{(\eta)}(\boldsymbol{k})\bar{b}_j^{(\eta)}(\boldsymbol{k})=\boldsymbol{e}^{(\eta)}(\boldsymbol{k})\cdot\bar{\boldsymbol{b}}^{(\eta)}(\boldsymbol{k})=0, \tag{5.5.1}$$

$$\hat{R}_i\hat{R}_je_i^{(\eta)}(\boldsymbol{k})\bar{b}_j^{(\eta)}(\boldsymbol{k})=0, \tag{5.5.2}$$

$$\hat{R}_k\varepsilon_{ijk}e_i^{(\eta)}(\boldsymbol{k})\bar{e}_j^{(\eta)}(\boldsymbol{k})=0. \tag{5.5.3}$$

However, it must be realised that the leading order, non-discriminatory E1E1 binding energy shift persists using linearly polarised light.

When circularly polarised light is used, on an argument based purely on symmetry considerations, it can be anticipated that the result (5.4.3) should lead to a non-zero discriminatory process. Using the following identity

$$e_i^{(\mathrm{L/R})}(\boldsymbol{k})\bar{b}_j^{(\mathrm{L/R})}(\boldsymbol{k})=\pm ie_i^{(\mathrm{L/R})}(\boldsymbol{k})\bar{e}_j^{(\mathrm{L/R})}(\boldsymbol{k})$$
$$=\tfrac{1}{2}\left[\pm i\left(\delta_{ij}-\hat{k}_i\hat{k}_j\right)+\varepsilon_{ijk}\hat{k}_k\right], \tag{5.5.4}$$

and once again taking the $\mu\mu\mu m$ term as an example - since $V_{ij}(k,\boldsymbol{R})$ is index symmetric only the first term in (5.5.4) contributes, giving the energy shift for $\boldsymbol{k}\perp\boldsymbol{R}$

$$\Delta E_{\mu\mu\mu m}^{\perp(\mathrm{L/R})}=\operatorname{Re}\frac{I}{8\pi\varepsilon_0^2c^2R^3}\alpha(\mathrm{A},\omega)G'(\mathrm{B},\omega)$$
$$\times\left[(\mp i)(\cos kR+kR\sin kR)\mp ik^2R^2\cos kR\right], \tag{5.5.5}$$

where I is the input laser irradiance used in previous chapters and is equal to $\left(n\hbar c^2 k/V\right)$.

Once again, following a similar analysis as above on the other three remaining terms ($\mu\mu m\mu$, $\mu m\mu\mu$, and $m\mu\mu\mu$) secures the energy shift for two neutral chiral molecules in the presence of circularly polarised light propagating perpendicular to R as

$$\Delta E^{\perp(\text{L/R})} = \frac{I}{8\pi\varepsilon_0^2 c^2 R^3}\left\{\left(\tilde{G}(\text{A},\omega)\alpha(\text{B},\omega)-\alpha(\text{A},\omega)\tilde{G}'(\text{B},\omega)\right)\right.$$
$$\left.\times\left[\pm(\cos kR + kR\sin kR)\pm k^2 R^2 \cos kR\right]\right\}, \tag{5.5.6}$$

where we have further simplified the notation using $\tilde{G}'(\xi,\omega)=iG'(\xi,\omega)$. The 'Re', which signifies to take the real part of the equation, has been dropped from equation (5.5.6) as no imaginary parts longer exist, due to the tensor G itself being imaginary, as noted earlier.

Following the methods above, the total energy shift for a pair of neutral chiral particles in the presence of circularly polarised light propagating parallel to R is found to be

$$\Delta E^{\parallel(\text{L/R})} = \frac{I}{4\pi\varepsilon_0^2 c^2 R^3}\left\{\left(\tilde{G}(\text{A},\omega)\alpha(\text{B},\omega)-\alpha(\text{A},\omega)\tilde{G}'(\text{B},\omega)\right)\right.$$
$$\left.\times\left[\mp(\cos kR + kR\sin kR)\pm k^2 R^2 \cos kR\right]\right\}\cos(kR). \tag{5.5.7}$$

5.6 PHASE-WEIGHTED PAIR ORIENTATIONAL AVERAGE ANALYSIS

The above results are clearly only valid for specific experimental setups, however a more general result applicable to molecular gases and liquids can be secured through a phase-weighted pair orientational average [31]. This more involved method averages over all k relative to R and over all relative orientations of the pair of molecules in the system. Because we are concerned with a pair interaction (the A-B coupling), the difference in optical phase of the input beam at each centre must be taken account of: a *phased* rotational average.

The phase rotational can be written in a generic form as

$$\Delta E^{\phi} = K \operatorname{Re} \left\langle S_{i_1 i_2}\left(\boldsymbol{k}\right) T_{\lambda_1 \lambda_2}\left(\boldsymbol{R}\right) e^{i\boldsymbol{k}\cdot\boldsymbol{R}} \right\rangle, \tag{5.6.1}$$

where $S_{i_1 i_2}\left(\boldsymbol{k}\right)$ and $\boldsymbol{k}$ are respectively tensors and vectors which are fixed in a laboratory frame of reference; in our specific example $\boldsymbol{k}$ relates to the wave vector of light and $S_{i_1 i_2}\left(\boldsymbol{k}\right)$ the two polarisation vectors: $T_{\lambda_1 \lambda_2}\left(\boldsymbol{R}\right)$ and $\boldsymbol{R}$ are tensors and vectors fixed in a molecular frame, with $T_{\lambda_1 \lambda_2}\left(\boldsymbol{R}\right)$ the appropriate retarded resonant dipole-dipole interaction tensor as given by (5.3.7) and (5.3.8); K is a constant. Through a rather involved analysis, the above expression can be cast as

$$I^{(m)\phi}_{i_1,\ldots,i_m:\lambda_1,\ldots,\lambda_m}\left(\alpha,\hat{k},\hat{R}\right) \equiv \left\langle l_{i_1\lambda_1} \cdots l_{i_m\lambda_m} e^{i\alpha\hat{k}\cdot\hat{R}} \right\rangle, \tag{5.6.2}$$

where $\alpha = \left|\boldsymbol{k}\right|\left|\boldsymbol{R}\right|$, m is the rank of the tensor to be averaged, and $l_{i_p\lambda_p}$ is the direction cosine of the angle between the laboratory axis i_p and the molecular axis $\lambda_{p..}$ The following results for $I^{(m)\phi}_{i_1,\ldots,i_m:\lambda_1,\ldots,\lambda_m}\left(\alpha,\hat{u},\hat{w}\right)$, defined by (5.6.2), are expressed in terms of spherical Bessel functions $j_m(\alpha)$ for $m \leq 2$:

$\underline{m = 0}$

$$I^{(0)\phi}\left(\alpha,\hat{k},\hat{R}\right) = j_0\left(\alpha\right). \tag{5.6.3}$$

$\underline{m=2}$

$$
\left.
\begin{aligned}
I^{(2)\phi}_{i_1 i_2 : \lambda_1 \lambda_2}\left(\alpha, \hat{k}, \hat{R}\right) &= \sum_{j=0}^{2} I^{(2:j)\phi}_{i_1 i_2 : \lambda_1 \lambda_2}, \\
I^{(2:0)\phi}_{i_1 i_2 : \lambda_1 \lambda_2} &= \tfrac{1}{3} j_0\left(\alpha\right)\delta_{i_1 i_2}\delta_{\lambda_1 \lambda_2}, \\
I^{(2:1)\phi}_{i_1 i_2 : \lambda_1 \lambda_2} &= \tfrac{i}{2} j_1\left(\alpha\right)\varepsilon_{i_1 i_2 i_\tau}\hat{k}_{i_\tau}\varepsilon_{\lambda_1 \lambda_2 \lambda_\tau}\hat{R}_{\lambda_\tau}, \\
I^{(2:2)\phi}_{i_1 i_2 : \lambda_1 \lambda_2} &= -\tfrac{3}{2} j_2\left(\alpha\right)\left(\hat{k}_{i_1}\hat{k}_{i_2} - \tfrac{1}{3}\delta_{i_1 i_2}\right)\left(\hat{R}_{\lambda_1}\hat{R}_{\lambda_2} - \tfrac{1}{3}\delta_{\lambda_1 \lambda_2}\right).
\end{aligned}
\right\}
\tag{5.6.4}
$$

Once again, a polarisation analysis can be carried out along with the phase averaging. Let us first look at the case of linear polarised light. Using the fact that $\operatorname{Re} V_{ij}\left(k, \boldsymbol{R}\right)$ is

$$
\begin{aligned}
\operatorname{Re} V_{ij}\left(k, \boldsymbol{R}\right) &= \frac{1}{4\pi\varepsilon_0 R^3}\left[\left(\delta_{ij} - 3\hat{R}_i\hat{R}_j\right)\left(1 - ikR\right) - \left(\delta_{ij} - \hat{R}_i\hat{R}_j\right)k^2 R^2\right]e^{ikR} \\[2mm]
&= \frac{1}{4\pi\varepsilon_0 R^3}\left[\left(\delta_{ij} - 3\hat{R}_i\hat{R}_j\right)\left(1 - ikR\right) - \left(\delta_{ij} - \hat{R}_i\hat{R}_j\right)k^2 R^2\right]\cos kR + i\sin kR \\[2mm]
&= \frac{1}{4\pi\varepsilon_0 R^3}\left[\left(\delta_{ij} - 3\hat{R}_i\hat{R}_j\right)\cos kR + kR\sin kR - \left(\delta_{ij} - \hat{R}_i\hat{R}_j\right)k^2 R^2\cos kR\right]. \tag{5.6.5}
\end{aligned}
$$

Taking the $\mu\mu\mu m$ term (5.4.2) (which has orientationally averaged molecules) and inserting (5.6.5) gives

$$
\begin{aligned}
\Delta E_{\mu\mu\mu m} &= \frac{n\hbar k}{4\pi V \varepsilon_0^2 R^3}\alpha\left(\mathrm{A}, \omega\right)G'\left(\mathrm{B}, \omega\right)e_i^{(\eta)}\left(\boldsymbol{k}\right)\bar{b}_j^{(\eta)}\left(\boldsymbol{k}\right) \\
&\quad \left[\left(\delta_{ij} - 3\hat{R}_i\hat{R}_j\right)\left(\cos kR + kR\sin kR\right) - \left(\delta_{ij} - \hat{R}_i\hat{R}_j\right)k^2 R^2\cos kR\right]e^{ik\cdot R}. \tag{5.6.6}
\end{aligned}
$$

Taking the relevant terms for the averaging procedure:

$$\left\langle \left(\delta_{ij} - 3\hat{R}_i\hat{R}_j\right) e_i^{(\eta)}(\boldsymbol{k}) \bar{b}_j^{(\eta)}(\boldsymbol{k}) e^{i\boldsymbol{k}\cdot\boldsymbol{R}} \right\rangle \left(\cos kR + kR\sin kR\right)$$
$$- \left\langle \left(\delta_{ij} - \hat{R}_i\hat{R}_j\right) e_i^{(\eta)}(\boldsymbol{k}) \bar{b}_j^{(\eta)}(\boldsymbol{k}) e^{i\boldsymbol{k}\cdot\boldsymbol{R}} \right\rangle k^2 R^2 \cos kR$$

$$= \left[\left\langle \delta_{ij} e_i^{(\eta)}(\boldsymbol{k}) \bar{b}_j^{(\eta)}(\boldsymbol{k}) e^{i\boldsymbol{k}\cdot\boldsymbol{R}} \right\rangle - \left\langle 3\hat{R}_i\hat{R}_j e_i^{(\eta)}(\boldsymbol{k}) \bar{b}_j^{(\eta)}(\boldsymbol{k}) e^{i\boldsymbol{k}\cdot\boldsymbol{R}} \right\rangle \right] \left(\cos kR + kR\sin kR\right)$$
$$- \left[\left\langle \delta_{ij} e_i^{(\eta)}(\boldsymbol{k}) \bar{b}_j^{(\eta)}(\boldsymbol{k}) e^{i\boldsymbol{k}\cdot\boldsymbol{R}} \right\rangle + \left\langle \hat{R}_i\hat{R}_j e_i^{(\eta)}(\boldsymbol{k}) \bar{b}_j^{(\eta)}(\boldsymbol{k}) e^{i\boldsymbol{k}\cdot\boldsymbol{R}} \right\rangle \right] k^2 R^2 \cos kR$$

$$= \left\langle \hat{R}_i\hat{R}_j e_i^{(\eta)}(\boldsymbol{k}) \bar{b}_j^{(\eta)}(\boldsymbol{k}) e^{i\boldsymbol{k}\cdot\boldsymbol{R}} \right\rangle \left(\cos kR + kR\sin kR\right)$$
$$- \left\langle 3\hat{R}_i\hat{R}_j e_i^{(\eta)}(\boldsymbol{k}) \bar{b}_j^{(\eta)}(\boldsymbol{k}) e^{i\boldsymbol{k}\cdot\boldsymbol{R}} \right\rangle k^2 R^2 \cos kR, \tag{5.6.7}$$

then the phase-weighted averaging is seen to be

$$\left\langle \hat{R}_i\hat{R}_j e_i^{(\eta)}(\boldsymbol{k}) \bar{b}_j^{(\eta)}(\boldsymbol{k}) e^{i\boldsymbol{k}\cdot\boldsymbol{R}} \right\rangle \left(\cos kR + kR\sin kR\right) = \hat{R}_\lambda \hat{R}_\mu e_i^{(\eta)}(\boldsymbol{k}) \bar{b}_j^{(\eta)}$$
$$\times \left[\tfrac{1}{3} j_0(kR)\delta_{ij}\delta_{\lambda\mu} + \tfrac{i}{2} j_1(kR)\varepsilon_{ijk}\hat{k}_k\varepsilon_{\lambda\mu\nu}\hat{R}_\nu \right.$$
$$\left. - \tfrac{3}{2} j_2(kR)\left(\hat{k}_i\hat{k}_j - \tfrac{1}{3}\delta_{ij}\right)\left(\hat{R}_\lambda\hat{R}_\mu - \tfrac{1}{3}\delta_{\lambda\mu}\right) \right]$$
$$\times \left(\cos kR + kR\sin kR\right);$$

$$\tag{5.6.8}$$

$$- \left\langle 3\hat{R}_i\hat{R}_j e_i^{(\eta)}(\boldsymbol{k}) \bar{b}_j^{(\eta)}(\boldsymbol{k}) e^{i\boldsymbol{k}\cdot\boldsymbol{R}} \right\rangle k^2 R^2 \cos kR = -3\hat{R}_\lambda \hat{R}_\mu e_i^{(\eta)}(\boldsymbol{k}) \bar{b}_j^{(\eta)}$$
$$\times \left[\tfrac{1}{3} j_0(kR)\delta_{ij}\delta_{\lambda\mu} + \tfrac{i}{2} j_1(kR)\varepsilon_{ijk}\hat{k}_k\varepsilon_{\lambda\mu\nu}\hat{R}_\nu \right.$$
$$\left. - \tfrac{3}{2} j_2(kR)\left(\hat{k}_i\hat{k}_j - \tfrac{1}{3}\delta_{ij}\right)\left(\hat{R}_\lambda\hat{R}_\mu - \tfrac{1}{3}\delta_{\lambda\mu}\right) \right]$$
$$\times k^2 R^2 \cos kR. \tag{5.6.9}$$

Expanding the square bracket in (5.6.9) gives the first term which involves j_0 as zero (see (5.5.1); the second term which involves j_1 is also zero due to the contraction of the index-symmetric $\hat{R}_\lambda\hat{R}_\mu$ with $\varepsilon_{\lambda\mu\nu}$, itself anti-symmetric in its indices; the final term involving j_2 is

also clearly zero due to the transverse nature of the electromagnetic field vectors and the wave vector.

Carrying out a similar analysis as above on the other term which involves $V_{ij}(k, \mathbf{R})$, namely the $m\mu\mu\mu$ term (5.3.16), highlights this contribution to the energy shift with linear polarised light is also zero.

The other two terms require the result of

$$\left\langle e_k^{(\eta)}(\mathbf{k}) e_l^{(\eta)}(\mathbf{k}) \operatorname{Im} U_{kl}(k, \mathbf{R}) e^{i\mathbf{k}\cdot\mathbf{R}} \right\rangle. \tag{5.6.10}$$

For linearly polarised light, the real part of $e_k^{(\eta)}(\mathbf{k}) e_l^{(\eta)}(\mathbf{k})$ is index symmetric, and if the expanded form (5.3.8) of $U_{kl}(k, \mathbf{R})$ is inserted into (5.6.10), it is clearly seen that the index symmetric polarisation product is contracted with the antisymmetric ε_{ijk}, and hence (5.6.10) is zero. Therefore, it can be concluded that the energy shift for a pair of freely tumbling chiral molecules in the presence of linearly polarised light is zero.

The case where the input radiation is circularly polarised is now looked at, and once again the analysis begins by looking at the $\mu\mu\mu m$ term. The relevant terms to look at whilst averaging are once again

$$\left\langle \left(\delta_{ij} - 3\hat{R}_i\hat{R}_j\right)\left(\cos kR + kR\sin kR\right) e_i^{(L/R)}(\mathbf{k}) \bar{b}_j^{(L/R)}(\mathbf{k}) e^{i\mathbf{k}\cdot\mathbf{R}} \right\rangle$$
$$-\left\langle \left(\delta_{ij} - \hat{R}_i\hat{R}_j\right)\left(k^2 R^2 \cos kR\right) e_i^{(L/R)}(\mathbf{k}) \bar{b}_j^{(L/R)}(\mathbf{k}) e^{i\mathbf{k}\cdot\mathbf{R}} \right\rangle. \tag{5.6.11}$$

To render the analysis easier to follow, we will look at each term in angular brackets in (5.6.11) on an individual basis. Beginning with the first in its expanded form

$$\left\langle \delta_{ij} e_i^{(\mathrm{L/R})}(\boldsymbol{k})\bar{b}_j^{(\mathrm{L/R})}(\boldsymbol{k})\mathrm{e}^{i\boldsymbol{k}\cdot\boldsymbol{R}}\right\rangle - \left\langle 3\hat{R}_i\hat{R}_j e_i^{(\mathrm{L/R})}(\boldsymbol{k})\bar{b}_j^{(\mathrm{L/R})}(\boldsymbol{k})\mathrm{e}^{i\boldsymbol{k}\cdot\boldsymbol{R}}\right\rangle. \tag{5.6.12}$$

Concentrating on the first term in (5.6.12)

$$\left\langle \delta_{ij} e_i^{(\mathrm{L/R})}(\boldsymbol{k})\bar{b}_j^{(\mathrm{L/R})}(\boldsymbol{k})\mathrm{e}^{i\boldsymbol{k}\cdot\boldsymbol{R}}\right\rangle = \left\langle \pm i e_i^{(\mathrm{L/R})}(\boldsymbol{k})\bar{e}_i^{(\mathrm{L/R})}(\boldsymbol{k})\mathrm{e}^{i\boldsymbol{k}\cdot\boldsymbol{R}}\right\rangle = \left\langle \pm i\,\mathrm{e}^{i\boldsymbol{k}\cdot\boldsymbol{R}}\right\rangle = \pm i j_0(kR), \tag{5.6.13}$$

where $\bar{b}_j^{(\mathrm{L/R})}(\boldsymbol{k}) = \pm i\bar{e}_j^{(\mathrm{L/R})}(\boldsymbol{k})$ has been used. The second term in angular brackets in (5.6.12) is

$$\left\langle 3\hat{R}_i\hat{R}_j e_i^{(\mathrm{L/R})}(\boldsymbol{k})\bar{b}_j^{(\mathrm{L/R})}(\boldsymbol{k})\mathrm{e}^{i\boldsymbol{k}\cdot\boldsymbol{R}}\right\rangle = \pm 3i\hat{R}_\lambda\hat{R}_\mu e_i^{(\mathrm{L/R})}(\boldsymbol{k})\bar{e}_j^{(\mathrm{L/R})}(\boldsymbol{k})\left[\tfrac{1}{3}j_0(kR)\delta_{ij}\delta_{\lambda\mu}\right.$$
$$+\tfrac{i}{2}j_1(kR)\varepsilon_{ijk}\hat{k}_\lambda\varepsilon_{\lambda\mu\nu}\hat{R}_\nu$$
$$\left.-j_2(kR)\left[\hat{k}_i\hat{k}_j-\tfrac{1}{3}\delta_{ij}\right]\left[\hat{R}_\lambda\hat{R}_\mu-\tfrac{1}{3}\delta_{\lambda\mu}\right]\right]. \tag{5.6.14}$$

Taking the above term by term:

$$\pm 3i\hat{R}_\lambda\hat{R}_\mu e_i^{(\mathrm{L/R})}(\boldsymbol{k})\bar{e}_j^{(\mathrm{L/R})}(\boldsymbol{k})\tfrac{1}{3}j_0(kR)\delta_{ij}\delta_{\lambda\mu} = \pm i j_0(kR), \tag{5.6.15}$$

$$\pm 3i\hat{R}_\lambda\hat{R}_\mu e_i^{(\mathrm{L/R})}(\boldsymbol{k})\bar{e}_j^{(\mathrm{L/R})}(\boldsymbol{k})\tfrac{i}{2}j_1(kR)\varepsilon_{ijk}\hat{k}_\lambda\varepsilon_{\lambda\mu\nu}\hat{R}_\nu = 0, \tag{5.6.16}$$

and

$$\mp\tfrac{9}{2}i\hat{R}_\lambda\hat{R}_\mu e_i^{(\mathrm{L/R})}(\boldsymbol{k})\bar{e}_j^{(\mathrm{L/R})}(\boldsymbol{k})j_2(kR)\left[\hat{k}_i\hat{k}_j-\tfrac{1}{3}\delta_{ij}\right]\left[\hat{R}_\lambda\hat{R}_\mu-\tfrac{1}{3}\delta_{\lambda\mu}\right] = \pm i j_2(kR). \tag{5.6.17}$$

Therefore, the overall phased average result for (5.6.12)

$$\left\langle \left(\delta_{ij} - 3\hat{R}_i\hat{R}_j \right) \left(\cos kR + kR \sin kR \right) e_i^{(\text{L/R})}(\mathbf{k}) \bar{b}_j^{(\text{L/R})}(\mathbf{k}) e^{i\mathbf{k}\cdot\mathbf{R}} \right\rangle$$
$$= \mp i j_2(kR) \left[\cos kR + kR \sin kR \right]. \tag{5.6.18}$$

Carrying out an analogous analysis on the second term in (5.6.11) gives

$$\left\langle e_i^{(\text{L/R})}(\mathbf{k}) \bar{b}_j^{(\text{L/R})}(\mathbf{k}) \left(\delta_{ij} - \hat{R}_i\hat{R}_j \right) \left(k^2 R^2 \cos kR \right) e^{i\mathbf{k}\cdot\mathbf{R}} \right\rangle$$
$$= \left(\pm \tfrac{2i}{3} j_0(kR) \mp \tfrac{i}{3} j_2(kR) \right) \left(k^2 R^2 \cos kR \right), \tag{5.6.19}$$

which gives the overall phase-averaged energy for the $\mu\mu\mu m$ term is

$$\left\langle \Delta E_{\mu\mu\mu m} \right\rangle = \left(\frac{I}{4\pi\varepsilon_0^2 c^2 R^3} \right) \alpha(A,\omega) \tilde{G}'(B,\omega) \left\{ \mp j_2(kR) \left[\cos kR + kR \sin kR \right] \right.$$
$$\left. - \left[\pm \tfrac{2}{3} j_0(kR) \mp \tfrac{1}{3} j_2(kR) \right] k^2 R^2 \cos kR \right\}. \tag{5.6.20}$$

A similar analysis for the $m\mu\mu\mu$ term gives

$$\left\langle \Delta E_{m\mu\mu\mu} \right\rangle = \left(\frac{I}{4\pi\varepsilon_0^2 c^2 R^3} \right) \tilde{G}(A,\omega) \alpha(B,\omega) \left\{ \pm j_2(kR) \left(\cos kR + kR \sin kR \right) \right.$$
$$\left. - \left(\mp \tfrac{2}{3} j_0(kR) \pm \tfrac{1}{3} j_2(kR) \right) k^2 R^2 \cos kR \right\}. \tag{5.6.21}$$

The final two terms, $\mu m\mu\mu$ and $\mu\mu m\mu$, which are dependent on $U_{ij}(k,\mathbf{R})$, are seen to be zero:

$$\left\langle e_i^{(L/R)}(\boldsymbol{k})\,\overline{e}_j^{(L/R)}(\boldsymbol{k})\,\varepsilon_{ijk}\hat{R}_k\,\mathrm{e}^{i\boldsymbol{k}\cdot\boldsymbol{R}}\right\rangle = \left\langle \frac{1}{2}\Big[\big(\delta_{ij}-\hat{k}_i\hat{k}_j\big)\mp i\varepsilon_{ijl}\hat{k}_l\Big]\varepsilon_{ijk}\hat{R}_k\,\mathrm{e}^{i\boldsymbol{k}\cdot\boldsymbol{R}}\right\rangle$$

$$= \left\langle \mp\frac{1}{2}i\varepsilon_{ijl}\hat{k}_l\varepsilon_{ijk}\hat{R}_k\,\mathrm{e}^{i\boldsymbol{k}\cdot\boldsymbol{R}}\right\rangle$$

$$= \left\langle \mp\frac{1}{2}i2\delta_{lk}\hat{k}_l\hat{R}_k\,\mathrm{e}^{i\boldsymbol{k}\cdot\boldsymbol{R}}\right\rangle$$

$$= \left\langle \mp i\,\mathrm{e}^{i\boldsymbol{k}\cdot\boldsymbol{R}}\right\rangle$$

$$= \mp ij_0(kR). \tag{5.6.22}$$

However, from (5.4.3) it follows that we require the imaginary part of this result, but the result is in fact real and so its contributions are zero.

To secure the final result, both contributions (5.6.20) and (5.6.21) are added together; expanding the spherical Bessel functions from table A5.1 in the Appendix 5.1 and using double-angle formulae we get:

$$\left\langle \Delta E^{(L/R)}\right\rangle = \pm\frac{I}{4\pi\varepsilon_0^2 c^2 R^3}\Big(\alpha(A,\omega)\tilde{G}'(B,\omega)-\tilde{G}(A,\omega)\alpha(B,\omega)\Big)$$

$$\times\left(\cos 2kR - \frac{kR\sin 2kR}{2} + \frac{3\sin 2kR}{2kR} + \frac{3\cos 2kR}{(kR)^2} - \frac{3\sin 2kR}{2(kR)^3}\right), \tag{5.6.23}$$

for, the energy shift experienced by two neutral, randomly orientated and tumbling chiral molecules bound together by the presence of an intense throughput of circularly polarised light [32].

5.7 α-G AND G-G COUPLING MECHANISMS

Evidently the result (5.6.23) depends linearly on the input beam irradiance, and the same is true for the dominant $\alpha-\alpha$ coupling. The discriminatory effects of the $\alpha-G$ coupling

(5.6.23) arise from the handedness of the circularly polarised radiation and the mixed electric-magnetic polarisabilities of the molecules. If both the chiral molecules were chemically identical and of opposite handedness (one left-handed and one right-handed), it is clear that the discriminatory binding energy contributions (5.5.7), (5.5.6) and (5.6.23) will be zero. It is worth noting, however, that when the chiral species A and B are not identical, their G tensors will generally differ in magnitude and the above will be nonzero. The energy shift experienced by pairs of chiral molecules with the same sense of handedness will differ, the sign of the energy shift being dependent on the relative handedness of the incident light and of the molecules. Take for example, if the incident beam is of a specific handedness, the optical binding energy between two left-handed molecules will differ in energy from the binding between two right-handed molecules. Upon changing the handedness of the incident light, the signs will reverse. These results are summarised in Figure 5.7.1.
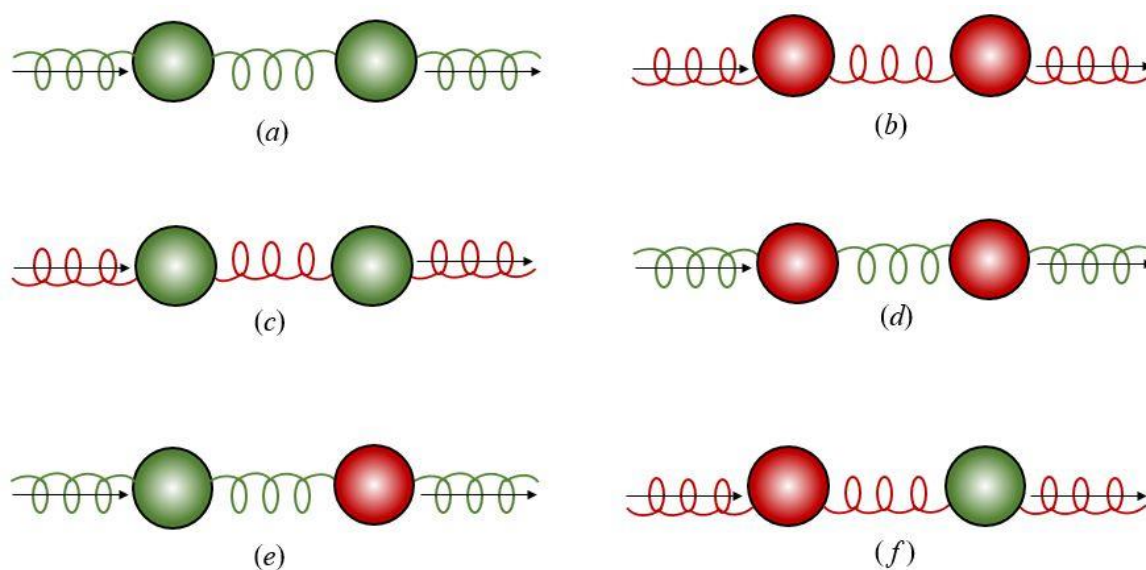
Figure 5.7.1 Illustration of the equivalences $a \equiv b$ and $c \equiv d$, and non-equivalences $a, b \neq c, d$, between the discriminatory optical binding forces for chiral particles of different handedness (depicted by red and green spheres) irradiated by circularly polarised light of either handedness (right- and left-handed forms shown with opposite twist). For cases e, f, where the two molecules are an enantiomeric pair, the $\alpha - G$ discriminatory force vanishes.

The presented analysis has focused upon a novel mechanism that operates between chiral particles subject to a sufficiently intense, circularly polarised laser beam. In particular, it has elucidated discriminatory optical binding forces which arise due to the $\alpha - G$ coupling terms. These discriminatory forces are seen to be both dependent on the handedness of the circularly polarised light - being zero for linearly polarised beams − and of the molecular handedness. The leading contributions to optical binding forces come from the E1E1-E1E1 interactions, i.e. the $\alpha - \alpha$ couplings. Their forces are non-discriminatory with regard to both the beam and the molecules, and they are of an order of magnitude 10^3 times larger than the $\alpha - G$ discriminatory contributions to the overall binding force. It is worth bearing in mind, however, that discriminatory binding forces can be made larger by exploiting pre-resonance enhancement of $G(\xi, \omega)$ by using an input wavelength approaching an absorption region for the material, though any enhancement will of course result in a corresponding increase in $\alpha(\xi, \omega)$

There also exists another form of discriminatory binding forces: the $G - G$ coupling mechanism (E1M1-E1M1), identified previously by Salam [18]. This term is in the order of 10^{-3} and 10^{-6} times smaller than the $\alpha - G$ and $\alpha - \alpha$ terms, respectively. However, it does offer different physics to both the larger contributions. The $G - G$ contribution to the energy shift for a pair of freely tumbling, randomly orientated chiral molecules is seen to be

$$\left\langle \Delta E^{(G-G)} \right\rangle = \frac{I}{8\pi\varepsilon_0^2 c^3 R^3} G(\mathrm{A}; \omega) G(\mathrm{B}; \omega) \left[\frac{4\sin 2kR}{kR} + \frac{6\cos 2kR}{(kR)^2} - \frac{3\sin 2kR}{(kR)^3} \right]. \tag{5.7.1}$$

This energy is also linearly dependent on the irradiance of the input beam, just as in the $\alpha - G$ and $\alpha - \alpha$ coupling terms. Importantly, the $G - G$ coupling is only chirally sensitive to the handedness of the molecules A and B, and is independent of the input light polarisation state: $\left\langle \Delta E_{(\mathrm{L/R})}^{(G-G)} \right\rangle = \left\langle \Delta E_{(\mathrm{Lin})}^{(G-G)} \right\rangle$, which is also in contrast to the $\alpha - G$ coupling in the sense it gives a non-zero result for linearly polarised radiation. Another important difference between the discriminatory $\alpha - G$ and $G - G$ contributions is that as we have shown in the former case, when the molecules A and B are chemically identical but of opposite

handedness, the energy shift is zero; however, in the latter the energy shift between a left-handed and a right-handed molecule is non-zero.

It is interesting and informative to speculate on why the $\alpha - G$ coupling was not reported before now. Firstly, the $\alpha - G$ coupling represents the interaction between two chiral molecules as we have shown, but it also represents the interaction between a chiral molecule with an achiral molecule. This is the crux: chiral molecules still engage their E1 moments and therefore still possesses a dynamic polarisability α. This is what has been overlooked by many. Just because a molecule is chiral, it does not necessarily mean its only molecular response is through its G tensor – the interferences between α and G must be included.

5.8 DISCUSSION

Two possible routes of exploiting these discriminatory optical binding forces are immediately evident. The first is concerned with helicity-dependent optical manipulation of particles. Optical nanomanipulation is a burgeoning field, wherein light is used to trap, rotate, and accelerate small particles of matter. In this sense, optical methods of manipulation offer distinct advantages due to their non-contact nature. A particular application of these optomechanical forces could be in chiral sorting. Although a host of established methods exist for chiral resolution at the molecular level, these methods generally rely on other chiral molecules or other materials to act as resolving agents. Recent work in the field has looked at using circular dichroism (the preferential absorption of left- and right-circularly polarised light) as a way to separate enantiomers in a fluidic environment [33]. Further contemporary work utilising optical methods have identified discriminatory optical forces as a potential tool in the separation of left- and right-handed molecules [34-37].

Although it may prove difficult at present to implement optical binding forces in the direct pursuit of enantiomer separation, there is another possible application in the development of identifying chirality in optically bound systems [38]. For example, consider an input laser beam that is modulated between right- and left-handed circular polarisations, the response of a system comprising chiral particles with the same handedness will be an oscillation from their equilibrium positions [39]. If the modulation frequency of the laser is tuned to

resonance with the essentially harmonic natural frequency of the optically bound pair, the small-scale oscillations should become readily detectable. Treating (5.6.23) as a correction to the standard $E1^2$-$E1^2$ $\alpha - \alpha$ coupling produces graphs of the form given in Figure 5.7.2. In producing the graph, the magnitude of the correction term $\alpha - G$ is taken to be of the order of the fine structure constant. It emerges that for a laser wavelength of 628 nm, there is a displacement of 5 nm between these minima. This verifies that a modulation of optical input between circular polarisations will produce a corresponding oscillation in their equilibrium positions [40, 41].
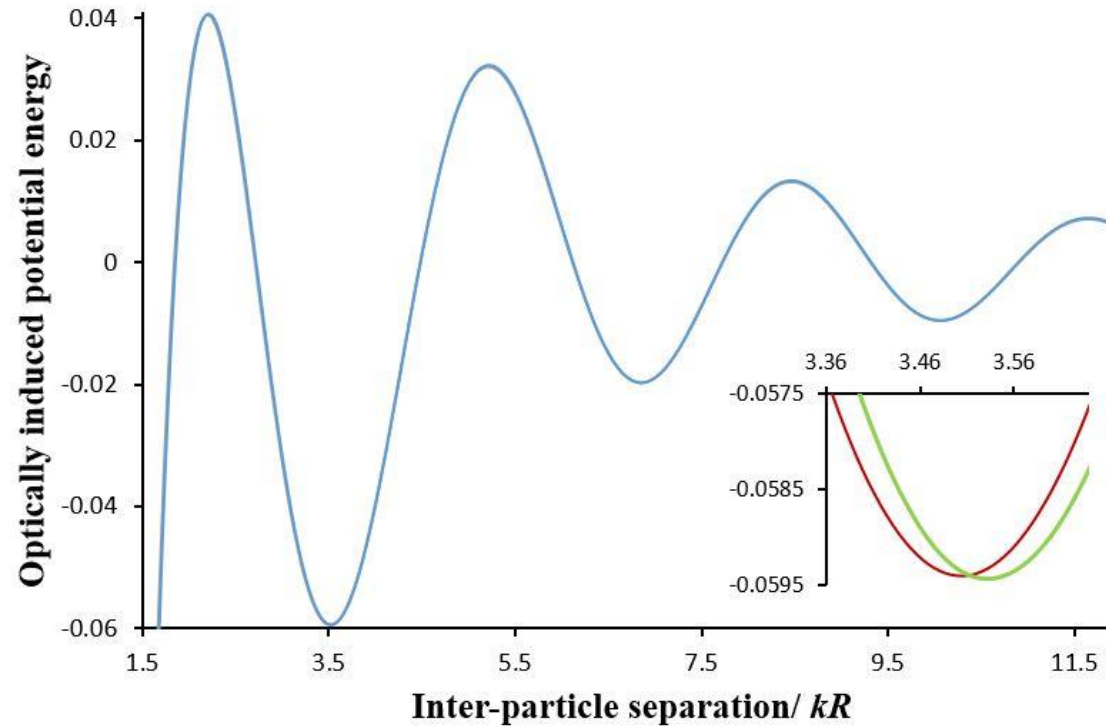
Figure 5.7.2 Plot of the optical binding potential energy (in arbitrary units) for two chiral particles in a circularly polarised beam. The abscissa scale measures the inter-particle distance R in dimensionless units of kR, the wave number k is defined as $2\pi/\lambda$ with λ as the laser wavelength. On the scale of the main graph there is an imperceptible difference between the results for particles who handedness is either the same, or opposite to, that of the radiation. The inset exhibits the difference between the two cases, around the position of the first potential energy minimum.

APPENDIX 5.1

Table A5.1. Spherical Bessel functions $j_n(kR)$, $n \leq 4$.

n	$j_n(kR)$
0	$\dfrac{1}{kR}\sin kR$
1	$\dfrac{1}{(kR)^2}\sin kR - \dfrac{1}{kR}\cos kR$
2	$\left[\dfrac{-1}{kR} + \dfrac{3}{(kR)^3}\right]\sin kR - \dfrac{3}{(kR)^3}\cos kR$
3	$\left[\dfrac{-6}{(kR)^2} + \dfrac{15}{(kR)^4}\right]\sin kR + \left[\dfrac{1}{kR} - \dfrac{15}{(kR)^3}\right]\cos kR$
4	$\left[\dfrac{1}{kR} - \dfrac{45}{(kR)^3} + \dfrac{105}{(kR)^5}\right]\sin kR + \left[\dfrac{10}{(kR)^2} - \dfrac{105}{(kR)^4}\right]\cos kR$

Higher-order results can be determined from the relation

$$j_{n+1}(\alpha) = (2n+1)^{-1} j_n(\alpha) - j_{n-1}(\alpha). \tag{A5.1}$$

REFERENCES

[1]   O. M. Maragò, P. H. Jones, P. G. Gucciardi, G. Volpe, and A. C. Ferrari, *Optical trapping and manipulation of nanostructures*, Nat. Nanotechnol. **8**, 807 (2013).

[2]   D. L. Andrews and D. S. Bradshaw, *Optical Nanomanipulation* (Morgan & Claypool Publishers, San Rafael, CA, 2016).

[3]   A. Bartoli, *Il calorico raggiante e il secondo principio di termodinamica*, Il Nuovo Cimento **15**, 193 (1884).

[4]   J. C. Maxwell, *A Treatise on Electricity and Magnetism, Volume 2* (Dover Publications, New York, 1954).

[5]   A. Ashkin, *Acceleration and trapping of particles by radiation pressure*, Phys. Rev. Lett. **24**, 156 (1970).

[6]   D. S. Bradshaw and D. L. Andrews, *Manipulating particles with light: radiation and gradient forces*, Eur. J. Phys. **38**, 034008 (2017).

[7]   A. Ashkin, J. M. Dziedzic, J. E. Bjorkholm, and S. Chu, *Observation of a single-beam gradient force optical trap for dielectric particles*, Opt. Lett. **11**, 288 (1986).

[8]   K. C. Neuman and S. M. Block, *Optical trapping*, Rev. Sci. Instrum. **75**, 2787 (2004).

[9]   H. B. G. Casimir and D. Polder, *The influence of retardation on the London-van der Waals forces*, Phys. Rev. **73**, 360 (1948).

[10]   T. Thirunamachandran, *Intermolecular interactions in the presence of an intense radiation field*, Mol. Phys. **40**, 393 (1980).

[11]   M. M. Burns, J.-M. Fournier, and J. A. Golovchenko, *Optical binding*, Phys. Rev. Lett. **63**, 1233 (1989).

[12]   K. Dholakia and P. Zemánek, *Colloquium: Gripped by light: Optical binding*, Rev. Mod. Phys. **82**, 1767 (2010).

[13]   T. Čižmár, L. C. Dávila Romero, K. Dholakia, and D. L. Andrews, *Multiple optical trapping and binding: New routes to self-assembly*, J. Phys. B: At. Mol. Opt. Phys. **43**, 102001 (2010).

[14]   V. Demergis and E.-L. Florin, *Ultrastrong optical binding of metallic nanoparticles*, Nano Lett. **12**, 5756 (2012).

[15]   Z. Yan, S. K. Gray, and N. F. Scherer, *Potential energy surfaces and reaction pathways for light-mediated self-organization of metal nanoparticle clusters*, Nat. Commun. **5**, 3751 (2014).

[16]   D. S. Bradshaw, K. A. Forbes, and D. L. Andrews, *Sculpting optical energy landscapes for multi-particle nanoscale assembly*, Proc. SPIE **9126**, 91260P (2014).

[17]   S. H. Simpson, P. Zemánek, O. M. Marago, P. H. Jones, and S. Hanna, *Optical binding of nanowires*, Nano Lett. (2017).

[18]   A. Salam, *On the effect of a radiation field in modifying the intermolecular interaction between two chiral molecules*, J. Chem. Phys. **124**, 014302 (2006).

[19]   R. P. Feynman, *Space-time approach to quantum electrodynamics*, Phys. Rev. **76**, 769 (1949).

[20]   R. D. Jenkins, D. L. Andrews, and L. C. Dávila Romero, *A new diagrammatic methodology for non-relativistic quantum electrodynamics*, J. Phys. B: At. Mol. Opt. Phys. **35**, 445 (2002).

[21]   D. Craig and T. Thirunamachandran, *New approaches to chiral discrimination in coupling between molecules*, Theor. Chem. Acc. **102**, 112 (1999).

[22]   E. A. Power and T. Thirunamachandran, *Quantum electrodynamics with nonrelativistic sources. III. Intermolecular interactions*, Phys. Rev. A **28**, 2671 (1983).

[23]   L. C. Dávila Romero and D. L. Andrews, *A retarded coupling approach to intermolecular interactions*, J. Phys. B: At. Mol. Opt. Phys. **42**, 085403 (2009).

[24]   D. Craig and E. Power, *The asymptotic Casimir–Polder potential from second-order perturbation theory and its generalization for anisotropic polarizabilities*, Int. J. Quant. Chem. **3**, 903 (1969).

[25]   D. Craig, E. Power, and T. Thirunamachandran, *The dynamic terms in induced circular dichroism*, Proc. R. Soc. A **348**, 19 (1976).

[26]   D. L. Andrews and T. Thirunamachandran, *A quantum electrodynamical theory of differential scattering based on a model with two chromophores. I. Differential Rayleigh-scattering of circularly polarized-light*, Proc. R. Soc. A **358**, 297 (1978).

[27]   E. Power and T. Thirunamachandran, *Casimir-Polder potential as an interaction between induced dipoles*, Phys. Rev. A **48**, 4761 (1993).

[28]   A. Salam, *Intermolecular interactions in a radiation field via the method of induced moments*, Phys. Rev. A **73**, 013406 (2006).

[29]   A. Salam, *A general formula obtained from induced moments for the retarded van der Waals dispersion energy shift between two molecules with arbitrary electric multipole polarizabilities: I. Ground state interactions*, J. Phys. B: At. Mol. Opt. Phys. **39**, S651 (2006).

[30]   D. L. Andrews and T. Thirunamachandran, *On three-dimensional rotational averages*, J. Chem. Phys. **67**, 5026 (1977).

[31]   D. L. Andrews and M. J. Harlow, *Phased and Boltzmann-weighted rotational averages*, Phys. Rev. A **29**, 2796 (1984).

[32]   K. A. Forbes and D. L. Andrews, *Chiral discrimination in optical binding*, Phys. Rev. A **91**, 053824 (2015).

[33]   G. Tkachenko and E. Brasselet, *Helicity-dependent three-dimensional optical trapping of chiral microparticles*, Nat. Commun. **5**, 4491 (2014).

[34]   D. S. Bradshaw and D. L. Andrews, *Chiral discrimination in optical trapping and manipulation*, New J. Phys. **16**, 103021 (2014).

[35]   D. S. Bradshaw and D. L. Andrews, *Laser optical separation of chiral molecules*, Opt. Lett. **40**, 677 (2015).

[36]   H. Chen, Y. Jiang, N. Wang, W. Lu, S. Liu, and Z. Lin, *Lateral optical force on paired chiral nanoparticles in linearly polarized plane waves*, Opt. Lett. **40**, 5530 (2015).

[37]   M. Wang, H. Li, Y. Dong, X. Zhang, M. Du, R. Wang, T. Xu, and J. Wu, *Manipulating the Lorentz force via the chirality of nanoparticles*, Opt. Mater. **62**, 411 (2016).

[38]   M. Kamandi, M. Albooyeh, C. Guclu, M. Veysi, J. Zeng, K. Wickramasinghe, and F. Capolino, *Enantiospecific Detection of Chiral Nanosamples Using Photoinduced Force*, Physical Review Applied **8**, 064010 (2017).

[39]   N. Metzger, K. Dholakia, and E. Wright, *Observation of bistability and hysteresis in optical binding of two dielectric spheres*, Phys. Rev. Lett. **96**, 068102 (2006).

[40]   D. S. Bradshaw, K. A. Forbes, J. M. Leeder, and D. L. Andrews, *Chirality in optical trapping and optical binding*, Photonics **2**, 483 (2015).

[41]   K. A. Forbes, D. S. Bradshaw, and D. L. Andrews, *Discriminatory effects in the optical binding of chiral nanoparticles*, Proc. SPIE **9548**, 95480M (2015).

CONCLUSION

Throughout this thesis the theory of molecular quantum electrodynamics has been employed to study fundamental interactions between light and matter. It has been explicitly highlighted how to implement the theory, and the powerful nature of its ability to predict new optical phenomena has been demonstrated.

All such theoretical predictions made throughout the thesis should be readily observable using modern laser techniques found in optics laboratories. Specific details of possible experimental methodology can be found at the end of each respective chapter. However, common to each potential experiment would be the need for a coherent light source, typically a femtosecond laser for experiments requiring high intensity and a tuneable frequency, supplemented by a continuous-wave source for other measurements. Other key components, included amongst the beam-steering and focusing units on an optical table, would be appropriate wave plates to obtain the desired polarisation state, especially useful for generating circularly polarised photons for studying chiroptical interactions. The production of twisted beams required in Chapter 4 may be achieved with spatial light modulators or spiral phase plates. The final key element being a suitable photodetector and associated electronic circuitry.

To conclude this work we shall now look towards the future, and in particular, how each project presented in the thesis might continue to evolve. In Chapter 2 a novel mechanism which involved the delocalised production of correlated photon pairs and optical harmonics was highlighted and quantitatively evaluated. Clearly, the next step would be to try an experimentally validate its existence. One of the more immediately obvious methods would be invoking the design criteria laid out for enhanced nonlinear optical processes using ideally-sized nanoparticle composites, and studying the output intensity. Another issue worth studying is how this mechanism affects the fidelity of entangled photon pairs produced in SPDC, and if any such manifestations may play an important role in the field of quantum information where correlated photon pairs are utilised extensively.

In Chapter 3, the often-neglected diamagnetic interactions with the radiation field were laid out for scattering and two-photon absorption. The work was concerned with highlighting the existence and unique characteristics of the diamagnetic couplings, whose origin of

importance comes from securing gauge invariant results. Although it may prove technically demanding, a potential scheme for observing their unique contribution to scattering rates was outlined.

Arguably Chapter 4 is the most open-ended and promising area for future developments. Now that the issue of whether the handedness of a vortex beam can play a role in chiroptical interactions has been given a firm theoretical grounding, one can anticipate that studying more complex optical processes will lead to further examples of optical rates that are sensitive to vortex beam handedness. Furthermore, there are theoretical questions to be answered with regards as to why it appears both the spin and orbital angular momentum need to be engaged to observe chiroptical effects in single-photon absorption with vortex beams – it suggests the route to take would be that of studying the total angular momentum of light in chiroptical interactions. Finally, as laid out at the end of Chapter 4, the results seem to highlight a mechanism of discriminatory effects using achiral material, this avenue requires further work as it potentially opens up chiroptical interactions to a much wider range of molecules.

The key issue developed in Chapter 5 concerned illuminating the fact that chiral molecules will still engage their electric polarisability, as well as their mixed electric-magnetic susceptibility. Firstly, this invites a reappraisal of past studies on chiroptical interactions in other two-centre optical processes and intermolecular interactions, for example the Casmir-Polder interaction. A more practical application worthy of development would be to quantitatively combine the discriminant optical trapping and optical binding forces into a single optical force experienced by molecules in an optical trap, and observing the interplay of altering parameters that are specific, or shared by, either optical force, potentially leading to an all optical method of chiral resolution.

With the rapid surge of research in the contemporary fields of photonics, plasmonics, and metamaterials, QED itself in the future should be adapted to be able to account for these types of interactions in what can be termed exotic materials, compared to the standard application to dielectric molecules. Quantum electrodynamics is the best theory we have to date, and the rewards of its successful application to these new and interesting fields should provide bountiful insights.